UNIVERSIDAD AUTÓNOMA DE SAN LUIS POTOSÍ

FACULTAD DE INGENIERÍA

CENTRO DE INVESTIGACIÓN Y ESTUDIOS DE POSGRADO

Design methodology for a free piston Stirling engine for electric power generation

Metodología de diseño para un motor Stirling de pistón libre para generación de energía eléctrica

TESIS

Que para obtener el grado de:
Maestro en ingeniería Mecánica
con Orientación Terminal en
Mecatrónica y Sistemas Mecánicos

Presenta:
Ing. José Rodrigo Ávila Pérez

Asesor:
Dra. Geydy Luz Gutiérrez Urueta
Co-Asesor:
Dr. Fidencio Tapia Rodríguez

San Luis Potosí, S. L. P **Septiembre de 2019**

UASLP
Universidad Autónoma de San Luis Potosí

FACULTAD DE
INGENIERÍA

20 de junio de 2019

ING. JOSÉ RODRIGO ÁVILA PÉREZ
P R E S E N T E.

En atención a su solicitud de Temario, presentada por los **Dres. Geydy Luz Gutiérrez Urueta y Fidencio Tapia Rodríguez**, Asesor y Co-asesor de la Tesis que desarrollará Usted, con el objeto de obtener el Grado de **Maestro en Ingeniería Mecánica con Orientación Terminal en Mecatrónica y Sistemas Mecánicos**, me es grato comunicarle que en la Sesión del H. Consejo Técnico Consultivo celebrada el día 20 de junio del presente, fue aprobado el Temario propuesto:

TEMARIO:

"Metodología de diseño para un motor Stirling de pistón libre para la generación de energía eléctrica"

Introducción
1. Estado del arte: Motores Stirling de pistón libre
2. Herramientas de diseño para motores Stirling de pistón libre
3. Intercambiadores de calor para motores Stirling
4. Metodología de diseño para motores Stirling de pistón libre

Conclusiones
Referencias

"MODOS ET CUNCTARUM RERUM MENSURAS AUDEBO"

A T E N T A M E N T E

M. I. JORGE ALBERTO PÉREZ GONZÁLEZ
DIRECTOR.

UNIVERSIDAD AUTONOMA
DE SAN LUIS POTOSI
FACULTAD DE INGENIERIA
DIRECCION

Copia. Archivo.
*etn.

www.uaslp.mx

Av. Manuel Nava 8
Zona Universitaria • CP 78290
San Luis Potosí, S.L.P.
tel. (444) 826 2330 al39
fax (444) 826 2336

To my family

Acknowledgments

To my supervisor Ph.D. Geydy Gutierrez Urueta, my co-supervisor Ph.D. Fidencio Tapia Rodríguez and also to Ph.D. Joseph Adhemar Araoz Ramos for their support and time.

To Ph.D. Sergio Rolando Cruz for his advises and invaluable time despite the significant amount of work he had, you always found some minutes.

To CONACyT, who provided the funding of this work.

Finally to my family and friends for always believing in me and for encouraging me.

Abstract

At present, Stirling engines are of interest for many research due to their capacity to use any source of heat, quiet operation and non-polluting character. Therefore, this devices are part the many alternatives for the development of new methods for sustainable energy transformation. Stirling engines are classified into kinematic (beta, alpha and gamma) and dynamic, which consist of Free Piston Stirling Engines (FPSE). A kinematic Stirling engine uses a typical crank mechanism with a flywheel to produce a 90° out of phase reciprocating motion of the piston parts. This type of Stirling engines are the most studied until now, both theoretically and experimentally. The FPSE is distinctive for the reason that it excludes all wearing mechanisms. It provides the possibility of extremely long operating life, higher efficiency and zero maintenance. This thesis centers on a new design methodology for FPSE. A complete design procedure for FPSE based on its stability and including fundamental components is described. Pressure losses in components (heater, regenerator and cooler) are included as an important part of the design methodology. Calculation of the friction factor and the Nusselt number are carried out using well-known experimental correlations. The variety of matrix types included and their design parameters add more calculation, which this suggest a more practical tool to automate the design process. An original Graphical User Interface (GUI) is developed through an original code generated using matlab. The implementation of a based-on genetic reproduction algorithm resulted in a powerful tool to find parameters that successfully satisfy the output power desired. This GUI includes the calculation of the natural oscillation frequency of the engine, based on the dynamic analysis, stability analysis and its representation in the complex plane. Besides, it offers the friction factors and Nusselt number according to the type heat exchanger. Given the significant amount of variables and the number of iterations needed to accomplish the desired parameters, the proposed design technique, summarized in the GUI, represents a fast and useful solution to new designers. The design parameters obtained are corroborated with reported results. A final technical data of the designed engine is offered using the GUI.

Resumen

En la actualidad, los motores Stirling son de interés para muchas investigaciones debido a su capacidad para utilizar cualquier fuente de calor, funcionamiento silencioso y carácter no contaminante. Por lo tanto, estos dispositivos son parte de las muchas alternativas para el desarrollo de nuevos métodos para la transformación de energía sostenible. Los motores Stirling se clasifican en cinemáticos (beta, alfa y gamma) y dinámicos, que consisten en motores Stirling de pistón libre (FPSE). Un motor Stirling cinemático utiliza un mecanismo de manivela típico con un volante para producir un movimiento alternativo desfasado a 90° de las partes del pistón. Este tipo de motores Stirling son los más estudiados hasta ahora, tanto teórica como experimentalmente. El FPSE es distinto por la razón de que excluye todos los mecanismos de uso. Ofrece la posibilidad de una vida útil extremadamente larga, mayor eficiencia y cero mantenimiento. Esta tesis se centra en una nueva metodología de diseño para FPSE. Se describe un procedimiento de diseño completo para FPSE basado en su estabilidad e incluyendo componentes fundamentales. Las pérdidas de presión en los componentes (calentador, regenerador y enfriador) se incluyen como una parte importante de la metodología de diseño. El cálculo del factor de fricción y el número de Nusselt se llevan a cabo utilizando correlaciones experimentales bien conocidas. La variedad de tipos de matriz incluidos y sus parámetros de diseño, agregan más cálculos, lo que sugiere una herramienta más práctica para automatizar el proceso de diseño. Una interfaz gráfica de usuario (GUI) novedosa se desarrolla a través de un código original generado en matlab. La implementación basada en un algoritmo genético es una herramienta poderosa para encontrar parámetros que satisfagan con éxito la potencia de salida deseada. Esta GUI incluye el cálculo de la frecuencia de oscilación natural del motor, basado en el análisis dinámico, el análisis de estabilidad y su representación en el plano complejo. Además, ofrece los factores de fricción y el número de Nusselt según el tipo de intercambiador de calor. Dada la cantidad significativa de variables y la cantidad de iteraciones necesarias para lograr los parámetros deseados, la metodología de diseño propuesta, resumida en la GUI, representa una solución rápida y útil para los nuevos diseñadores. Los parámetros de diseño obtenidos se corroboran con los resultados informados. Se ofrece una información técnica final del motor diseñado utilizando la GUI.

Nomenclature

Variables

P	Pressure	c_p	Gas constant
V	Volume	c_v	Gas constant
T	Temperature	r	Vector
Q	Heat or non potencial force	q	Degree of freedom
F	Force	s	Complex variable
X or x	Displacement	h	Heat transfer coefficient
f	Frequency	u	Velocity
K	Spring stiffness	d	Hydraulic diameter
M	Mass	NTU	Number of transfer units
C	Damping coefficient	C_f	Friction coefficient
t	Time	Re	Reynolds number
$\dot{x}$	Velocity	Nu	Nusselt number
$\ddot{x}$	Acceleration	d_s	Sphere diameter
A	Area	S_x	Wetted perimeter
R	Gas constant	n	number of elements
m	Mass gas	L	Length or Lagrangian

Greek symbols

μ	Micro or viscosity	η	Efficiency
ω	Angular frequency	α	Phase angle
ϕ	Phase angle of the displacer with respect to the piston	ε	Porosity
ρ	Density	δ	Phase angle of the compression space volume with respect to the piston
θ	Angle	τ	Kinetic energy
ν	Potencial energy	Δ	Difference

Subscript

max	Maximum	min	Minimum
C	Compression	E	Expansion
w	working gas	o	Initial or output
D	Displacer	P	Piston
R	Rod	k	Cooler
h	Heater	r	Regenerator
wk	Wetted cooler	wh	Wetted heater
$h1$	Heater higher	$h2$	Heater lower
$k1$	Cooler higher	$k2$	Cooler lower
i	Input	f	Free flow

Contents

Índice

List of Figures

List of Tables

Introduction

The demand for energy increases continuously in the modern world due to overpopulation. This scenario, together with the shortage of fossil fuels, have given rise to the development of new methods for energy transformation during the past decades.

The primary goal is to utilize the higher amount of energy available from fuel or other source, which will result in more efficient technologies. For the past decades, the boom of renewable energy has exponentially increased with solar panels and wind turbines as the most known technologies, but there are many others which are trying to join the seek of solutions, like wave energy converters. The topic of this document is the Stirling engine which has characteristics of an external combustion engine but the advantage of clean energy conversion.

The Stirling engine was invented in 1816 by Reverend Robert Stirling [3]. At that time the machine was better known as a "Hot Air" engine, although for that time the device occupied a relatively unimportant role among other engines. Now Stirling engines rearise due to their high efficiency, their capacity to use any source of heat, their quiet operation, and non-polluting character [4]. These represent a notable advantages in the current energy context, and explain the increasing number of works focused on developing this technology.

They are classified into kinematic (beta, alpha and gamma) and dynamic, which includes free piston Stirling engines. A kinematic Stirling engine uses a classic crank mechanism with a flywheel to produce a 90°out of phase reciprocating motion of the piston parts. These type of Stirling engines are the most studied until now and there are well resumed works on both theoretical and experimental studies (Ipci and Karabulut, 2018; Cheng et al., 2017; Altin et al., 2018; Sowale et al., 2018; Cinaret al., 2018, among others).

The micro cogeneration (μCHP) is one of the principal applications, although there are many others like vehicle propulsion to produce a zero or low level of pollution, to directly pump blood, generate electricity or generate hydraulic power, as summarized by Valent et al., (2015). The Free-piston Stirling engine(FPSE) is distinctive for the reason that it excludes all wear mechanisms related with a kinematic Stirling engine and thus eliminates the need for lubricant. It replaces the crank mechanism of the kinematic Stirling engine by a linear mechanical storage device such as a compression spring. It provides the FPSE with the possibility of extremely long operating life, higher efficiency and zero maintenance (Deetlefs, 2014).

In order to design an FPSE, a theoretical simulation model needs to be developed. The key complication to design useful FPSE is to assure the stability of the oscillations, which is not a minor mission because of the decoupled pistons and the sensibility of some parameters. The aim of this study is to achieve the coupling between the kinematic and dynamic constrains, considering the stability for a practical design of a FPSE. A code is developed with the purpose of pursuing a set of parameters which enables the engine to generate a desired power output or other variables using genetic algorithms. Considering the fact that these machines can be activated with heat, they represent an additional alternative for the use of renewable energy.

Main Objective

Develop a design methodology for a Free Piston Stirling engine for electricity production, based on dynamic and thermal analysis.

Specific Objectives

1. Obtain a mathematical model that describes the dynamics of the engine components and includes the thermodynamic description of the working fluid.
2. Simulate the operation of the Stirling engine subject to variation of parameters such as various fluids and real geometries.
3. Compare the resulting model with technical data found in the literature.
4. Obtain design parameters (lengths, areas, spring stiffness and cylinder size) that, together with the operating parameters, generate a specific power.
5. Establish a series of steps to follow the development of a free piston Stirling engine (FPSE).
6. Develop computer tools that support the different stages of the design of FPSE.

Methodology

The study was divided into several parts: the first part represents the study of the isothermal model and the coupling of the dynamics of the system. The second part is the study of the engine stability, and the third part integrates both studies, see Figure 1.

1. A literature review of Stirling engines and the Free pistons arrangement from published reports, articles and books.
2. Study the dynamics of the system.
3. Study the thermodynamics of the system.
4. Use a simplified thermal model to study a first order engine.

5. Study the specifications of the engine (masses, springs, coefficients, working fluid, pressure and temperatures) to generate different net powers.
6. Analysis of stability.
7. Analysis and evaluation of the results.
8. Development of the design methodology.

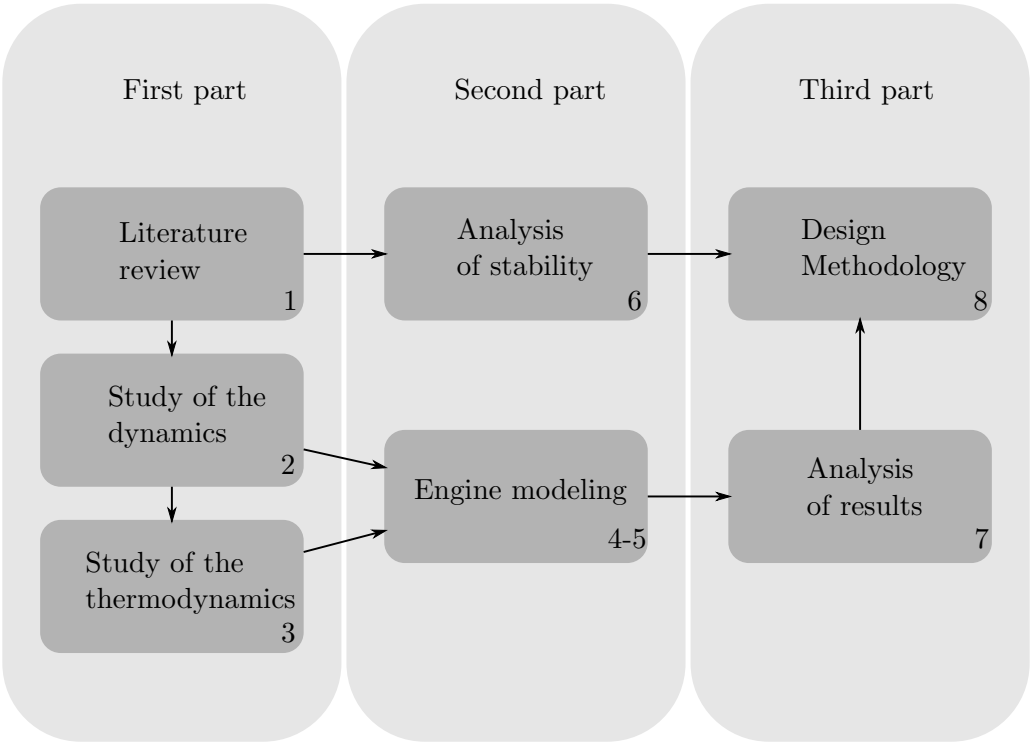

Figure 1: Methodology

Structure of the Thesis

The thesis is divided into five chapters:

- **Introduction:** In the introductory chapter, the work purposes are presented as well as the methodology used for the development of the Thesis in order to achieve such purposes.
- **Chapter 1:** Presents the state of the art on Free Piston Stirling Engines, and its functioning.
- **Chapter 2:** The first order model analysis is presented as an approach for the designer to know the output power and the size of the engine. Furthermore, the adiabatic model is presented as a more realistic mathematical description.
- **Chapter 3:** Useful correlations for the Nusselt number and the friction coefficient are presented as part of the heat exchangers design.

- **Chapter 4:** A design methodology for FPSE is performed. It gives directions to help the engineer to design a functional machine, based on a stability study combined with the dynamic and thermodynamic studies. Moreover, a graphic user interface is developed to facilitate the design of FPSE.
- **Conclusions:** summarizes the conclusions obtained in this Thesis and suggest possible lines of future research.

Chapter 1

State of the art: Free piston Stirling engines

This type of engines has received many attention from the scientists in the recent years due to its varied applications in renewable energy technologies. Recent works on Free Piston Stirling Engine (FPSE) can be summarized as follow: Zhu et al.[5] presented a theoretical study on a micro-combined heat and power system combined with a FPSE. An experimental validation was carried out, showing good agreement with the model and a cycle efficiency up to 90% (combined heat and power performance). Acoustic impedance is the base of the model. In this paper, as well as Tavakolpour-Saleh et al.[6], reported a well-summarized review on modeling of FPSE. The works developed by Tavakolpour-Saleh et al.[7], Zare and Tavakolpour-Saleh [8], Mou et al. [9] are examined, making evident that most of the FPSE models developed so far were established on dynamic or thermodynamic analysis of the system. Remiorz et al. [10] compared a micro-cogeneration unit based on FPSE and a heat pump in terms of thermodynamic effectiveness and cost. They found the efficiency of electric energy generation in the micro-cogeneration unit and the overall efficiency and sensitivity analysis of cost. For the heating season, the operation of the heat pump resulted slightly better in terms of cost, but it changes with the price of both natural gas and electricity.

Conroy et al. [4] found that operating a WhisperGen Mk IV Stirling engine unit in the house resulted in an energy saving of 2063 kWh of electricity and generated a thermal output of 20095 kWh during the trial period, operated for 2512 h and produced an annual saving of 180 euros; also there was a decrease in the emissions by 1040 kg per annum. The interest in developing this kind of technology has been growing not only as a common subject for research but as a device which companies can take a profit. That is the case of United Stirling of Sweden with his P-75, 75kW truck engine and Sunpower of Athens, Ohio with his atmospheric air engine which can produce 850 watts, to mention a few [1].

Formosa [11, 12] developed and validated an analytical thermodynamic model that considers the effectiveness and flaws of the heat exchangers and regenerator. Later, a semi-analytical dynamic model of an FPSE was developed Formosa [11]. Formosa and Fréchette [13] also studied the scaling laws for FPSE design. A simple model capable of predicting the geometrical parameters of the heat exchangers and the mass of the pistons was thus proposed.

Karabulut [14] presented a nonlinear dynamic model of a passive FPSE and then, studied the dynamic response of the engine system corresponding to the variations of engine parameters such as hot source temperature, damping coefficients of the pistons, diameter of displacer rod, initial positions of the power piston and displacer, mean pressure, and stiffness of the pistons' springs. Some works are found in the literature, showing the use of renewable energies using FPSE [15, 16, 17]. Other researchers are interested in the design, but fixing parameters like frequency [18] or using scaling laws [13].

1.1 Working principle of a Stirling engine

A Stirling engine is a thermo-mechanical device that operates on a closed regenerative thermodynamic cycle (there is no mass transfer across the engine) with cyclic compression and expansion of the working fluid (Figure 1.1) at different temperature levels [19]. This last description includes a wide variety of configurations, functions, and characteristics. Also, this particular type of engine (FPSE) has the advantage of being a mechanism-free, as is discussed later.

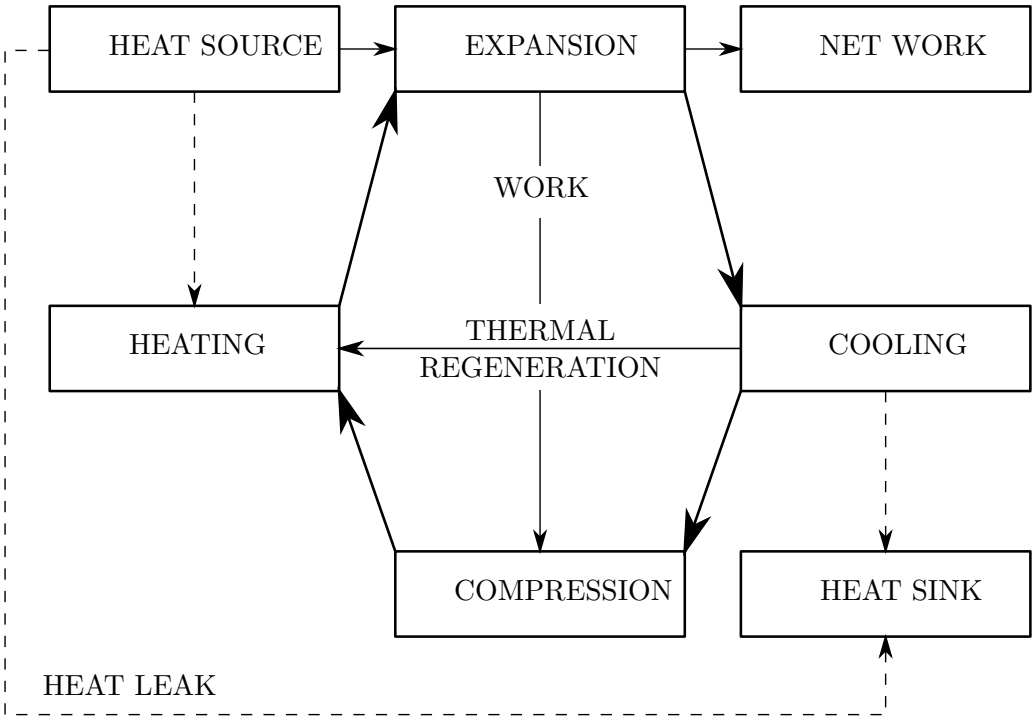

Figure 1.1: Process for regenerative heat engines

Figure 1.1 shows the working principle for any regenerative heat engine. Even though the engine and the cycle have the same name, this ideal cycle does not represent the actual engine operation, since the Stirling Engine (SE) follows more complicated processes. For this reason, the use of the ideal cycle for the engine analysis is not advisable for design for purposes.

The Stirling cycle is an ideal thermodynamic cycle built by two isothermal curves and two isometric regenerative processes. To fully understand the com-

plete cycle the next part describes each one of the processes.

Consider the two pistons shown in Fig. 1.2 and the PV diagram shown in Fig. 1.3. The pistons are one on each end of the cylinder, and between them a regenerator, which may be thought as a thermodynamic sponge, releasing and absorbing heat alternately. One of the volumes between the regenerator and a piston is called the *expansion space*, and it's maintained at a high temperature (T_{max}). The remaining volume is named *compression space* kept at a low temperature (T_{min}). Therefore the temperature gradient is $T_{max} - T_{min}$ through the longitudinal direction; also it is assumed that there is no thermal conduction between these two volumes.

It is essential to get the initial configuration of the pistons and the fluid, to describe the cycle; thus the following assumptions are made, see Figure 1.2:

- As an initial configuration the compression space piston is at the outer dead point and the expansion space piston is at the inner dead point (near the regenerator).
- All the fluid is at the compression space.
- At this position the volume is a maximum.
- The pressure and temperature are minimum values.

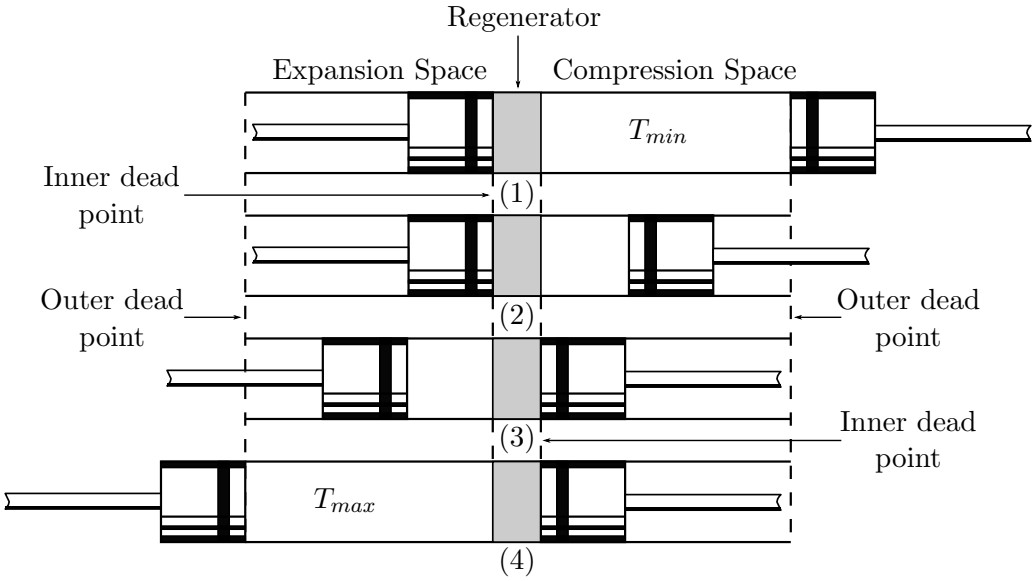

Figure 1.2: Stirling cycle

Process 1-2: Caused by the movement of the compression piston and the lack of motion of the expansion piston, the working fluid is squeezed. At the same instant, the temperature remains constant due to the transfer of heat (Q_c) from the compression space to the surrounds or external sink, and therefore the pressure increases, see Figure 1.3a.

Process 2-3: Also named as transfer process, both pistons move, the compression piston towards the regenerator and the expansion piston simultaneously

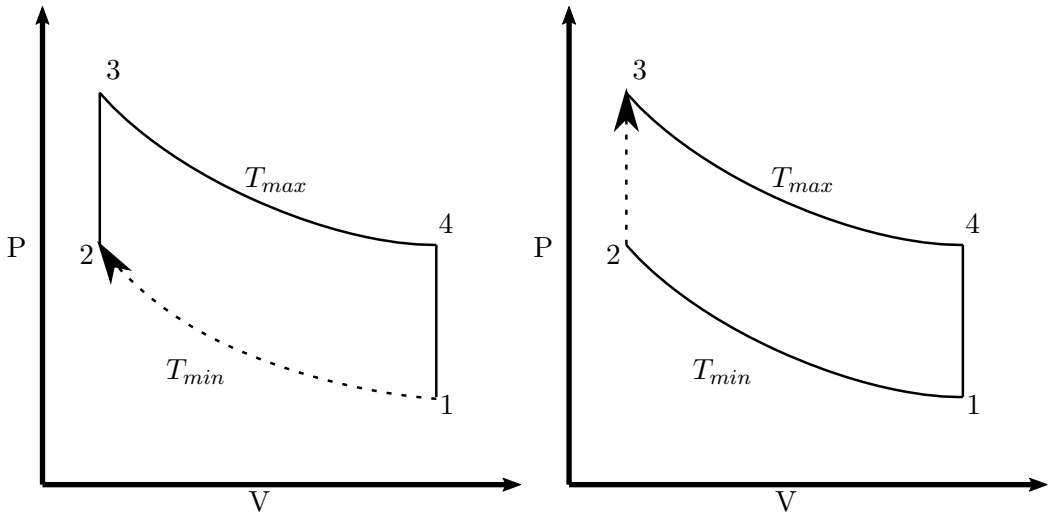

(a) Compression process

(b) Increase of temperature

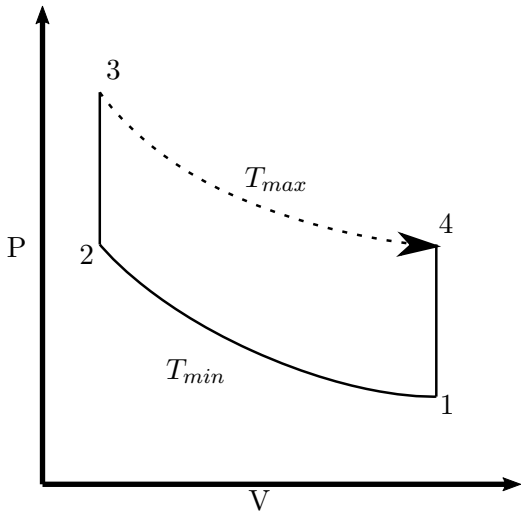

(c) Expansion process

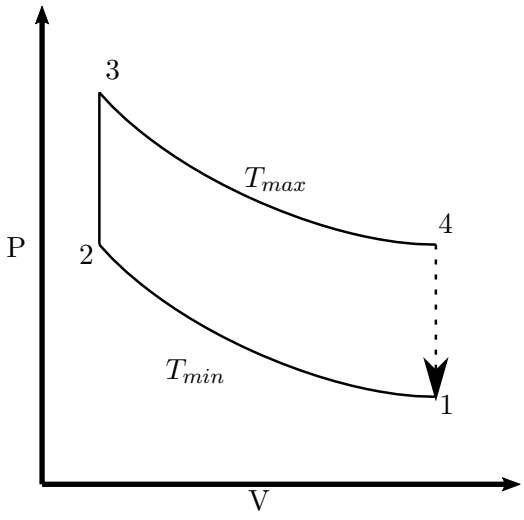

(d) Decrease in temperature

Figure 1.3: Pressure-Volume diagram for the ideal Stirling cycle

away. So the volume remains constant. Now the fluid is passing through the regenerator, from the compression space to the expansion space. Also while moving the fluid is heated up, from T_{min} to T_{max}. The gradual increase of temperature at constant volume also causes the increase in pressure, see Figure 1.3b.

Process 3-4: Now the expansion piston keeps moving to the outer dead point, and the compression piston remains stationary at the central dead point. As the volume increases, the pressure decreases also heat is added (Q_E) to the system from an external source, see Figure 1.3c.

Process 4-1: Another transfer process describes the closure of the cycle, as in process 2-3 the pistons move simultaneously enclosing the same volume and transferring the fluid back to the compression space but passing before through the regenerator. Therefore a change in temperature occurs as before but in the opposite direction which means $T_{max} \rightarrow T_{min}$, see figure 1.3d.

In comparison with Carnot cycle, the theoretical efficiency (η) is the same[20][3].

$$\eta = \frac{T_{max} - T_{min}}{T_{max}} \tag{1.1.1}$$

The significant advantage lies in work generated, due to the isovolumetric processes the area inside the PV diagram is higher than in the Carnot cycle which instead has two isentropic processes [1][19].

Stirling engines can be arranged in three main configurations, shown in Fig. 1.4. The alpha type uses two pistons, which compress the fluid in the cold space, then the fluid is displaced to the hot volume where it is expanded. The cooler, regenerator and heater are in series. The beta type has only one power piston and one displacer piston in the same cylinder, the expansion space is solely determined by the movement of the displacer, and the compression space depends on the motion of both pistons, as the alpha configuration the three heat exchangers are in series. Similar to the beta type, the gamma configuration utilizes only one cylinder, and within it, the piston and displacer lie inside, the significant difference is an offset from the displacer to the piston to allow a simpler mechanical arrangement. See Figure 1.4

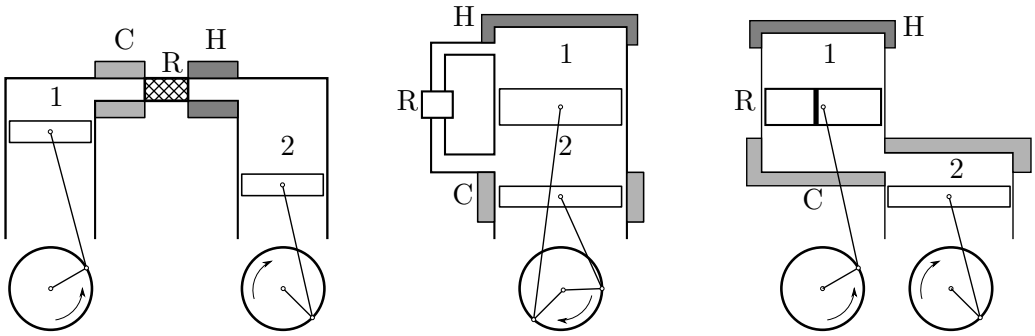

Alpha Beta Gamma

Figure 1.4: Main types of Stirling engine arrangement,(1: Compression, 2: Expansion)

The Free-Piston Stirling engine has no kinematic linkages coupling the reciprocating mechanical elements to each other or common flywheel, see Figure 1.5. Pistons move entirely in response to the fluctuating gas or spring forces. The engine consists of a heavy power piston and a lightweight displacer within an enclosed cylinder. In some arrangements, there is the so-called bounced space, which acts as a gas spring; therefore, the need for mechanical springs is substituted by this.

The natural frequency of the system is determined by the combination of mass and spring stiffness (this will be shown in the next chapters). Due to the resonant characteristic, the motion of the displacer may be sinusoidal.

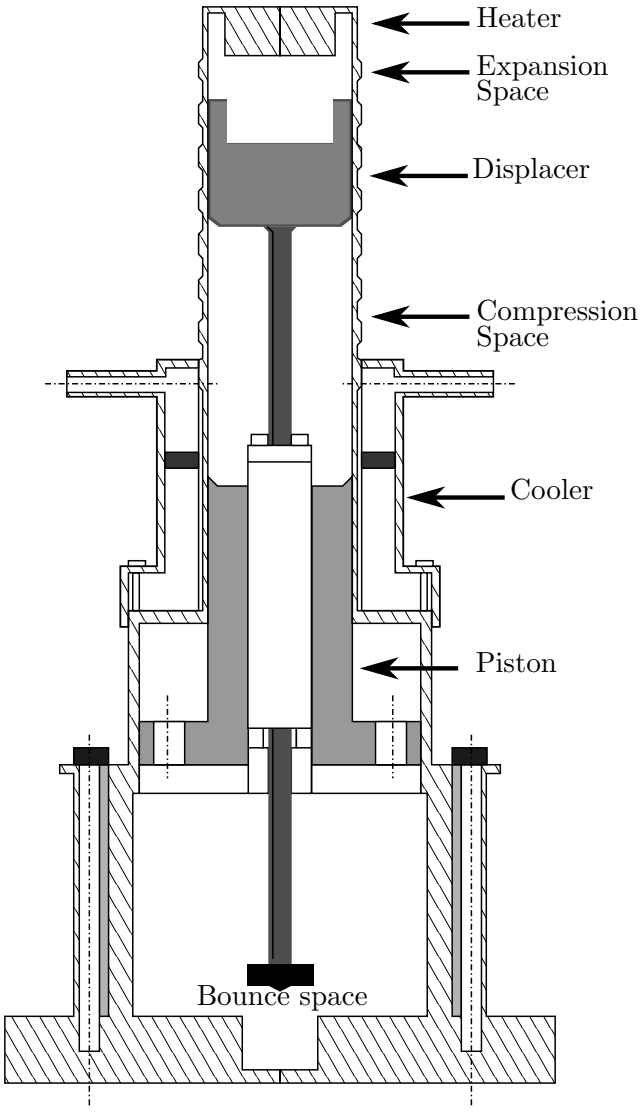

Figure 1.5: FPSE Diagram

As discussed before, there are at least three principal types of Stirling engines, now a fourth arrangement is added to the list. The Free-Piston is not a new version but a subtype. All three can be Free-piston, excluding wearing mechanisms. FPSE has several advantages. It operates at a more or less constant frequency, and it is self-starting. Also, there are no side thrusts exerted by the reciprocating devices against the engine cylinder. The lack of linkages reduces to zero the losses due to mechanical transmissions. Since the container is sealed, dust particles are maintained outside.[1]

This thermal machine is not perfect, so it is worth to mention some of the disadvantages: Due to the lack of rotating shaft, the coupling between other devices results complicated (e.g., alternators, pumps and compressors). Also, the decoupling between pistons induces more hazardous tasks to the designer (e.g., stability study).

1.2 How a Free-Piston Stirling engine works

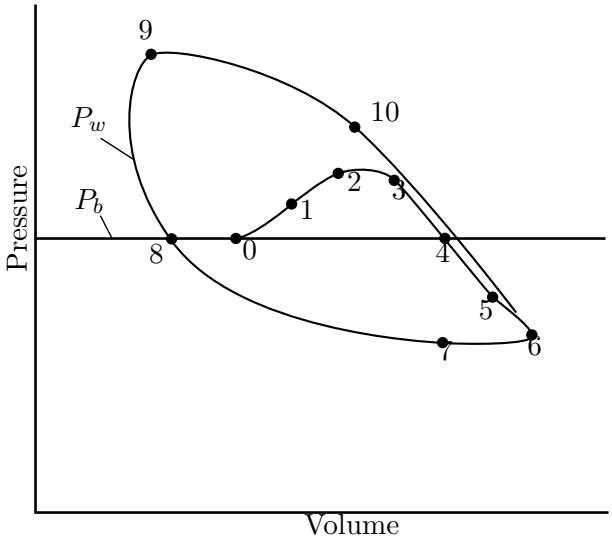

Figure 1.6: Pressure-Volume Diagram

Figure 1.6 shows the transcendent behavior of the engine and the stable operation of it.

As soon as the temperature increases inside the hot volume, the temperature in the expansion space starts to rise and so the pressure P_w (Figure 1.6). This will move the displacer and piston down the cylinder (Process 0-1), see Figure 1.7a.

Due to the bigger mass of the power piston, the displacer will move more than the piston. This is going to reduce the compression volume above the piston and below the displacer. Therefore the fluid is displaced out of the compression space through the regenerator to the expansion space. Then the gas is heated, and so the pressure increases further (Process 1-2) see Figure 1.7b.

At some point, the compression space has no volume due to the physical contact among displacer and piston; and no cold gas is transferred to the regenerator. At this state, the working pressure is higher than the one inside the bounce space; therefore the pistons are still in motion, see Figure 1.7c [1].

The working volume within the cylinder increases until the pressures stabilize and then it begins to fall as the gas expands (Process 2-3), see Figure 1.7d.

The process of expansion continues until the pressure inside the working space equals the pressure of the bounce space, but the inertia of the piston keeps the piston moving. This will produce a significant decrement in the working pressure so the bounce pressure will be higher (Process 4-5), see Figure 1.7e.

Then the gas forces acting are reversed and decelerate both piston and displacer. The displacer, due to its lightweight, will move up faster than the piston till the top of the cylinder (Process 5-6). Since the displacer had moved there is not expansion volume (the displacer is in contact with the top part of the cylin-

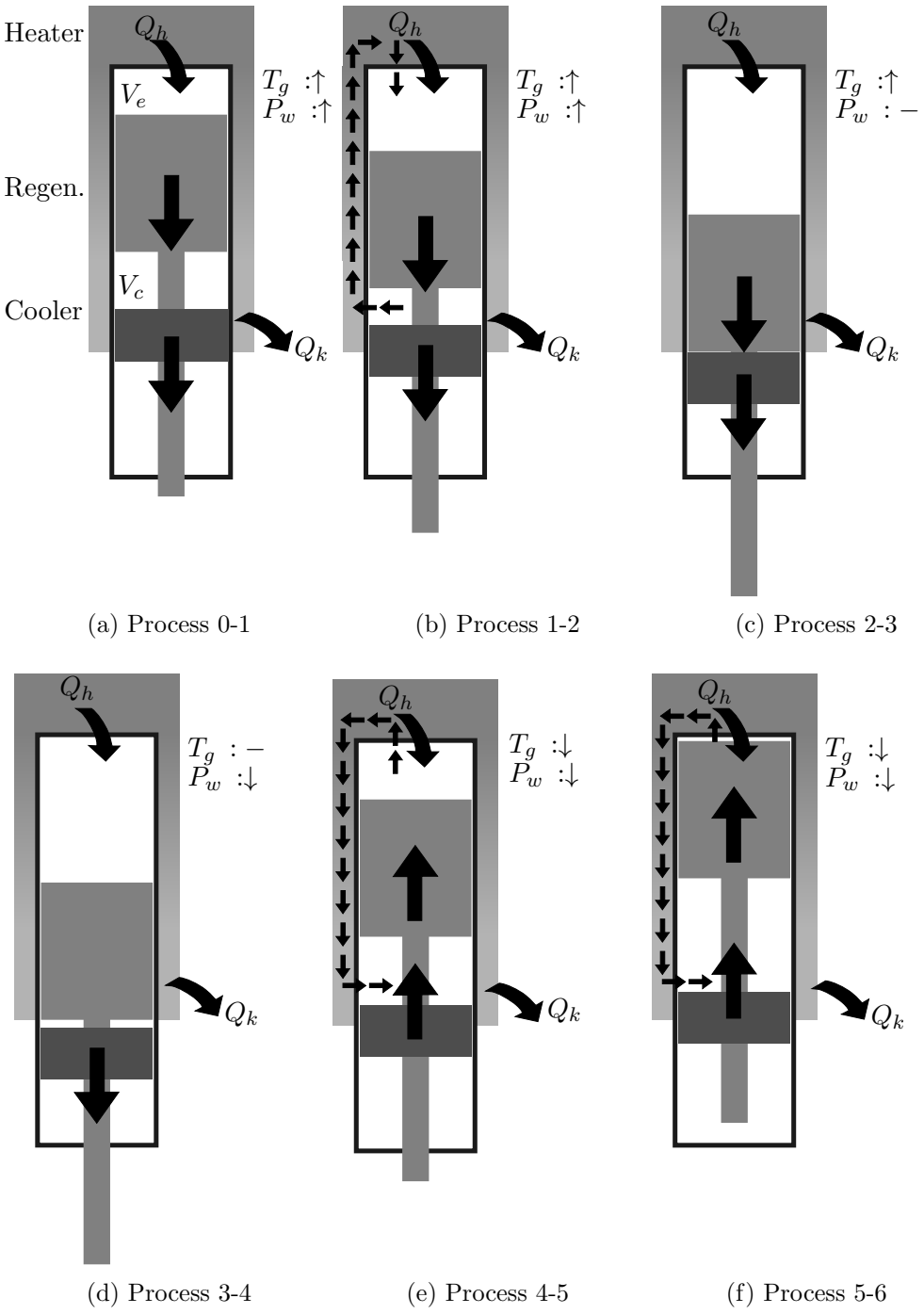

(a) Process 0-1 (b) Process 1-2 (c) Process 2-3

(d) Process 3-4 (e) Process 4-5 (f) Process 5-6

Figure 1.7: Piston motion inside one cylinder ruled by the Stirling cycle

der), and all the mass that once was there now is pushed through the regenerator to the compression space, and consequently, its temperature decreases and further so the pressure, see Figure 1.7f.

A considerably differential in pressure reverses the motion of the power piston and, then cause it to start ascending the cylinder. The compression process continues until the pressure inside the working space increases to the bounce space pressure (Process 6-7 and 7-8), see Figure 1.7g.

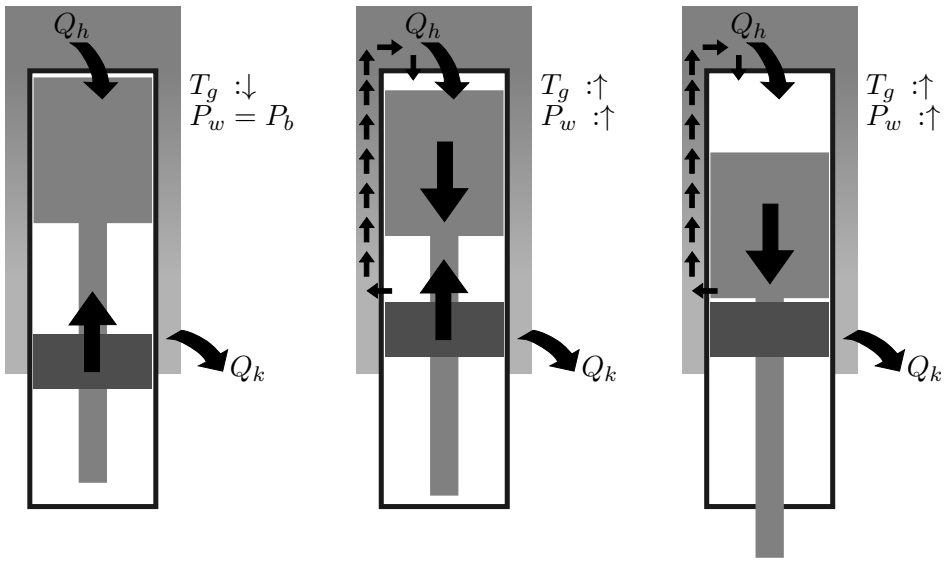

(g) Process 6-7 (h) Process 8-9 (i) Process 10

Figure 1.7: Piston motion inside one cylinder ruled by the Stirling cycle (cont.)

Inertia force of the piston then carries it past the pressure balance point causing a higher pressure in the working space. Then the displacer starts to fall toward the piston, and the mass inside the compression volume moves to the expansion (hot area) and, therefore increasing the pressure in the working space (Process 8-9) see Figure 1.7h. Finally, the displacer is now again in contact with the piston (Process 10). See Figure 1.6 and Figure 1.7i [1].

1.3 Types of Free-Piston Stirling engines

The classification of the FPSE begins with the single common feature that the machine has at least one reciprocating element. The motion of this component can be:

- Simple harmonic in which the engine is oscillating.
- Non-resonant in which the engine is described as 'over-driven'.

A single acting (From only one piston work is obtained) FPSE can be also classified as i) two-piston engine, ii) piston-displacer machines. See figure 1.8

1.4 Dynamics of Free-Piston Stirling engine

The study of Stirling engines is a multidisciplinary task. It includes knowledge from solid mechanics, thermodynamics, fluid mechanics and heat transfer. Although it results in an attractive project, that is one of the complications for the development of these machines. Since the difference in temperatures and the

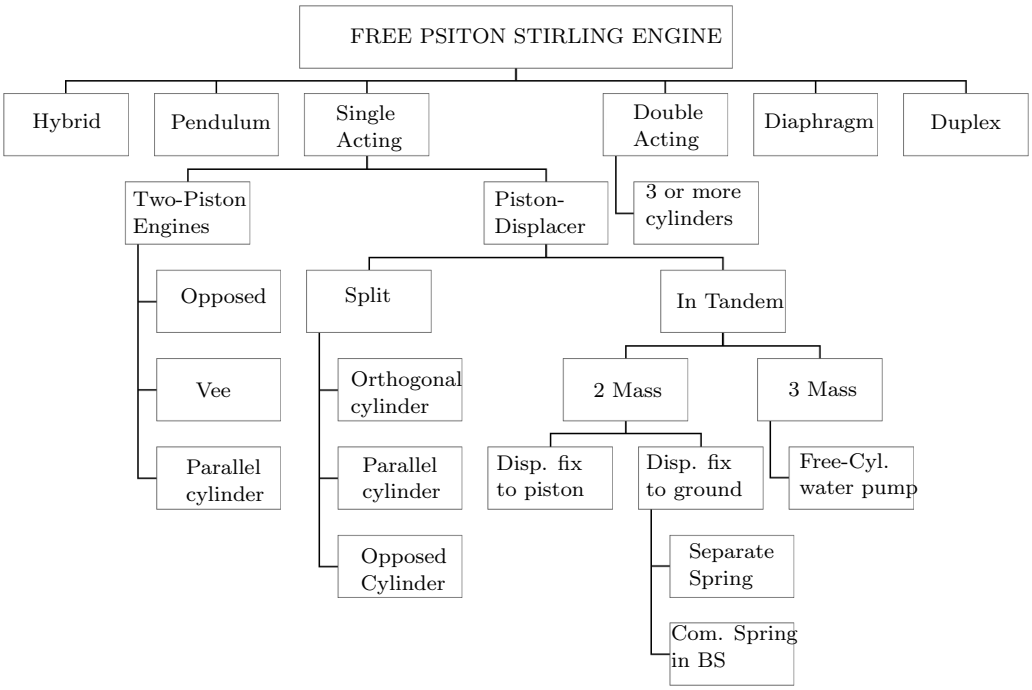

Figure 1.8: Types of Free-Piston Stirling engines [1]

motion of the pistons within the cylinder together determine the variation in pressure, the analysis should be studied as a whole and not only the solid mechanic part but also the thermodynamic phenomena.

FPSE as a vibrating system

Newton's Second Law of motion describes the motion of the mass, where the sum of forces is equal to the mass times the acceleration. The free vibration of the mass shown in Figure 1.9 represents an under-damped behavior, which means that at some time the mass will return to its equilibrium position. It is important to notice that no external forces (dynamic forces) are applied to the mass.

Then, when external forces act upon the system (usually periodic forces $F(t) = F_o \sin \omega t$), the resulting motion tends to follow the behavior of the force; this is called forced vibration. A particular phenomenon appears when the frequency of excitation matches to the damped natural frequency, this is called resonance, and it causes an increase in the amplitude of vibration [21][22].

In a system with steady state forced vibration with viscous damping the displacement of the piston is harmonic but never in phase with the driving force. Therefore if the driving force is at the form $F(t) = F_o \sin \omega t$ the displacement will be $x(t) = X_o \sin(\omega t - \alpha)$, then the angle α depends on the frequency ratio $r = f/f_n$ and the degree of viscosity. When $r = 1$ damping then the angle is $90°$ regardless of the degree of damping in the system.

Also, non-viscous damping is presented inside the engine. The most common is described as Coulomb damping which is the appropriate model of frictional drag of dry sliding surfaces. It is autonomous of velocity and exercises a nearly

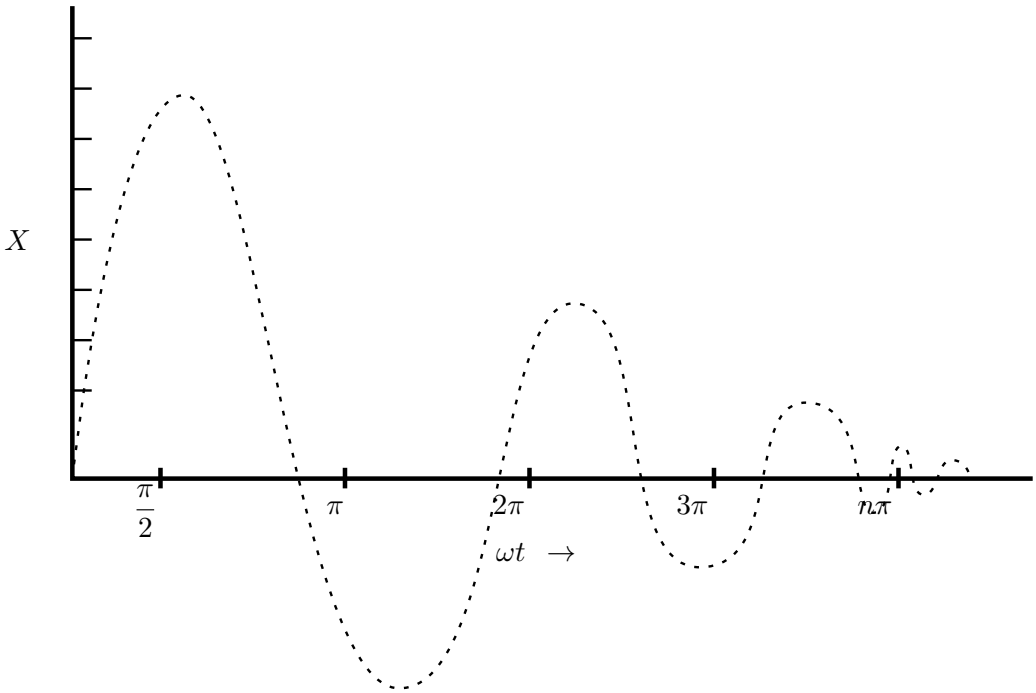

Figure 1.9: Time response of a single DOF

constant pull resisting the motion.

Due to their multiple degrees of freedom FPSEs are more complicated than the standard internal combustion engines. They are constituted by three masses although, in many cases, the piston or cylinder is fixed to the ground, so the three DOF reduces to two. Also, various springs and dashpots connect the moving devices.

In Figure 1.10, the diagram shows two masses: For the piston P and for the displacer D, three dashpots and two springs of stiffness K_D and K_P, two sinusoidal external forces F_D and F_P of the same frequency and in phase but with different amplitudes which are applied to D and P respectively. The magnitude of oscillation of the two masses are shown in Figure 1.11.

Phasor representation

Reciprocating harmonic movement can be easily represented by the projection of the endpoint of a rotating vector. For example, in Figure 1.12, $X \sin \omega t$ is denoted as a phasor of magnitude x and angular velocity ω. Then for FPSE motion, displacement, velocity and acceleration are determined using Eq. 1.4.1:

$$\begin{aligned} x &= X \cos \omega t \\ \dot{x} &= -\omega X \sin \omega t = \omega X \cos \left(\omega t + \frac{\pi}{2} \right) \\ \ddot{x} &= -\omega^2 X \cos \omega t = \omega^2 X \cos(\omega t + \pi) \end{aligned} \tag{1.4.1}$$

Its phasor diagram is shown in Figure 1.13. Forces applied to the mass, can also be projected in the phasor diagram.

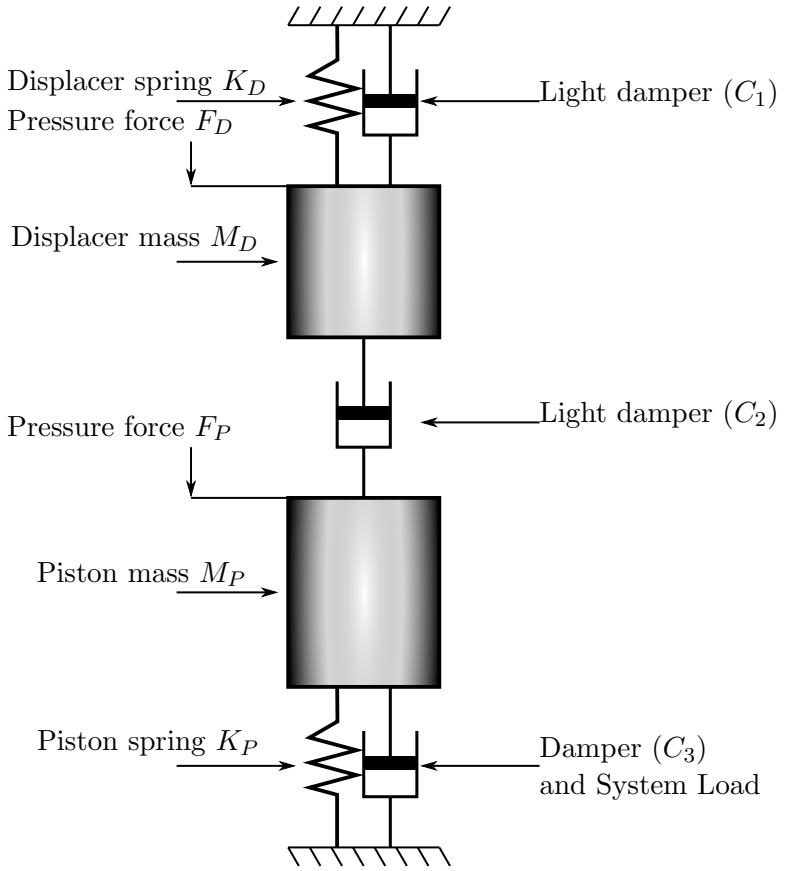

Figure 1.10: System with two DOF

The spring force is always resisting the displacement of the displacer, so its representation is collinear of x but in the opposite direction; then the damping force has the opposite direction of the mass velocity and the only magnitude which points to the same direction of the displacement is the acceleration force. Finally the excitation force is α degrees ahead from the acceleration force (Figure 1.14).

All the horizontal projections, of these phasors correspond to the equation of motion.

$$M\ddot{x} + C\dot{x} + Kx = F\cos(\omega t + \alpha) \tag{1.4.2}$$

From mechanical vibration books [21][23][24], the work done per cycle by harmonic excitation force to sustain a harmonic vibration is:

$$W = \pi\, F\, X \sin\alpha \tag{1.4.3}$$

The work input is necessary to overcome the total frictional losses.

The power produced by the engine is the work done per cycle times the frequency:

$$\begin{aligned} P &= W f \\ &= \frac{\omega}{2}\, F\, X\, \sin\alpha \end{aligned} \tag{1.4.4}$$

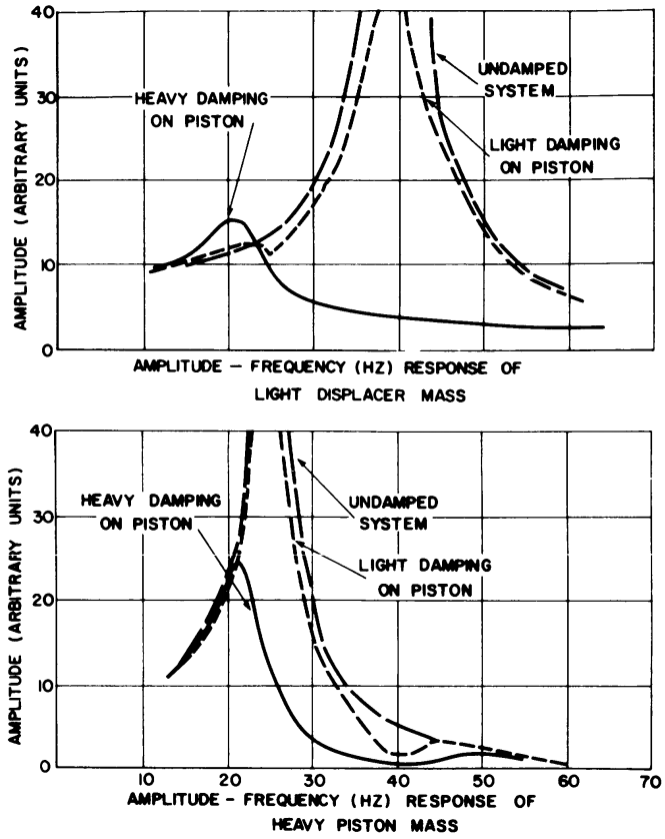

Figure 1.11: Amplitude oscillation as a function of exitation frequency for the two masses P and D [1]

In conclusion, it is crucial to know that the excitation force F is made up of two components, the perpendicular part of the displacement overcomes the damping resistance, and the horizontal portion corresponds to a spring force and does negligible work and consumes no power, se Figure 1.14 [1].

Based on the vibrating principles, the necessary condition of operation is the dynamic equilibrium of forces. The main forces acting inside the cylinder are the damping, spring and working pressure forces. The damping forces include the aerodynamic drag force as well as the resistance to motion by loading devices like alternators (magnetic fields) or the movement of other fluid for the pumping arrangement. The spring forces are produced by gas springs or mechanical springs, which are going to support the reciprocating devices. Then, the pressure force is the result of the cyclic variation of the working fluid pressure during expansion and compression process, due to the motion of the piston. This complicated situation where the oscillation is maintained because of its response is described as a "limit cycle."

In Figure 1.15a, the piston displacer X_P represents the horizontal axis reference. The displacer phasor X_D leads the piston by angle ϕ. It is important to mention that O is the mid-stroke position for both the piston and displacer. Then the phasor V_e is in line but 180° out of phase with the displacer phasor X_D. The other important variable is the compression volume which depends on

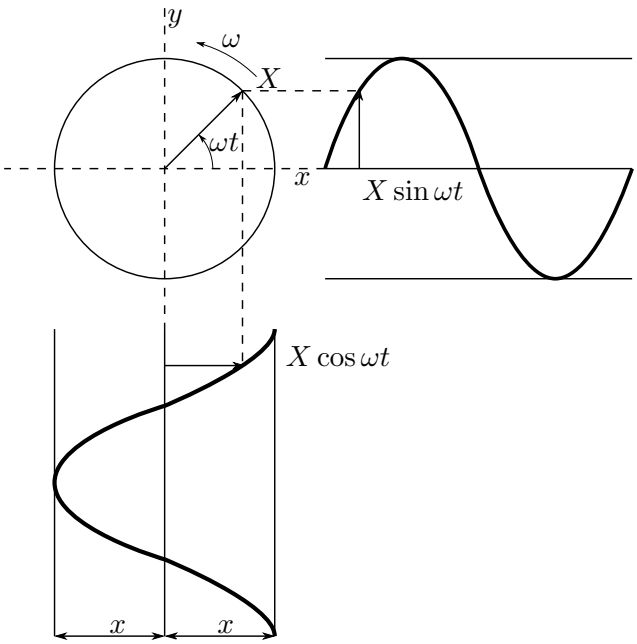

Figure 1.12: Vector representation of simple harmonic motion

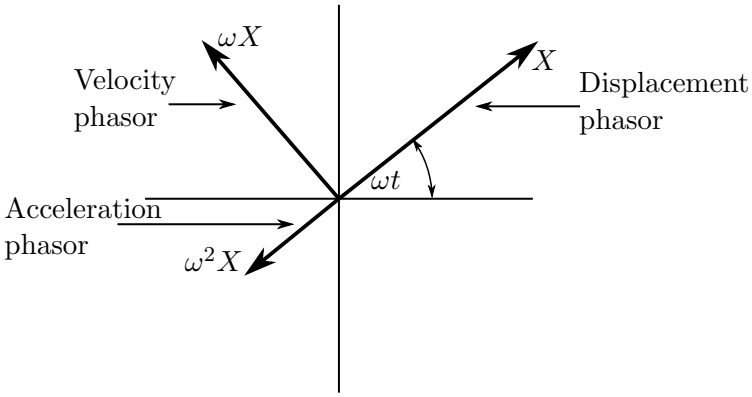

Figure 1.13: Phasor representation of displacement, velocity and acceleration

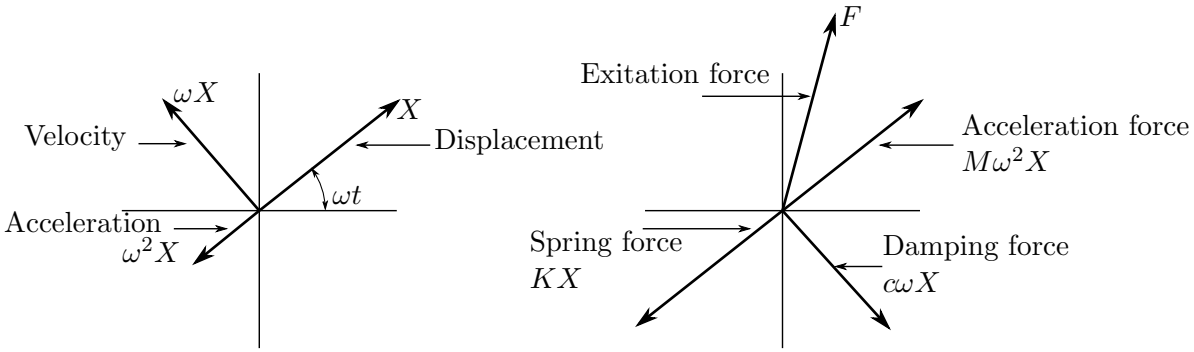

Figure 1.14: Phasor representation of forces

the displacer and the piston motion. When the displacer moves from the mid-stroke position to the top dead center (TDC) (Figure 1.2) the compression space increases but a similar motion of the piston will decrease the same volume. Then one can say that the difference in the displacements is going to determine the

compression volume. The phasor subtraction of X_P from X_D gives the resultant vector V_c.

Now, to understand better the relationship among pressure and displacement, holding the piston stationary and moving the displacer a short distance to the TDC the fluid tends to travel from the expansion space through the regenerator to the cold part, resulting in a small decrease in the pressure. This can be represented by P_D, acting in the reverse direction of X_D. Since the volume above and below the displacer varies due to the rod volume, if more displacer rod enters the compression space then above the piston the pressure tends to increase. It can be represented by P_R; however, the effect is so small that frequently it is ignored.

In the same manner, if the motion of the piston tends to move to the TDC with the displacer fixed, the pressure increases, this vector can be represented as P_P and acts in the same direction as the piston. Adding P_P and P_D results in the phasor P which trails the piston displacement by β. It is also important to remark that an increase in pressure results in a greater force acting on the piston and displacer.

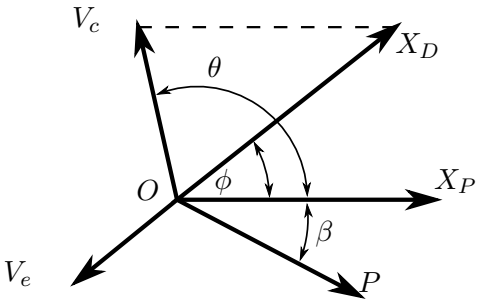

(a) Displacement and volume phasors

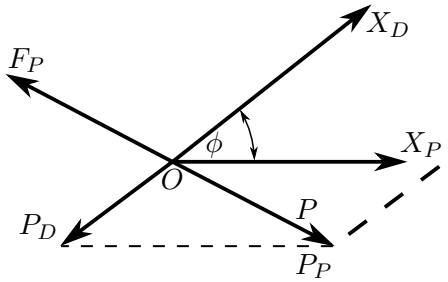

(b) Pressure phasor

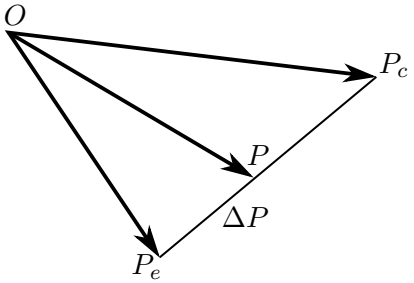

(c) Variation in pressure

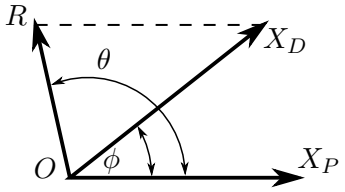

(d) Relative motion of piston and displacer

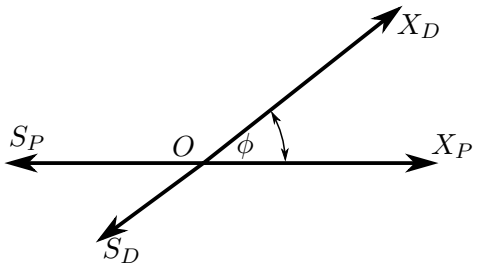

(e) Spring phasor

Figure 1.15: Phasor representation of a FPSE

In practical engines, a pressure drop will occur in the regenerator, heater, and cooler (dead volume). This will produce a phase lag among the pressure changes and the compression and expansion spaces. Other forces like C_2 represent the sealing generated by the fluid between the displacer rod and the piston. Therefore, it can be obtained by the difference of the vector X_P and X_D which is described by the vector R at angle θ. The rest of the forces acting on the piston and displacer are the spring forces S_P and S_D which are collinear to X_P and X_D respectively but pointing at the opposite direction. See Figure 1.15.

For the piston force polygon, See Figure 1.16a:

- **a-b**: F(S) is the spring force acting on the piston, opposed to the piston displacement.
- **b-c**: F(C_3) is the damping force caused by the damping device C_3. It absorbs the work output of the piston and acts opposite to the pistons velocity.
- **c-d**: It acts perpendicular to the OR phasor.
- **d-e**: F(I) is the inertial force of the piston which has the same direction of its displacement due to its lead (180°) from the acceleration phasor.
- **e-a**: F(P) is the excitation force generated by the pressure and acts along the line, but in the opposite direction of the phasor P, *if the polygon does not close it means the engine cannot operate at those conditions*[1].

- **On the piston:**

$$\begin{aligned} \mathrm{F(S)} &= K\, x_P \\ \mathrm{F}(C_3) &= C_3 \dot{x}_P = \omega X_P \\ \mathrm{F}(C_2) &= C_2 \dot{x}_R = C_2 \omega R \\ \mathrm{F(I)} &= M_P\, \ddot{x_P} = M_P \omega^2 X_P \\ \mathrm{F(P)} &= (A_c - A_R) P \end{aligned}$$

- **On the displacer:**

$$\begin{aligned} \mathrm{F(S)} &= K\, X_D \cos(\psi - \phi) \\ \mathrm{F}(C_1) &= C_1 \dot{x}_D = C_1 \omega X_D \\ \mathrm{F}(C_2) &= C_2 \dot{x}_R = C_2 \omega R \\ \mathrm{F(I)} &= M_D\, \ddot{x_D} = M_D \omega^2 X_D \\ \mathrm{F(P)} &= A_R P \end{aligned}$$

1.5 Practical considerations

FPSE appear to be simple due to the small number of moving parts. However, their proper design and operation require a high level of experience. The following has to be considered:

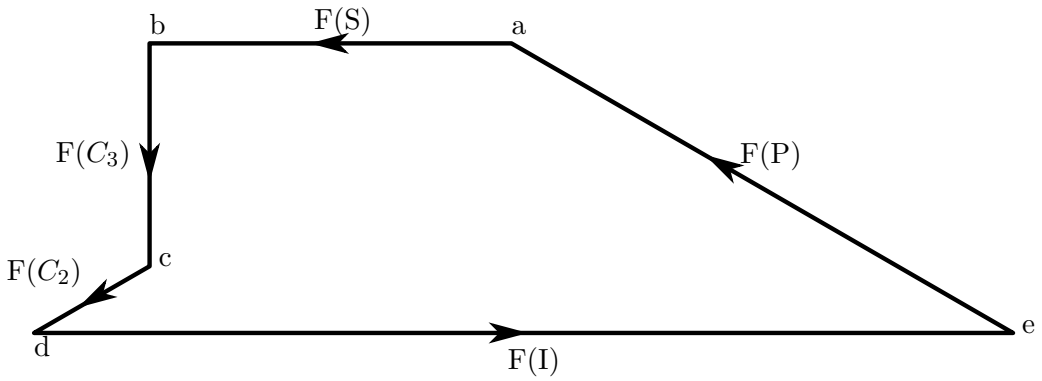

(a) Piston forces

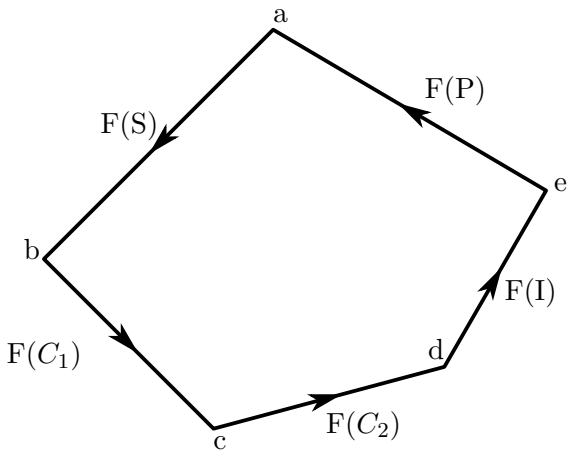

(b) Displacer forces

Figure 1.16: Phasor forces polygons

- **Piston centering:** There are some leakages from the working space to the bounce space; this is an inevitable situation due to the slightest imperfections in the seal or on the machined surface (e.g., taper or varying eccentricity will increase the flow). Two methods developed by Sunpower Inc. involve the control of the leak among the spaces (Figure 1.17) [3].

  In Figure 1.18b can be seen a more complicated method which is the active method for centering pistons. It uses a microprocessor to control a valve which connects the pressurized spaces. Although it means a more reliable way it is only suitable for bigger engines due to its cost-output power relation.

- **Seals:** The permanent problem in Stirling engines is the seal. However, in FPSE things are more manageable due to the lack of kinetic linkages. For the kinetic mechanisms, the presence of lube is essential. Therefore the working gas eventually will get contaminated, and this will block the porous construction of the regenerator. Also, a preferable material for low clearance seals is the hard anodized aluminum due to its low mass and sturdy surface.

  Another advantage of FPSE is the absence of side forces, generated by mechanical transmissions which demand the use of new supports. Widely spread in the Stirling field, the use of gas bearings are preferable because

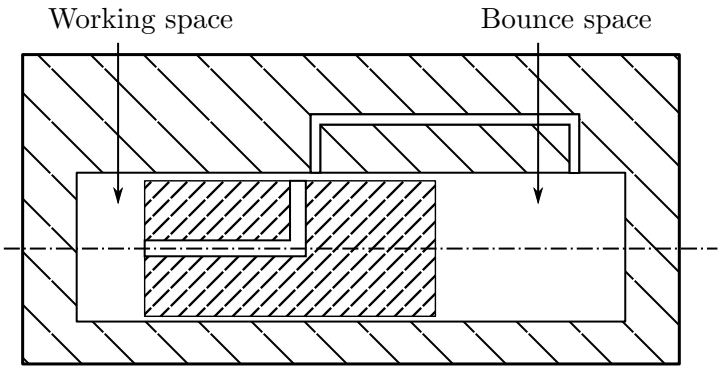

(a) Centering solution manifold

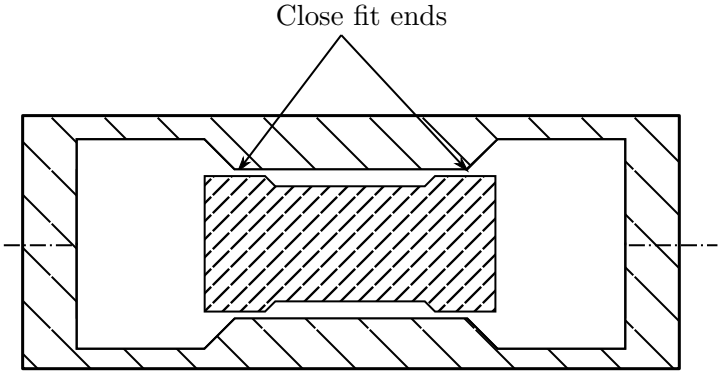

(b) Centering solution flat

Figure 1.17: Piston centering by controlled leaks

of their high precision tolerances plus low friction seals. Grinnel has shown that the amount of leakage of gas in close tolerances seals [25].

$$\dot{m} \propto \frac{h^3}{L}\left(P_1^2 - P_2^2\right) \tag{1.5.1}$$

Where,
$\dot{m}$ = mass rateof leakage,
h = clearance,
L = length of seal,
P_1 and P_2 are the fluid pressures across the seal.

From Eq.1.5.1 is deduced that the clearance h is a critical dimension of a close tolerance seal.

- **Bearings:** The lack of transversal forces acting upon the piston shell supports the use of gas bearings to escape the contamination problem because of oil present in standard bearings.

There are two types of gas bearings:

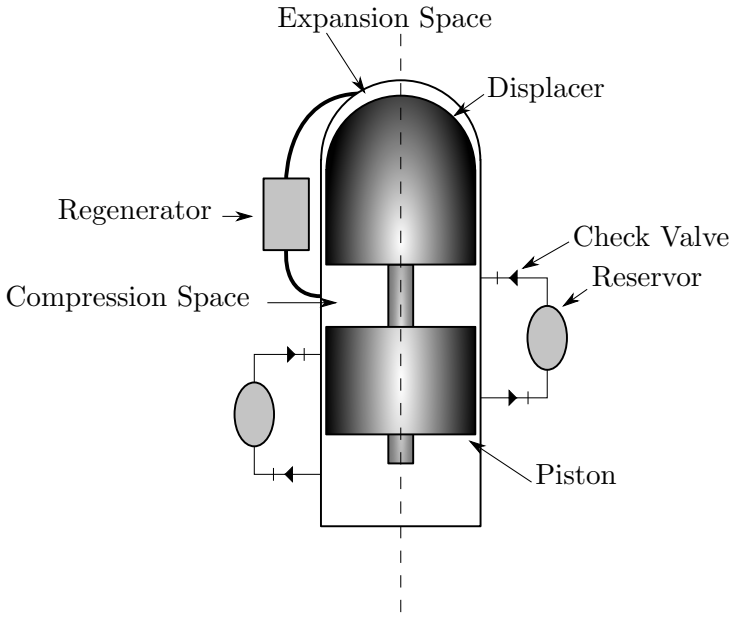

(a) The store and dump technique

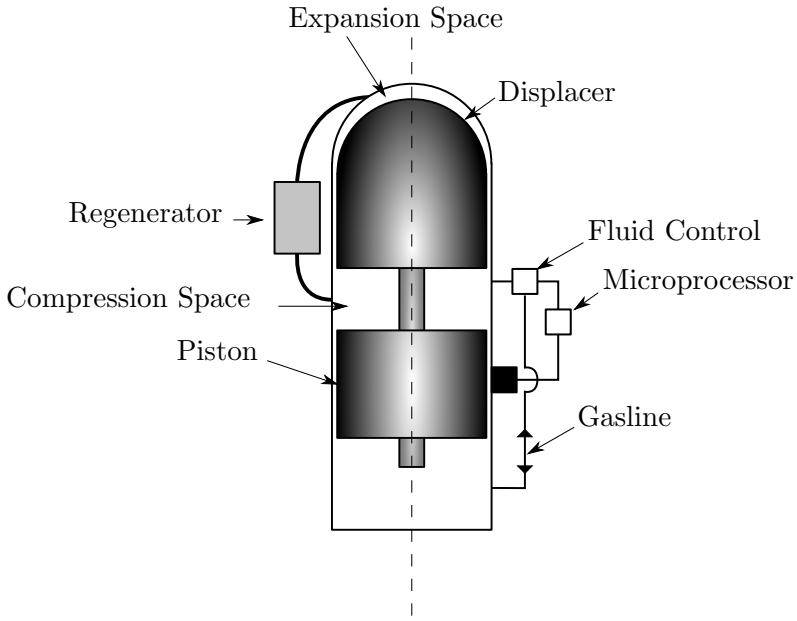

(b) Active method

Figure 1.18: Piston centering, other methods

– Hydrostatic: Externally pressurized and requires an external source of pressure plus adequate drains. Hydrostatic bearings are capable of more significant loads. The shaft is supported in a bearing journal by a supply of gaseous lubricant. Compared with liquids, gases are highly mobile due to their low viscosity, and low density. These bearing lead to a very rigid shaft with virtually zero radial movement. See Figure 1.19a.

– Hydrodynamic: They are self-acting which eliminate the need for external facilities. Its most notable disadvantage lands in the contact

between the two surfaces at the beginning of the motion. To establish the hydrodynamic lubricant film, the moving parts will touch each other until a required velocity is achieved. Because of the reciprocating motion and the zero speed at the top and end of the strokes, there will always be physical contact. A solution is to cause a rotation of the piston during the whole stroke. See Figure 1.19b.

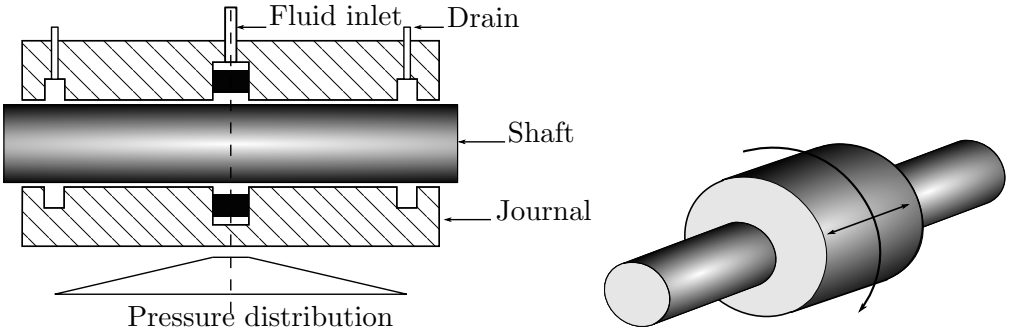

(a) Hydrostatic gas bearing (b) The rotary stroker

Figure 1.19: Types of gas bearings

- **Materials**: As in other fields of engineering, the material selection results in a crucial task. Especially with Stirling engines, the hot part stands under the spotlight; not only the materials surrounding the hot part have to withstand but also the constant stresses generated by the change in temperatures cycle by cycle. Stainless steels are conventionally used for the heater ends. For example:

  - Type 316 has the best creep properties of stainless steel, 10000 hours, 650 °C rupture strength of 304 SS.
  - Iron-based type N-155 has about twice the rupture strength of Type 316 SS.
  - Nickel-based alloy Udimet 700 has a rupture strength about four times that of 316 SS

  Away from the hot zones of the engine, aluminum is widely used due to its low density, ease of fabrication, availability of processes to provide a hard surface finish and high thermal conductivity.

- **Springs:** The restoring forces are a product of the springs. To maintain a cyclic operation of the engine suited springs must be selected. There are two main types of springs:

  - Mechanical springs: These have the main advantage of low losses but are subject to mechanical failures due to fatigue as well as uneven force distribution.
  - Gas springs: These kinds of springs have no side loading and are not subject to fatigue. However, the hysteresis loss in gas springs can be appreciable as well as some leakages.

The most important characteristic of the springs is the stiffness which is directly related to the operating frequency. For gas springs this constant is described in Eq.1.5.2.

$$K = \frac{\gamma p A^2}{V} \tag{1.5.2}$$

Where,
K = spring constant,
γ = ratio of specific heats of the spring gas,
p = mean pressure of the gas spring,
A = gas spring piston area,
V = mean volume of the gas spring.

Chapter 2

Free piston Stirling engines design tools

The mathematical representation of the reciprocating fluid inside the machine results in a very challenging problem. Due to the movement of the two pistons, the process within a Stirling engine is complicated. For a kinematic type engine, the variation inside the volumes (compression and expansion) is known, the mechanical linkages determine how the motion of the displacer moves concerning the power piston.

The analysis of a FPSE is more complicated due to the fact that there are no mechanical connections; therefore the ratio of motion between the moving parts is not determined. However, the movement is going to be defined by the dynamics of the system. The designer should have in mind that the dynamics is directly connected to the fluid response.

"A poorly designed crank engine (kinetic type) will usually have less than expected performance, whereas a poorly designed FP engine will likely not run at all." (Wood 1982)

2.1 Preliminary calculations, "Zero order analysis"

One of the essential characteristics of an engine is its power capacity. For a FPSE, it is often necessary to rawly compute, under specific operation parameters, its power as well as efficiency. The starting point is the ideal Stirling cycle [1].

$$W = \oint p\, dV = mR(T_E - T_C)\ln(V_2/V_1) \tag{2.1.1}$$

With a specific frequency (f), one can predict the engine's power.

$$P = fW \tag{2.1.2}$$

Of course, Eq.2.1.1 is only valid for the ideal cycle, and it is well known that practical machines are far from the perfect models. Some of the real aspects that make the first approximation not a right approach are non-isothermal processes, continuous piston motion, dead space, etc. Martini [19] proposed to departure

from the ideal model and then multiplied its power by a fraction by an "experience factor".

Rarely the designer knows at first glance the amount of fluid mass inside of the engine or the maximum values of the volumes. However, it is better to reform Eq.2.1.1 in terms of characteristic parameters. William Beale evaluates the following dimensionless quantity [1].

$$B_n = \frac{P}{fV_oP_m}$$

where,
$P =$ engine net or brake power,
$f =$ frequency,
$P_m =$ mean cycle pressure,
$V_o =$ total volume variation (swept volumes).

For well-designed machines, B_n was always about 0.15 in the international system (SI).

$$P = 0.15fV_oP_m \tag{2.1.3}$$

The above was calculated for engines operating among 65°C for the chiller and 650°C for the heater.

West [26] discovered a similar formula but taking the temperature effect. The factor proposed (W_n) is 0.35 (SI).

$$P = W_nfV_oP_m\frac{T_e - T_c}{T_e + T_c} \tag{2.1.4}$$

With these basic calculations, there is nothing but accept the results as a first guide since the gas behavior is not included as well as some other physic phenomena (e.g., the motion of the pistons, hysteresis, and imperfect regeneration).

Another design parameter directly related to the output work is the frequency (f). For the first calculation, the rate of oscillation might be equal to the natural frequency of the system, Beale recommended reducing the frequency by 20%. Although the studies are focused on steady-state behavior, the frequency usually varies due to the variation in volume caused by loads and mean pressure.

$$f = f_n = \frac{1}{2\pi}\sqrt{\frac{K}{M}} \tag{2.1.5}$$

where,
$M =$ total mass of the piston,
$K =$ net spring constant.

It is important to highlight that K is the sum of the constants of all the springs acting upon the mass which includes "the spring effect" of the working space K_g (gas spring):

$$K_g = \frac{\gamma P_m A^2}{V_m} \tag{2.1.6}$$

Where,
γ = ratio of specific heats of the spring gas,
P_m = mean pressure of the gas spring,
A = gas spring piston area,
V_m = mean volume of the gas spring.

If the piston is arranged with a large mechanical spring, then the effect of K_g is less crucial and in some circumstances negligible.

The charge pressure can also modify the frequency by the ratio:

$$f \propto \sqrt{P_m} \tag{2.1.7}$$

However, this variation will also change the amplitude of the piston strokes.
Lastly, the engine efficiency of the ideal Stirling cycle is identical to:

$$\bar{\eta} = 1 - \frac{T_c}{T_e} \tag{2.1.8}$$

The similarity among this efficiency and the Carnot's efficiency lays in the same amount of heat absorbed by the gas during one constant volume process, and the heat rejected during another constant volume process. Although this is not possible in practice, really efficient regenerator can be manufactured. However, Eq. 2.1.8 remains a positive approach.

In practical engines, the designer is more focused on brake efficiency which relates the useful power output (e.g., at the shaft or the piston rod) and the heat absorbed by the machine. It is more convenient to measure the heat added to the cooling water at the chiller, which is the sum of heat absorbed by the water. Again this efficiency should be multiplied by an "experience factor" which oscillates around 28% and 69% of $\bar{\eta}$; thus half the Carnot efficiency should be expected for a well designed Stirling engine [1].

2.2 Schmidt Analysis

It gets its name after Gustav Schmidt of the German Polytechnic Institute of Prague who published this analysis in 1871.

The analysis is based on mainly five assumptions:

1. the working fluid obeys the ideal gas law,
2. the mass inside the engine is constant,
3. the instantaneous pressure is consistent within the working space,
4. there are isothermal regions throughout the engine,
5. the piston and displacer motions behave sinusoidally [27].

For real engines assumption 3 is not valid, the friction generated by the translation of the gas may cause pressure drops, these drops are more present in high-speed engines than in low-speed machines.

However, the most crucial assumption is the fourth one, best known as isothermal analysis, which pretends that while the fluid passes through the heat exchangers, it will automatically change its temperature. The last behavior is not achievable unless an infinite heat transfer capability of the gas. In practical engines, the isothermal compression and expansion are more similar to an adiabatic process [19].With the first four assumptions, the pressure within the cylinder is fully described:

$$m = m_c + m_k + m_r + m_h + m_e$$

$$M = \frac{PV}{RT}$$

$$m = \frac{P}{R}\left(\frac{V_c}{T_c} + \frac{V_k}{T_c} + \frac{V_r}{T_r} + \frac{V_h}{T_e} + \frac{V_e}{T_e}\right)$$

where,
V_c: Compression volume,
V_k: Cooler volume,
V_r: Regenerator volume,
V_h: Heater volume,
V_e: Expansion volume,
T_c: Compression temperature,
T_k: Cooler temperature,
T_r: Regenerator temperature,
T_h: Heater temperature,
T_e: Expansion temperature,
P: Pressure,
R: Gas constant,
m: Total mass inside the engine.

The mean effective temperature inside the regenerator should be calculated from the maximum temperature (T_e) and the minimum temperature (T_c). It is assumed that the distribution is linear thus the function is:

$$T(x) = \frac{T_e - T_c}{L_r}x + T_c$$

where L_r is the regenerator length.

Also, the total mass of the gas m_r in the regenerator void space V_r is given by:

$$m_r = \int_0^{V_r} \rho dV_r$$

where $\rho =$ is the density,

$$m_r = \frac{V_r P}{R}\int_0^{L_r} \frac{1}{(T_e - T_c)x + T_c L_r}dx$$

$$m_r = \frac{V_r P}{R}\frac{\ln(T_e/T_c)}{T_e - T_c} \tag{2.2.1}$$

Then the mean effective temperature T_r of the gas in terms of ideal gas equation of state:

$$m_r = \frac{V_r P}{R T_r} \tag{2.2.2}$$

Substituting Eq. 2.2.2 into Eq. 2.2.1

$$T_r = \frac{T_e - T_c}{\ln\left(\frac{T_e}{T_c}\right)} \tag{2.2.3}$$

$$P = \frac{mR}{\frac{V_c}{T_c} + \frac{V_k}{T_c} + \frac{V_r}{T_r} + \frac{V_h}{T_e} + \frac{V_e}{T_e}}$$

$$P = \frac{mR}{\frac{V_c}{T_c} + \frac{V_k}{T_c} + \frac{V_r \ln\left(T_e/T_c\right)}{T_e - T_c} + \frac{V_h}{T_e} + \frac{V_e}{T_e}} \tag{2.2.4}$$

Eq. 2.2.4 shows that parameters that change are the compression (V_c) and expansion (V_e) volumes. From assumption 5, the volumes are periodic functions; thus the work done per cycle is shown in Eq. 2.2.5 and the integration is carried out over the common period of the volumes.

$$W = mR \oint \frac{d(V_e + V_c)}{\frac{V_c}{T_c} + \frac{V_k}{T_c} + \frac{V_D \ln\left(T_e/T_c\right)}{T_e - T_c} + \frac{V_h}{T_e} + \frac{V_e}{T_e}} \tag{2.2.5}$$

With assumption 5, it is possible to integrate Eq. 2.2.5 and so obtain a closed-form expression for the work (W). Now the problem is to find the optimum values of phase angle, swept volume ratios to maximize the desirable power.

Part of the engine analysis must be focused on the point of view of energy flow. Due to the isothermal simplification, the boundary conditions are T_e, and T_c, the heater, regenerator, and cooler are connected in series as Fig. 2.1 shows. The point of start is the working gas energy equation.

A general cell is shown in Fig.2.2, it represents each of the spaces of the machine (either working space or a heat exchanger). By means of mass flow m_i' and temperature T_i, enthalpy is transported. In the same manner, out of the cell the flow of mass m_o' and temperature T_o.

$$\begin{array}{c}\textit{rate of heat}\\ \textit{transfer}\\ \textit{into the cell}\end{array} + \begin{array}{c}\textit{net enthalpy}\\ \textit{convected}\\ \textit{into the cell}\end{array} = \begin{array}{c}\textit{rate of}\\ \textit{work done}\\ \textit{on the}\\ \textit{surroundings}\end{array} + \begin{array}{c}\textit{rate of increase}\\ \textit{of internal}\\ \textit{energy}\\ \textit{in the cell}\end{array} \tag{2.2.6}$$

For an ideal gas, the specific enthalpy $h = c_p T$ and the specific internal energy $u = c_v\, T$, where c_v and c_p are the specific heat capacity at constant volume and pressure respectively. Substituting in Eq. 2.2.6:

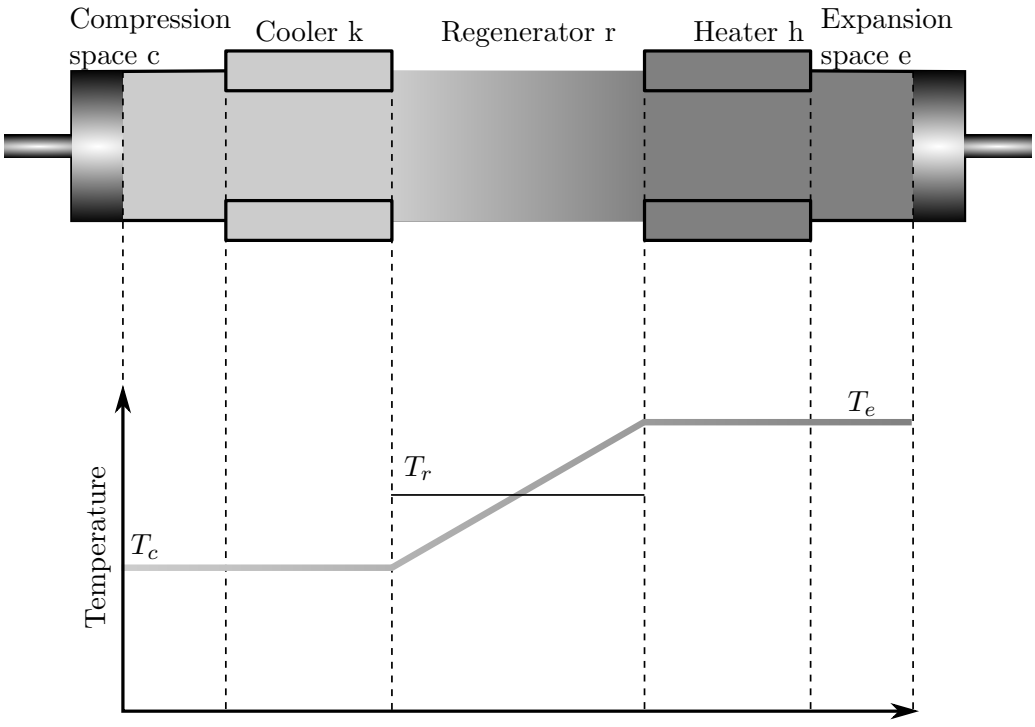

Figure 2.1: Isothermal model

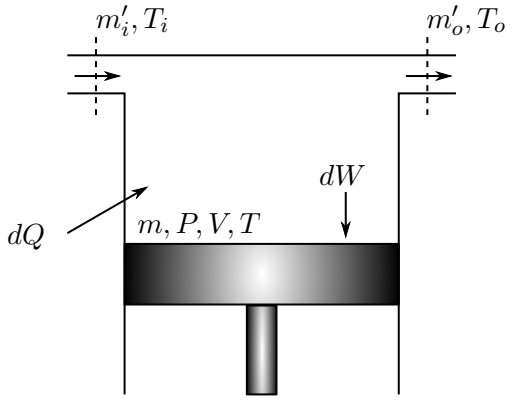

Figure 2.2: Generalized cell

$$dQ + (c_p\, T_i\, m'_i - c_p\, T_o\, m'_o) = dW + c_v\, d(m\, T) \tag{2.2.7}$$

Eq. 2.2.7 represents the energy equation for non-steady flow in which kinetic and potential energy are neglected. For heat exchanger, the input temperature (T_i) and the output temperature (T_o) are the same $T_i = T_o = T$, also the rate in the mass flow $(m'_i - m'_o) = dm$. Then for heat exchangers Eq. 2.2.7 simplifies to:

$$\begin{aligned} dQ + c_p\, T\, dm &= dW + c_v\, T\, dm \\ dQ &= dW - R\, T\, dm \end{aligned} \tag{2.2.8}$$

For ideal gases $R = c_p - c_v$.

For the working spaces the cyclic integration of Q implies that the cyclic change in mass of the working gas (m) is zero, thus:

$$Q_c = W_c$$
$$Q_e = W_e$$

For heat exchanger where there is no work done:

$$Q_k = 0$$
$$Q_h = 0$$

For ideal regenerator, the heat exchange between the regenerator and the working fluid is internal (there is no external heat transferred), thus $Q_r = 0$

$$\eta = \frac{W}{Q_e} \tag{2.2.9}$$

where $Q_e = W_e = \oint P \frac{dV_e}{d\theta} d\theta$ and $W = W_e + W_c$

Beta type (One cylinder)

Beta type machines differ from the alpha type due to the compression space which depends on the displacer and piston motion. Eq. 2.2.10 describes both volumes.

$$\begin{aligned} V_c &= V_{clc} + V_{swc}(1 + \cos(\theta + \delta))/2 \\ V_e &= V_{cle} + V_{swe}(1 + \cos(\theta + \delta + \alpha))/2 \end{aligned} \tag{2.2.10}$$

where,

$$\alpha = \pi + \phi - \delta$$

θ: Independent variable,
V_{cle}: Clearance expansion volume,
V_{clc}: Clearance compression volume,
ϕ: Phase advance of the displacer with respect to the piston,
δ: Phase advance of the compression space volume with respect to the piston,
α: Phase advance of the expansion space volume with respect to the compression space volume,
V_{swe}: Sweep expansion volume,
V_{swc}: Sweep compression volume.

The variation of the compression and expansion volumes with respect to the cycle will be used to compute the work done and thus the power.

$$\frac{dV_c}{d\theta} = -\frac{V_{swc}}{2}\sin(\theta + \delta)$$
$$\frac{dV_e}{d\theta} = -\frac{V_{swe}}{2}\sin(\theta + \delta + \alpha)$$

Substituting Eq. 2.2.10 at Eq. 2.2.4 results in Eq.2.2.11

$$P = \frac{mR}{S + \frac{V_{swc}}{2T_c}\cos(\theta + \delta) + \frac{V_{swe}}{2T_e}\cos(\theta + \delta + \alpha)} \tag{2.2.11}$$

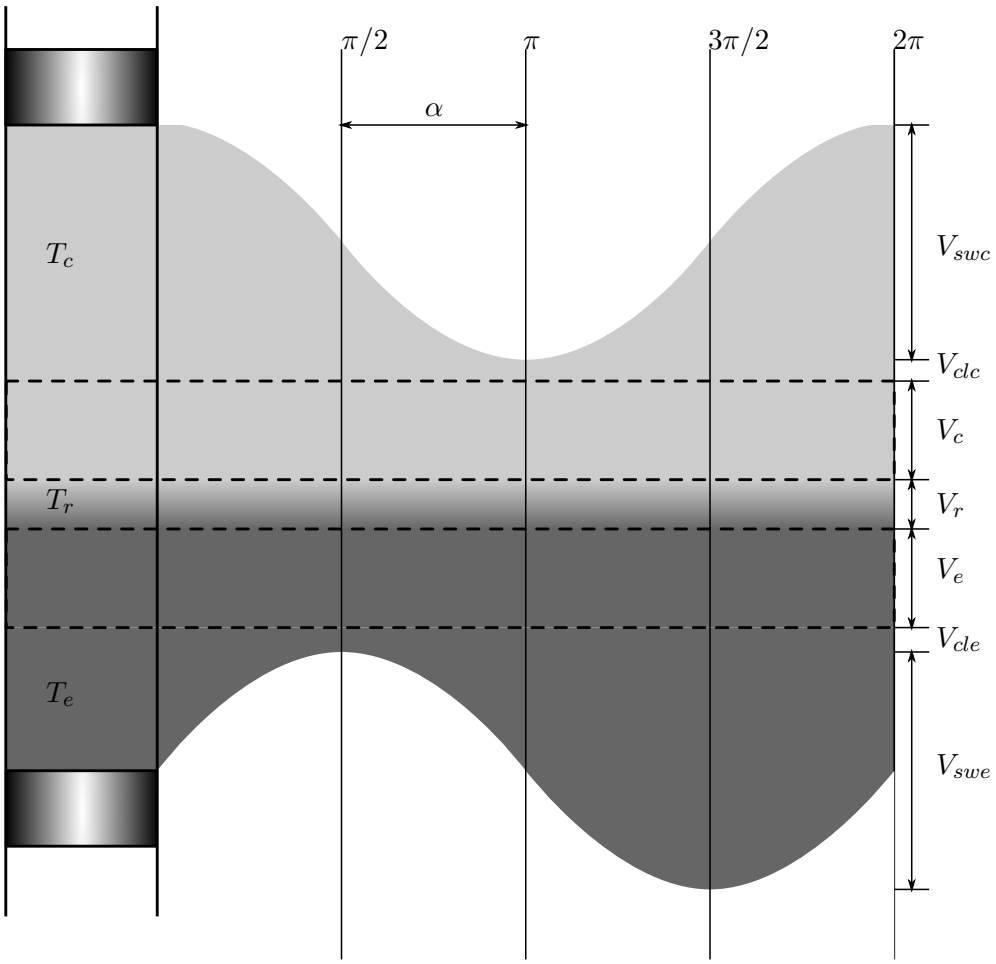

Figure 2.3: Volume variation

where,

$$S = \frac{V_{clc}}{T_c} + \frac{V_{swc}}{2T_c} + \frac{V_k}{T_c} + \frac{V_{cle}}{T_e} + \frac{V_{swe}}{2T_e} + \frac{V_h}{T_e} + \frac{V_r \ln(T_E/T_c)}{T_e - T_c}$$

The next trigonometric identity is utilized for the analysis.

$$\cos(a+b) = \cos a \cos b - \sin a \sin b$$

$$\begin{aligned} \frac{V_{swc}}{2T_c}\cos(\theta+\delta) &= \frac{V_{swc}}{2T_c}(\cos\theta\cos\delta - \sin\theta\sin\delta) \\ \frac{V_{swe}}{2T_e}\cos(\theta+\delta+\alpha) &= \frac{V_{swe}}{2T_e}(\cos\theta\cos\psi - \sin\theta\sin\psi) \\ \psi &= \delta + \alpha \end{aligned} \tag{2.2.12}$$

Rearranging the denominator of 2.2.11 with Eq. 2.2.12

$$P = \frac{mR}{S + \left(\frac{V_{swc}}{2T_c}\cos\delta + \frac{V_{swe}}{2T_e}\cos\psi\right)\cos\theta - \left(\frac{V_{swc}}{2T_c}\sin\delta + \frac{V_{swe}}{2T_e}\sin\psi\right)\sin\theta} \tag{2.2.13}$$

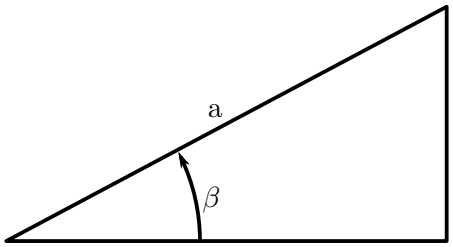

$$\mathrm{a}\sin\beta = \left(\frac{V_{swc}}{2T_c}\sin\delta + \frac{V_{swe}}{2T_e}\sin\psi\right)$$

$$\mathrm{a}\cos\beta = \left(\frac{V_{swc}}{2T_c}\cos\delta + \frac{V_{swe}}{2T_e}\cos\psi\right)$$

Figure 2.4: Triangle representation

From Fig. 2.4

$$\tan\beta = \frac{\frac{V_{swc}}{2T_c}\sin\delta + \frac{V_{swe}}{2T_e}\sin\psi}{\frac{V_{swc}}{2T_c}\cos\delta + \frac{V_{swe}}{2T_e}\cos\psi} \tag{2.2.14}$$

$$a = \sqrt{\left(\frac{V_{swc}}{2T_c}\sin\delta + \frac{V_{swe}}{2T_e}\sin\psi\right)^2 + \left(\frac{V_{swc}}{2T_c}\cos\delta + \frac{V_{swe}}{2T_e}\cos\psi\right)^2} \tag{2.2.15}$$

Substituting in the pressure equation 2.2.13 the Eq. 2.2.14 and 2.2.15.

$$P = \frac{mR}{S + a\cos(\beta + \theta)} \tag{2.2.16}$$

The maximum and minimum values of the pressure are calculated when the maximum and minimum values of the cosine are presented.

$$P_{max} = \frac{mR}{S - a}$$
$$P_{min} = \frac{mR}{S + a}$$

Then, the work of the engine can be calculated from Eq. 2.2.17 and 2.2.18.

$$\begin{aligned} Q_e = W_e &= \oint_0^{2\pi} \left(P\frac{dV_e}{d\theta}\right) d\theta \\ Q_c = W_c &= \oint_0^{2\pi} \left(P\frac{dV_c}{d\theta}\right) d\theta \end{aligned} \tag{2.2.17}$$

$$\begin{aligned} Q_e = W_e &= -\frac{mRV_{swe}}{2}\oint_0^{2\pi} \frac{\sin(\theta + \delta + \alpha)}{S + a\cos(\theta + \beta)} d\theta \\ Q_c = W_c &= -\frac{mRV_{swc}}{2}\oint_0^{2\pi} \frac{\sin(\theta + \delta)}{S + a\cos(\theta + \beta)} d\theta \end{aligned} \tag{2.2.18}$$

From Eq. 2.2.19 the total work is calculated.

$$W = W_e + W_c \tag{2.2.19}$$

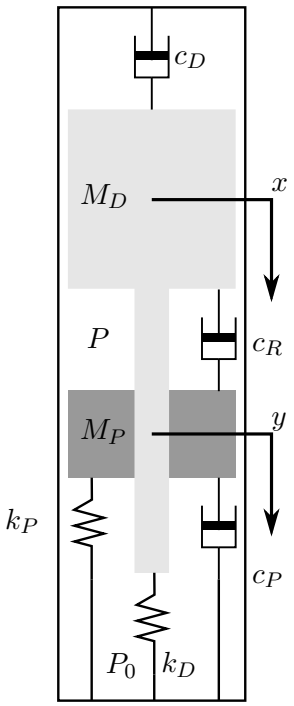

Figure 2.5: FPSE dynamic diagram

Dynamics of the Free-Piston Stirling engine

Due to the fact that a FPSE lacks mechanical connections, the study of this type of machines must have a pre-study before applying the first order analysis. The most significant difference of the FPSE and the kinetic engines is that the piston and displacer strokes are unspecified, as well as the phase angle. Not only the fact that the amplitudes are unknown is hard to lead but also the dependence of these parameters with loads adds more complexity to the study. Therefore, the study of the dynamics is fundamental and thus it is the first step. The equations below describe the behavior of the engine in Figure 2.5.

Equations of Motion

$$\frac{d}{dt}\frac{\partial L}{\partial \dot{q}_k} - \frac{\partial L}{\partial q_k} = Q_k \tag{2.2.20}$$

$$Q_k = \sum_{j=1}^{p} \vec{F}_j \cdot \frac{\partial \vec{r}_j}{\partial q_k}$$

where Q_k is are the generalized forces and k is the number of degrees of freedom, there are p forces acting upon the system, $\vec{F}$ are the external forces and$\vec{r}$ are displacements.

Kinetic energy

$$\tau_{Displacer} = \frac{1}{2} m_D \cdot \dot{\vec{r}}_1^2 \tag{2.2.21a}$$

$$\tau_{Piston} = \frac{1}{2} m_P \cdot \dot{\vec{r}}_2^2 \tag{2.2.21b}$$

$$\tau_{Total} = \frac{1}{2} (m_D \cdot \dot{\vec{r}}_1^2 + m_P \cdot \dot{\vec{r}}_2^2) \tag{2.2.21c}$$

Potential energy

$$\nu_{Displacer} = \frac{1}{2} (k_D \vec{r_1}^2 + k_R (\vec{r_2} - \vec{r_1})^2) \tag{2.2.22a}$$

$$\nu_{Piston} = \frac{1}{2} (-k_P \vec{r_2}^2 + k_R (\vec{r_2} - \vec{r_1})^2) \tag{2.2.22b}$$

$$\nu_{Total} = \frac{1}{2} (k_D \vec{r_1}^2 + k_R (\vec{r_2} - \vec{r_1})^2 + k_R (\vec{r_2} - \vec{r_1})^2 - k_P \vec{r_2}^2) \tag{2.2.22c}$$

Non-potential forces

$$Q_1 = \sum_{j=1}^{3} \vec{F_j} \cdot \frac{\partial \vec{r_j}}{\partial q_1}$$

Where $q_1 = \vec{x_d}$ and $\vec{r_1} = \vec{x}_d + l_d$

$$\vec{F_1} = - c_D \dot{\vec{r_1}} \cdot 1 \tag{2.2.23a}$$

$$\vec{F_2} = c_R (\dot{\vec{r_2}} - \dot{\vec{r_1}}) \cdot 1 \tag{2.2.23b}$$

$$\vec{F_3} = \Delta P \cdot A_c \tag{2.2.23c}$$

$$Q_2 = \sum_{j=1}^{3} \vec{F_j} \cdot \frac{\partial \vec{r_j}}{\partial q_2}$$

Where $q_2 = \vec{x}_p$ and $\vec{r_2} = \vec{x}_p + l_p$

$$\vec{F_1} = - c_P \dot{\vec{r_2}} \cdot 1 \tag{2.2.24a}$$

$$\vec{F_2} = c_R (\dot{\vec{r_2}} - \dot{\vec{r_1}}) \cdot 1 \tag{2.2.24b}$$

$$\vec{F_3} = \Delta P \cdot (A_c - A_r) \tag{2.2.24c}$$

$$L = \frac{1}{2} (k_D \vec{r_1}^2 + k_R (\vec{r_2} - \vec{r_1})^2 + k_R (\vec{r_2} - \vec{r_1})^2 - k_P \vec{r_2}^2) - \frac{1}{2} (m_D \cdot \dot{\vec{r}}_1^2 + m_P \cdot \dot{\vec{r}}_2^2) \tag{2.2.25}$$

$$\frac{d}{dt} \frac{\partial L}{\partial \dot{x}_d} = m_D \ddot{\vec{r_1}} \qquad \frac{\partial L}{\partial x_D} = -k_D \cdot \vec{r_1} + k_R \cdot \vec{r_2} - k_R \cdot \vec{r_1} \tag{2.2.26}$$

Substituting 2.2.23 and 2.2.26 at 2.2.20

$$m_D \ddot{\vec{r_1}} + k_D \vec{r_1} - k_R \vec{r_2} + k_R \vec{r_1} = -c_D \dot{\vec{r_1}} + c_R (\dot{\vec{r_2}} - \dot{\vec{r_1}}) + \Delta P \cdot A_c$$

In a similar way

$$m_P \ddot{\vec{r_2}} + k_P \vec{r_2} + k_R \vec{r_2} - k_R \vec{r_1} = -c_P \dot{\vec{r_2}} - c_R (\dot{\vec{r_2}} - \dot{\vec{r_1}}) + \Delta P \cdot (A_c - A_r)$$

$$\begin{aligned} m_D \ddot{x} + (c_D + c_R) \dot{x} + (k_D + k_R) x - c_R \dot{y} - k_R y &= \Delta P \cdot A_r \\ m_P \ddot{y} + (c_P + c_R) \dot{y} + (k_P + k_R) y - c_R \dot{x} - k_R x &= \Delta P \cdot (A_c - A_r) \end{aligned} \tag{2.2.27}$$

2.3 Stability of the Free-Piston Stirling engine

A stability analysis is presented as an essential step to study how different design parameters influence the behavior of the thermomechanical machine.

The section starts with the new dynamic model, which includes a new velocity dependent mechanical loss. The latter is included with the purpose of studying how the motion of the pistons influence each other. The mathematical tool used is the Laplace transform, due to its simplicity at the moment of implementation and most important for the study of the localization of the poles.

Other approaches like the matrix representation of the system, tends to find the complex frequencies of the engine. The purpose of this calculation is to find the eigenvalues of the matrix to dismiss their real part and transform them in pure imaginary eigenvalues.

The main obstacle to design functional Free Piston Stirling engines is to guarantee the stability of the oscillations, which is not a trivial task due to the decoupled pistons and the sensibility of some parameters.

In a new way, the dynamics of a more complete dynamic model is presented, this time taking into account the loss of momentum, acknowledging the dependence of motion among the displacer and the piston. Consequently, the analysis and calculation of a new model is required based on the methodology presented in [28].

The difference between a kinematic engine and a dynamic one lays on the lack of linkages between piston and displacer, because of the motion inside is not easily described nor completely understood. One path to follow in order to describe the motion is the integration either analytical or numerically of the linearized model. Their major disadvantage lies in the consumption of time and accuracy talking about the numerical approach. Therefore, there should be a way to find some intrinsic parameters that let us understand in a specific manner the behavior of the engine.

The study of stability in dynamic problems results in a powerful tool to describe a specific system without the need of solving its equations of motion. There are several techniques at our disposal, being the first approach the transformation of the differential equations into the frequency domain (making use of the Laplace transform). Many important rules are addressed in [22] on how to find the Laplace transform for specific mathematical forms.

A few articles proposed dynamic systems control strategies to tackle the stability problem, tools like the root locus let the engineer know some of the fundamental characteristics of the system (e.g., frequency, amplitude and the localization of the roots). The primary consideration in these papers is that the system is linear; therefore the amount of input is going to modify the output in a proportional scale. Works like [29] presents other tools like the Bode diagrams and the Nyquist Plot, along with the document the transformation of simple Laplace equation into block enhance the analysis in a more graphical interpretation letting the reader

understand clearly the input and output of the system for both degrees of freedom (displacer and piston motion).

More recent articles intend to find design parameters based on the study of the natural frequency of the system [30]. The authors propose a design method for selecting the physical parameters, as in the previews articles the engine is represented in its frequency equivalent (transfer function) and based on the Nyquist stability criterion is used to derived operation condition. Then their results are compared with the well known RE-1000 engine, tested by NASA. Formosa and Frechette also studied the scaling laws for FPSE design [13].

Aside from the frequency representation, alternative reports utilize more specific methods. Hopf instabilities are discussed in [31], where a mathematical method described with the goal of seeking periodic solutions, then the comparison of the analytical versus the numerical approach is executed.

The first analysis of the next part is based on previews studies about stability, such is the case of [32] and [18]. These documents propose simpler dynamic models for the sake of focus on the stability part.

Bégot et.al [33] use the analysis presented in [32] and add pressure losses, therefore a more complete calculation is exposed. Works like [34] propose an active control concerning the complicated motion of the pistons, which allows the adjustment of the pressure inside the chambers (buffer and compression space inside the gas springs). Some novel techniques of adjustments are discussed (e.g., genetic algorithms) all the work done by the controller is to maintain the phase angle between the displacer and piston.

Based on the analysis of [32], the more complete dynamic system described in Eq. 2.2.27 is now studied. The spring constant between the displacer and the piston is assumed negligible in comparison to the mechanical piston spring constant and the mechanical displacer spring constant.

$$\left(m_D s^2 + (c_D + c_R)s + k_D + A_r \frac{\partial P}{\partial x_D}\right) X_D = \left(c_R s - A_r \frac{\partial P}{\partial x_P}\right) X_P \tag{2.3.1a}$$

$$\left(m_P s^2 + (c_P + c_R)s + k_P + A_P \frac{\partial P}{\partial x_P}\right) X_P = \left(c_R s - A_P \frac{\partial P}{\partial x_D}\right) X_D \tag{2.3.1b}$$

For simplicity,

$$c_D + c_R = D_D \qquad k_D + A_r \frac{\partial P}{\partial x_D} = K_D$$

$$c_P + c_R = D_P \qquad k_P + A_P \frac{\partial P}{\partial x_P} = K_P$$

$$c_R s - A_r \frac{\partial P}{\partial x_P} = \varpi_P(s) \qquad c_R s - A_P \frac{\partial P}{\partial x_D} = \varpi_D(s)$$

$$\left(m_D s^2 + D_D s + K_D\right) X_D = \varpi_P(s) X_P \tag{2.3.2a}$$

$$\left(m_P s^2 + D_P s + K_P\right) X_P = \varpi_D(s) X_D \tag{2.3.2b}$$

$$\omega_D = \sqrt{\frac{K_D}{m_D}} \qquad Q_D = \frac{\omega_D m_D}{2\pi D_D}$$
$$\omega_P = \sqrt{\frac{K_P}{m_P}} \qquad Q_P = \frac{\omega_P m_P}{2\pi D_P}$$
$$H_D(s) = m_D \left(s^2 + \frac{\omega_D}{2\pi Q_D} + \omega_D^2 \right)$$
$$H_P(s) = m_P \left(s^2 + \frac{\omega_P}{2\pi Q_P} + \omega_P^2 \right)$$

Then,

$$H_D(s) X_D = \varpi_P(s) X_P \tag{2.3.3a}$$
$$H_P(s) X_P = \varpi_D(s) X_D \tag{2.3.3b}$$

$$\begin{vmatrix} H_D(s) & -\varpi_P(s) \\ -\varpi_D(s) & H_P(s) \end{vmatrix} = 0 \qquad \rightarrow \qquad H_D(s) H_P(s) - \varpi_P(s) \varpi_D(s) = 0$$

$$H_D(s) = 0 = -\frac{1}{2} \left(\frac{\omega_D}{2\pi Q_D} \pm \sqrt{\left(\frac{\omega_D}{2\pi Q_D} \right)^2 - 4\omega_D^2} \right) \tag{2.3.4a}$$
$$H_P(s) = 0 = -\frac{1}{2} \left(\frac{\omega_P}{2\pi Q_P} \pm \sqrt{\left(\frac{\omega_P}{2\pi Q_P} \right)^2 - 4\omega_P^2} \right) \tag{2.3.4b}$$

From Fig. 2.6,

$$\tan^{-1} \left(\frac{\omega_c - \omega_D}{-\dfrac{\omega_D}{4\pi Q_D}} \right) = \tan^{-1} \left(\frac{\omega_c - \omega_P}{\dfrac{\omega_P}{4\pi Q_P}} \right)$$
$$\omega_c = \frac{\omega_D \omega_P (Q_D + Q_P)}{\omega_P Q_P + \omega_D Q_P} \tag{2.3.5}$$

$$\text{If } Q_D >> Q_P \text{ then } \omega_c \approx \omega_D$$
$$\text{If } Q_D << Q_P \text{ then } \omega_c \approx \omega_P$$

If $\omega_D = \omega_P$ then ω_c is independent of Q_D and Q_P, one can say that is better to design for $Q_D >> Q_P$ so the frequency is not going to depend on the piston load.

$$P_0 = \frac{mR}{V_{swc}/(2T_c) + V_k/T_c + V_r/T_r + V_h/T_e + V_{swe}/(2T_e)} \tag{2.3.6}$$

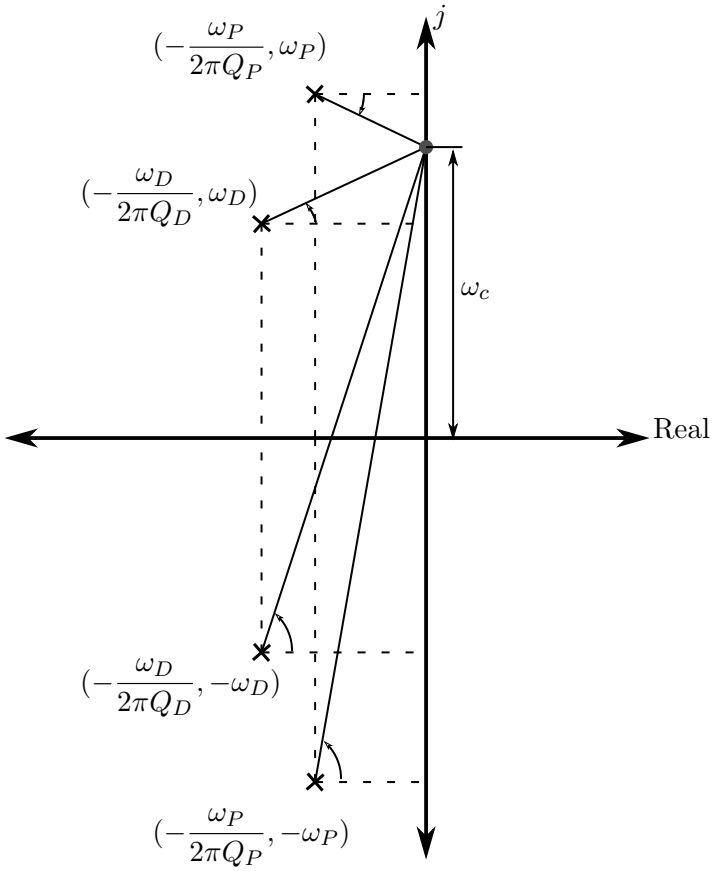

Figure 2.6: Localization of the poles

or

$$P_0 = \frac{mRT_0}{V_0} \tag{2.3.7}$$

From Eq. 2.3.6 and Eq. 2.3.7,

$$\frac{V_0}{T_0} = V_{swc}/(2T_c) + V_k/T_c + V_r/T_r + V_h/T_e + V_{swe}/(2T_e) \tag{2.3.8}$$

$$\begin{aligned} \frac{\partial P}{\partial x_D} &= \frac{\partial P}{\partial V_e}\frac{\partial V_e}{\partial x_D} + \frac{\partial P}{\partial V_c}\frac{\partial V_c}{\partial x_D} \\ \frac{\partial P}{\partial x_P} &= \frac{\partial P}{\partial V_e}\frac{\partial V_e}{\partial x_P} + \frac{\partial P}{\partial V_c}\frac{\partial V_c}{\partial x_P} \end{aligned} \tag{2.3.9}$$

Based on Eq. 2.3.9,

$$\frac{\partial P}{\partial V_e} = -\frac{mR}{T_e}\left(\frac{V_c}{T_c} + \frac{V_k}{T_c} + \frac{V_r}{T_r} + \frac{V_h}{T_e} + \frac{V_e}{T_e}\right)^{-2}$$

$$\frac{\partial P}{\partial V_c} = -\frac{mR}{T_c}\left(\frac{V_c}{T_c} + \frac{V_k}{T_c} + \frac{V_r}{T_r} + \frac{V_h}{T_e} + \frac{V_e}{T_e}\right)^{-2}$$

$$\frac{\partial V_e}{\partial x_D} = -A_r$$

$$\frac{\partial V_c}{\partial x_D} = A_P = (A - A_r)$$

$$\frac{\partial V_c}{\partial x_P} = -A_P = -(A - A_r)$$

$$\frac{\partial V_e}{\partial x_P} = 0$$

Assuming that the average pressure P_0 occurs when the compression and expansion volumes are $V_c = V_{swc}/2$ and $V_e = V_{swe}/2$ respectively[32].

$$\frac{\partial P}{\partial x_D} = -\frac{T_0 P_0}{V_0}\left(\frac{A_P}{T_c} - \frac{A_r}{T_e}\right) \qquad \frac{\partial P}{\partial x_P} = \frac{A_P T_0 P_0}{V_0 T_c} \tag{2.3.10}$$

The machine has to fulfill the next criteria shown in Eq. 2.3.11.[32]

$$|H_D(j\omega_c)H_P(j\omega_c)| < |\varpi_P(j\omega_c)\varpi_D(j\omega_c)| \tag{2.3.11}$$

In practice, oscillation amplitude is limited by non-linearities, either artificially induced by means of closed loop mechanisms that control Q_p or Q_d in response to piston amplitude , or inherent in the working gas process, when equilibrium is reached, piston and displacer motion are expressible in complex form as Eq. 2.3.12 [32].

$$\begin{aligned} x_d(t) &= X_D e^{j\omega_c t} \\ x_p(t) &= X_P e^{j\omega_c t} \end{aligned} \tag{2.3.12}$$

If at some instant the amplitude were greater, the energy dissipation would be greater than the input, which would gradually diminish the kinetic energy of the system until the equilibrium amplitude is reached [21]. This is due to the fact that the work done by the viscous forces is $\pi c \omega x_0^2$ and the work done by an external force is $\pi P_0 x_0$, thus the quadratic behavior will be greater than the linear from the force.

The amplitudes are not uniquely determined in this analysis, but are strongly related through the frequency and phase angle. A first assumption could be to take the piston stroke half the displacer amplitude (Eq.2.3.13) [1] or based on the geometry of the cylinder [35].

$$\frac{X_D}{X_P} = \frac{\varpi_P}{H_D(j\omega_c)} \tag{2.3.13}$$

Results

Table 2.1 shows the values utilized for the design of several engines. Tables 2.2, 2.3, and 2.4 show some of the design and operational parameters for specific output power.

The results shown in Tables 2.5, 2.6, and 2.7 represent the implementation of the first order analysis for a beta type engine, based on Urieli's work, and the stability analysis, which took into consideration the loss between the power piston and the displacer. The error shown is between the comparison of the first order analysis and the stability study develop in this section and the Schmidt analysis deduced from Urieli [36]. The maximum error presented is 2.6% which seems

Table 2.1: Engine parameters

Parameter	Quantity
$M(kg)$	0.001006
$R(J/kg\,K)$	2077
$V_c(m^3)$	2.096×10^{-5}
$V_e(m^3)$	1.74×10^{-5}
$V_k(m^3)$	1.91×10^{-5}
$V_r(m^3)$	1.17×10^{-4}
$V_h(m^3)$	2.95×10^{-5}
$T_c(K)$	300
$T_e(K)$	900
$T_r(K)$	$(T_e - T_c)/(\ln(T_e/T_c))$
$A(m^2)$	3.62×10^{-3}
$A_r(m^2)$	$(\pi/4)(1.06\times10^{-2})^2$
$m_P(kg)$	1
$m_D(kg)$	0.25
$V_{clc}(m^3)$	0.001
$V_{cle(m^3)}$	0.001
$x_{da}(m)$	0.06
$x_{pa}(m)$	0.03
$\alpha(rad)$	$90\pi/180$
$\theta(rad)$	$0\rightarrow2\pi$
$K_P(Nm)$	6.8828×10^5
$K_D(Nm)$	1.7207×10^5
$c_r(Nm/s)$	10
$c_D(Nm/s)$	40
$c_P(Nm/s)$	60
$D_P(Nm/s)$	$c_r + c_P$
$D_D(Nm/s)$	$c_r + c_D$

acceptable.

Figures 2.7, 2.8, and 2.9 show the variation of the compression and expansion space of some of the engines described in Tables 2.5, 2.6, and 2.7. Similarly, Figures 2.10, 2.11, and 2.12 show the "Pressure-Volume" diagram of some of the engines described in Tables 2.5, 2.6, and 2.7.

Table 2.2: Engine parameters for 500w, First order analysis

Engine	$A\,(m^2)$	$A_r\,(m^2)$	m (kg)	T_c (K)	T_e (K)	f (Hz)	Power (w)
1	0.0038	0.0008	0.0079	421.6194	975.2985	58.7237	343.9067
2	0.0040	0.0006	0.0099	318.4509	930.7242	57.7029	494.0768
3	0.0048	0.0002	0.0073	309.8165	829.0394	59.6881	498.1949
4	0.0045	0.0007	0.0091	310.6355	903.8053	52.9452	499.8550
5	0.0047	0.0001	0.0075	396.2645	912.3510	57.1180	494.3517
6	0.0048	0.0003	0.0090	481.3007	910.2128	55.4410	512.1503

Table 2.3: Engine parameters for 1000w, First order analysis

Engine	$A\,(m^2)$	$A_r\,(m^2)$	m (kg)	T_c (K)	T_e (K)	f (Hz)	Power (w)
1	0.0048	0.0004	0.0128	493.0304	1097.0824	58.8041	1012.9638
2	0.0044	0.0001	0.0189	458.4954	839.5971	62.4070	977.4794
3	0.0049	0.0004	0.0125	369.8578	981.6834	57.8149	990.1325
4	0.0040	0.0003	0.0159	322.3066	947.5976	64.1755	1004.7297
5	0.0046	0.0001	0.0111	376.4419	1081.0567	62.4589	1012.7449
6	0.0048	0.0005	0.0159	398.2282	842.0762	62.6464	991.7534

Table 2.4: Engine parameters for 1500w, First order analysis

Engine	$A\,(m^2)$	$A_r\,(m^2)$	m (kg)	T_c (K)	T_e (K)	f (Hz)	Power (w)
1	0.0045	0.0007	0.0200	343.2570	1006.9345	64.8695	1491.0204
2	0.0046	0.0001	0.0149	340.6029	1076.9969	68.4743	1513.1085
3	0.0050	0.0008	0.0182	300.8922	1110.4421	54.7821	1527.1635
4	0.0043	0.0003	0.0177	338.1772	1049.6459	66.5712	1474.5268
5	0.0037	0.0006	0.0149	346.8556	1121.9814	65.1180	906.9729
6	0.0044	0.0002	0.0158	355.5930	1125.9821	65.3857	1470.5873

Table 2.5: Engine parameters for 500w, First order and stability analysis

Engine	$A\,(m^2)$	$A_r\,(m^2)$	P_{mean} (Bar)	T_c (K)	T_e (K)	m_P (kg)	m_D (kg)	f(Hz)	Phase angle(rad)	Power (w)	Error (%)
1	0.0041	0.0007	5.2	363.2142	979.1728	1.1082	0.6143	107.4295	0.3034	502.7092	-1.1527
2	0.0041	0.0007	6.2	323.6616	623.4138	1.3777	0.6439	100.5405	0.3562	439.2926	-1.5255
3	0.0043	0.0006	5.4	447.5266	1168.1496	1.7752	0.8127	88.9970	0.3284	505.2463	-1.3078
4	0.0048	0.0006	3	486.7184	1095.8697	0.9968	0.9035	75.1350	0.6781	505.7672	-0.8983
5	0.0040	0.0003	3	491.2869	866.5982	1.1771	0.6430	83.7340	1.3501	504.0891	0.4540
6	0.0043	0.0008	2.6	350.0169	1137.8459	0.6715	0.3695	138.2825	0.3862	505.3635	-0.9557
7	0.0045	0.0001	5.7	348.8346	885.9448	0.6048	0.6479	118.7463	0.1953	489.2612	-1.8968
8	0.0043	0.0004	5	465.8161	906.0242	1.7391	0.6862	92.8550	0.4428	497.7360	-1.6764
9	0.0047	0.0005	3.08	437.5158	1194.2287	2.2703	0.8466	80.5112	0.5161	506.5841	-1.1494
10	0.0037	0.0003	6.2	337.3224	1037.5930	1.5758	0.7966	92.2493	0.2945	495.7784	-1.0289

Table 2.6: Engine parameters for 1000w, First order and stability analysis

Engine	$A\,(m^2)$	$A_r\,(m^2)$	P_{mean} (Bar)	T_c (K)	T_e (K)	m_P (kg)	m_D (kg)	f(Hz)	Phase angle(rad)	Power (w)	Error (%)
1	0.0045	0.0006	3.0	399.0865	1052.3007	2.0547	0.4547	93.4856	2.0482	996.1320	-0.0962
2	0.0047	0.0001	2.5	361.6235	890.2314	1.5472	0.4432	104.1543	1.0744	1002.6841	0.1161
3	0.0048	0.0004	2.2	365.2878	1159.8359	2.0072	0.4397	94.6912	2.0749	1005.0044	-0.0959
4	0.0044	0.0003	6.5	342.8332	990.7492	1.5137	0.6356	98.2458	0.4146	997.7022	-1.2160
5	0.0040	0.0008	5.1	398.0866	932.8574	2.6982	0.6021	81.5023	2.0766	985.5610	-0.1020
6	0.0039	0.0006	3.9	326.4109	1180.6006	2.7000	0.7314	79.4879	1.1773	998.6065	0.1071
7	0.0049	0.0005	5.3	376.9360	662.3828	1.9573	0.6082	91.4292	0.7866	996.3391	-0.8581
8	0.0050	0.0001	6.9	331.8653	704.3730	0.6201	0.4468	133.0718	0.2896	1013.5687	-2.5977
9	0.0043	0.0006	4.9	471.4736	863.2944	2.1966	0.5186	89.7326	1.8219	998.3121	0.0440
10	0.0043	0.0005	4.1	374.7670	884.3692	1.5335	0.4729	103.4211	0.8662	1009.3330	-0.2748

Table 2.7: Engine parameters for 1500w, First order and stability analysis

Engine	$A\,(m^2)$	$A_r\,(m^2)$	P_{mean} (Bar)	T_c (K)	T_e (K)	m_P (kg)	m_D (kg)	f(Hz)	Phase angle(rad)	Power (w)	Error (%)
1	0.0044	0.0003	3.5	438.9074	876.6793	2.0103	0.1956	159.8870	1.1030	1497.5464	0.2136
2	0.0039	0.0005	6.3	482.0272	1011.1602	0.5646	0.2238	162.8118	0.6887	1487.2601	-0.6584
3	0.0047	0.0006	5.7	353.0556	728.9397	2.0238	0.5648	91.4204	1.1097	1502.3071	0.2240
4	0.0041	0.0001	5.9	352.8515	1092.5765	2.4847	0.7137	82.1555	0.9594	1563.7921	-0.1024
5	0.0047	0.0001	6.7	335.9755	1172.3150	2.0392	0.7371	87.6036	0.5371	1581.1131	-1.0587
6	0.0047	0.0003	3.6	453.7310	976.7617	1.4901	0.3628	108.5317	1.6685	1481.2765	0.2609
7	0.0049	0.0001	6.6	304.9608	1081.0392	1.8816	0.7166	89.9046	0.4628	1515.1925	-1.2941
8	0.0043	0.0002	4.8	446.4842	1102.2620	2.3471	0.5696	86.5128	1.7083	1497.2688	0.1664
9	0.0047	0.0002	6.3	332.1147	1083.1604	2.6662	0.8455	78.0777	0.6631	1494.1717	-0.7749
10	0.0046	0.0005	6.8	498.4021	1137.6945	0.9015	0.6983	83.9907	0.8670	1518.1369	-0.3161

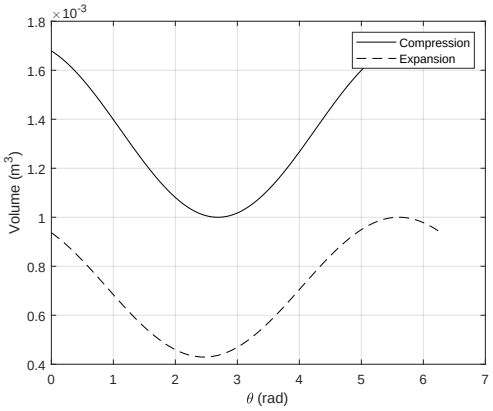

(a) Engine 1

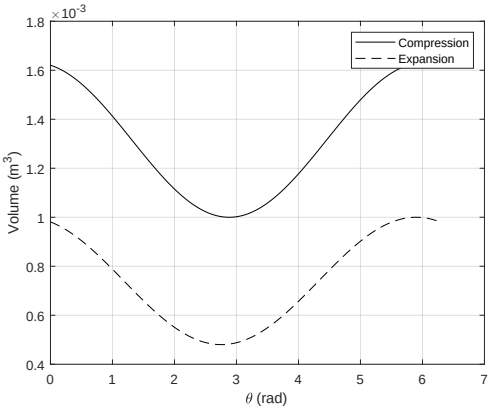

(b) Engine 4

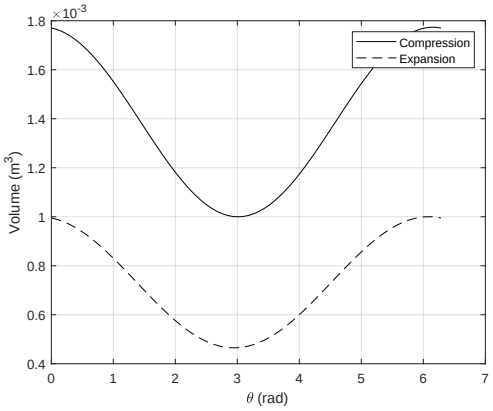

(c) Engine 5

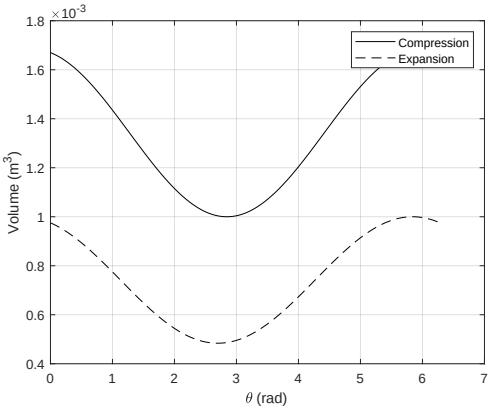

(d) Engine 6

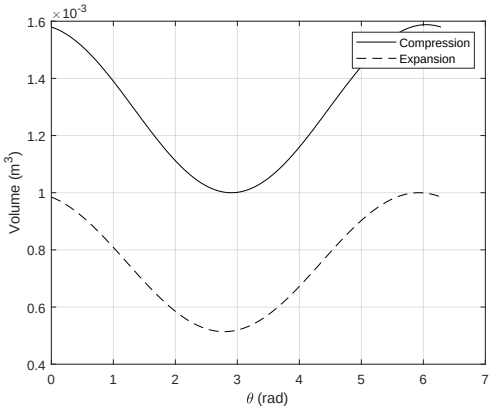

(e) Engine 8

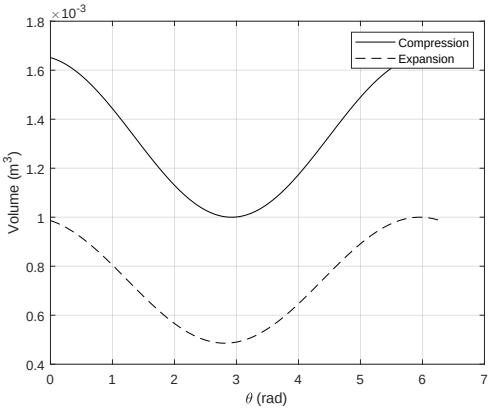

(f) Engine 9

Figure 2.7: Volume variation for 500w engines

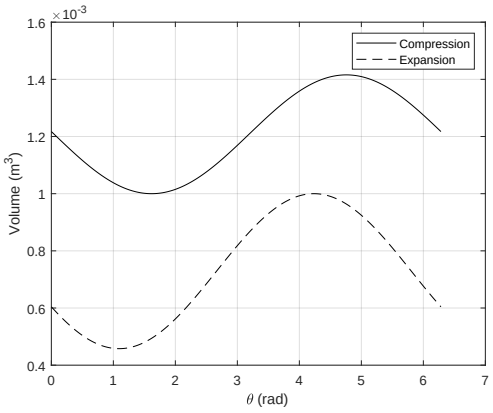

(a) Engine 1

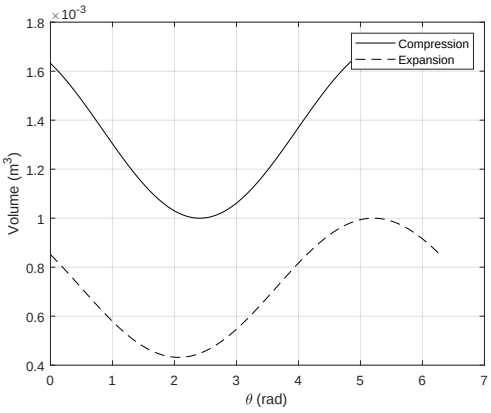

(b) Engine 2

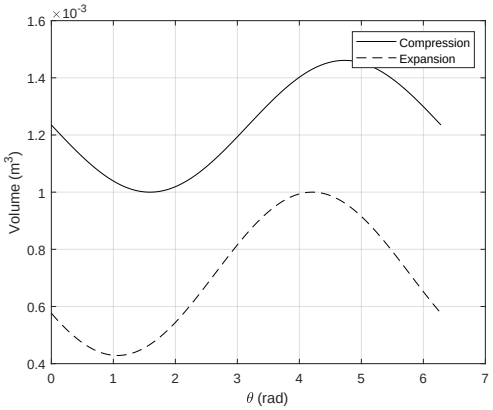

(c) Engine 3

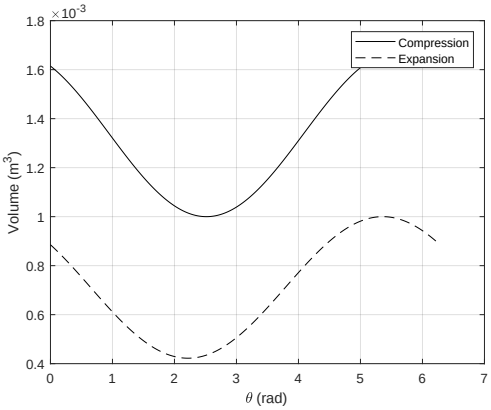

(d) Engine 4

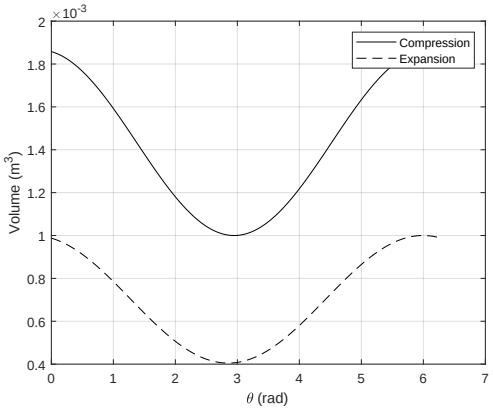

(e) Engine 9

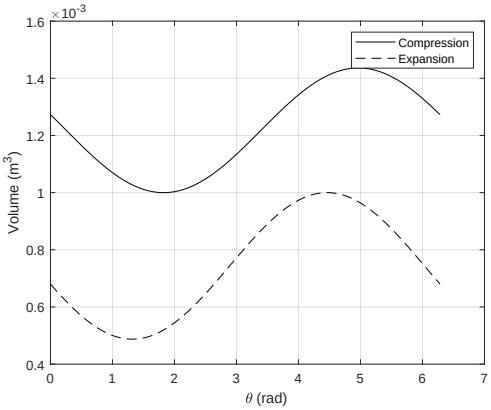

(f) Engine 10

Figure 2.8: Volume variation for 1000w engines

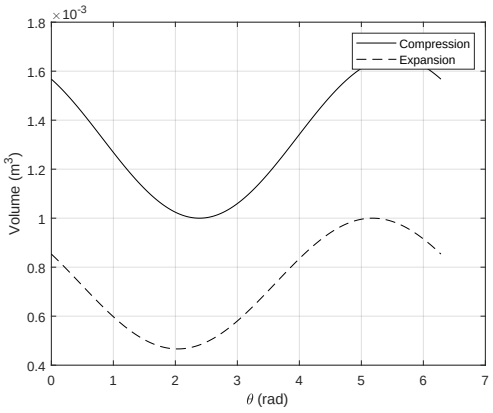

(a) Engine 1

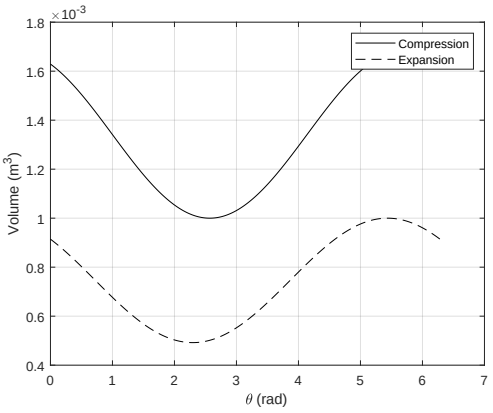

(b) Engine 3

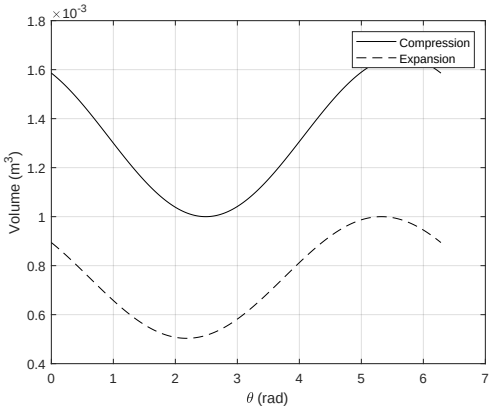

(c) Engine 4

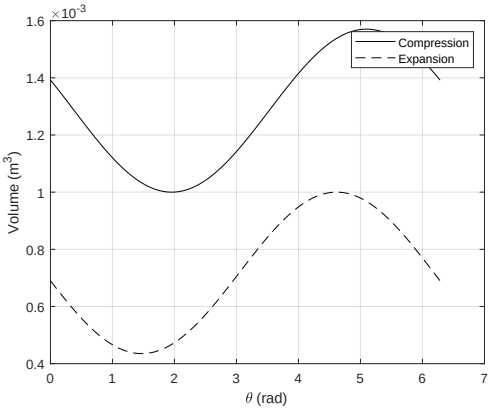

(d) Engine 6

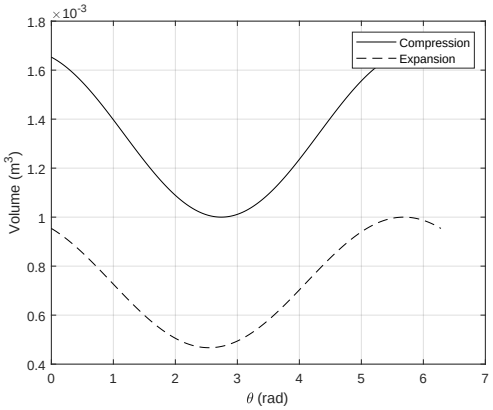

(e) Engine 7

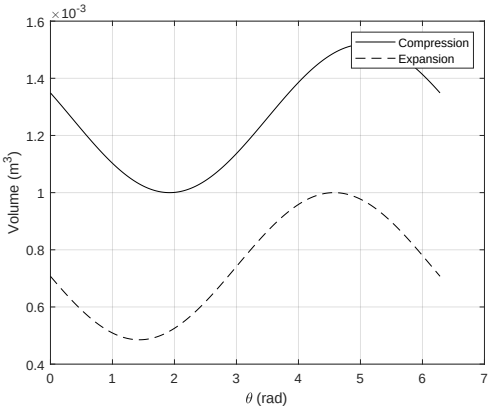

(f) Engine 8

Figure 2.9: Volume variation for 1500w engines

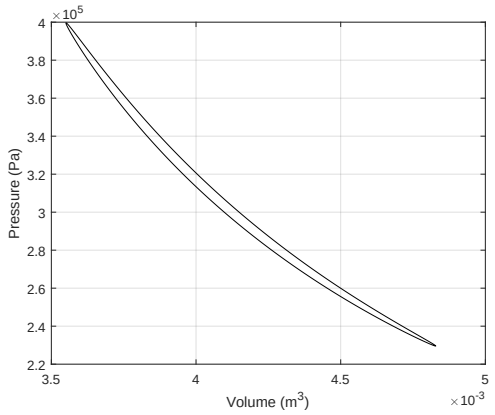

(a) Engine 1

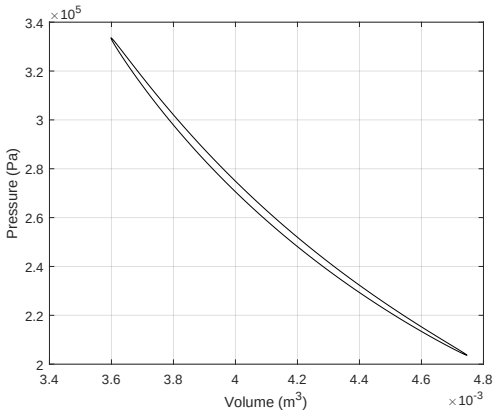

(b) Engine 4

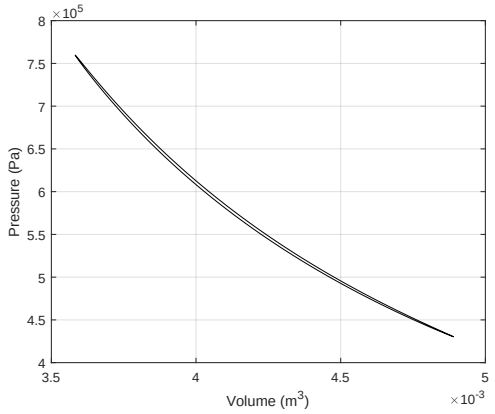

(c) Engine 5

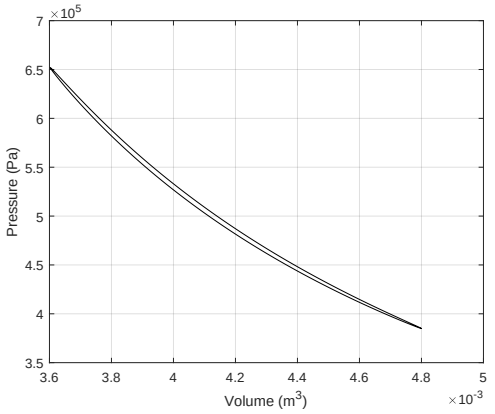

(d) Engine 6

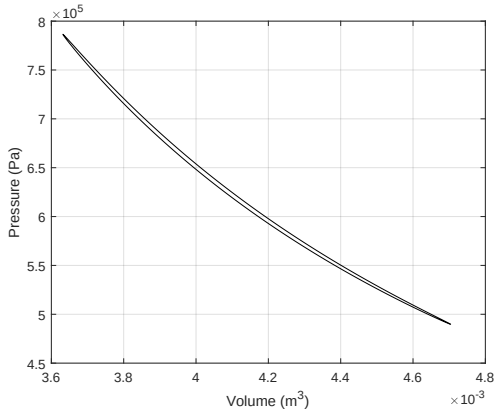

(e) Engine 8

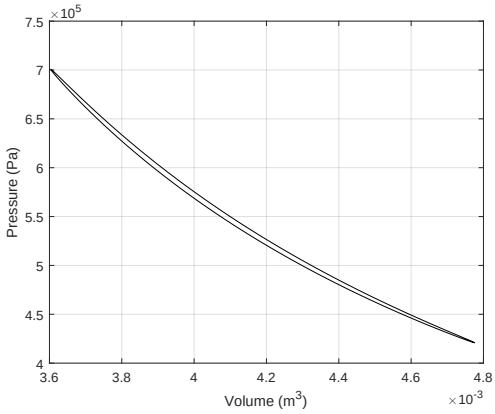

(f) Engine 9

Figure 2.10: PV diagram for some 500w engines

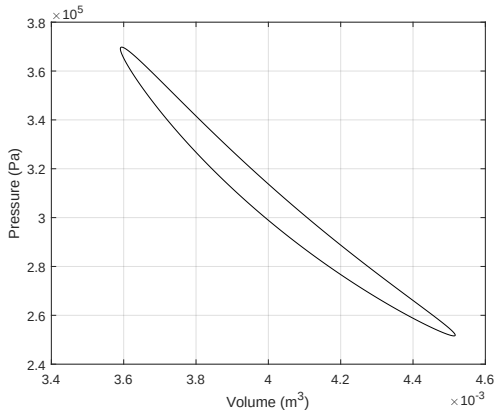

(a) Engine 1

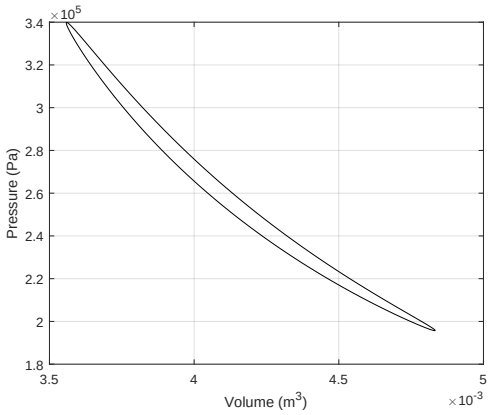

(b) Engine 2

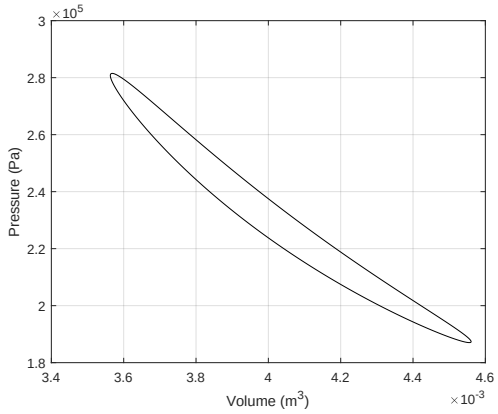

(c) Engine 3

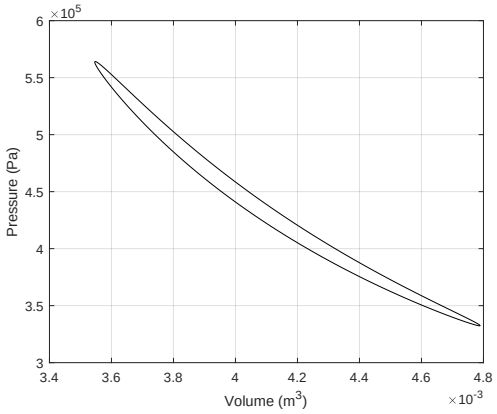

(d) Engine 4

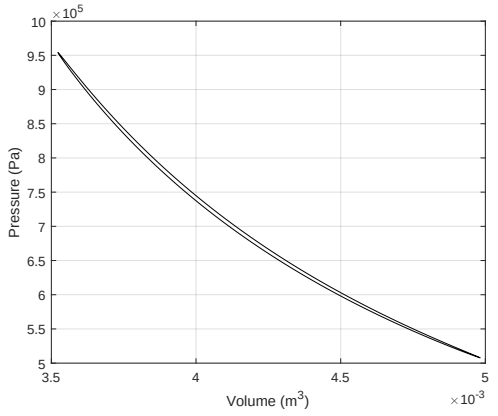

(e) Engine 9

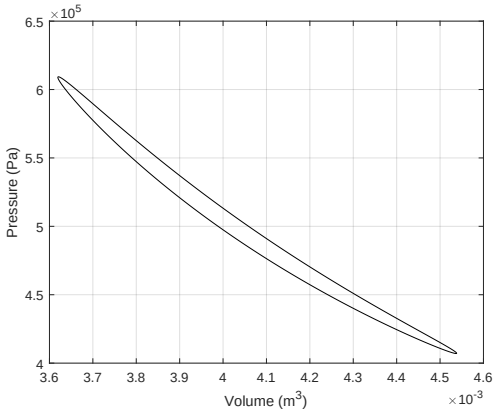

(f) Engine 10

Figure 2.11: PV diagram for some 1000w engines

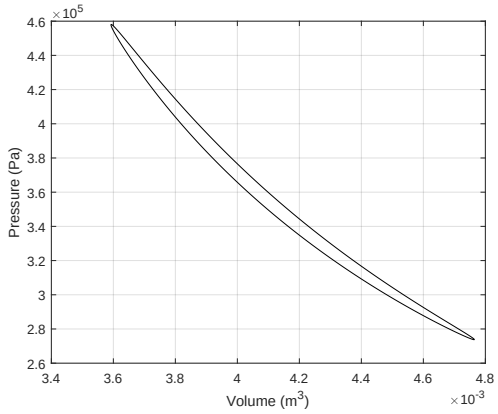

(a) Engine 1

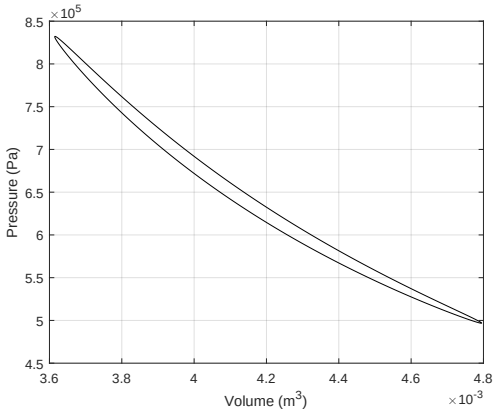

(b) Engine 3

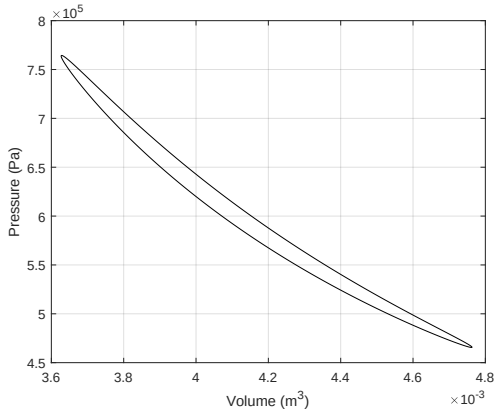

(c) Engine 4

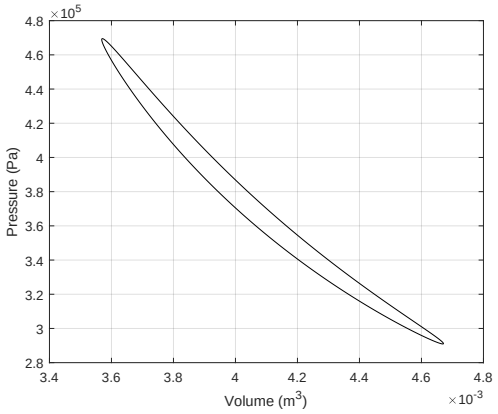

(d) Engine 6

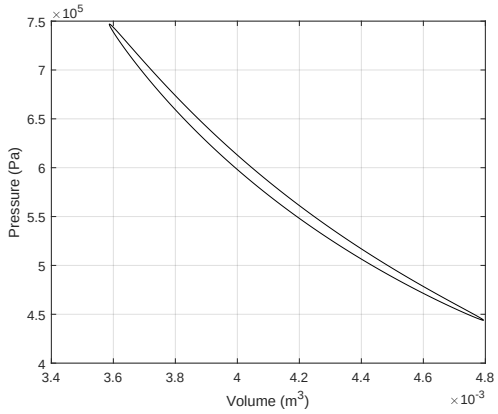

(e) Engine 7

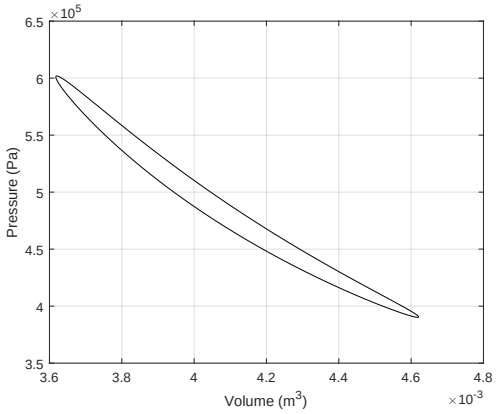

(f) Engine 8

Figure 2.12: PV diagram for some 1500w engines

Table 2.6 shows ten different combination of parameters, which represent ten different engines working in a stable mode, and with power outputs closer to the desired 1 kW. There are also some designs with lower power outputs, like engine 1 and engine 5. This indicates that under certain conditions, there is a maximum limit for the power output, that would not affect the stable operation of the engine. The proposed procedure does not explore in detail the influence of a particular parameter, the objective is to search through all the potential designs, ensuring the stability of each proposed engine. This represent a valuable tool for early stage design of free piston engines. In general, the error for the predicted power is lower than 1% for the majority of the simulations, which validates the proposed models.

Figures 2.8a and 2.8c show the variation of the volume inside the compression and expansion spaces for the same engines. Figure 2.11a and 2.11c represent the Pressure-Volume diagrams of a pair of engines enlisted in Table 2.6.

Figure 2.11a, and Figure 2.11c reflect the characteristic shape for a PV diagram in Stirling engines. This shape differs largely from the theoretical PV cycle, and thus indicates the relevance of using adequate tools to analyze Stirling cycles. Some conclusions can be inferred from this kind of diagrams. For example, according to Figures 2.11a and 2.11c, both engines follow a similar volume variation, but the design 3 gives a higher power output. This difference can be explained due to the operation at higher pressures observed in Figure 2.11c, when compared with the pressure levels of engine 1, Figure 2.11a. This supports a known fact about Stirling engines, when two engines present similar geometrical characteristics, the operation at higher pressures will translate into higher power outputs.

Entropy analysis

In the heat addition process the main source is the heater. Similarly the cooler, for rejecting heat from the fluid to the heat sink. In Figure 2.13a and 2.13b the PV diagram and TS diagram for imperfect regeneration is shown. The big difference between the ideal cicle and the non-ideal lies in the amount of heat provided from the regenerator (process 2-2') and from the gas to the regenerator (process 4-4')

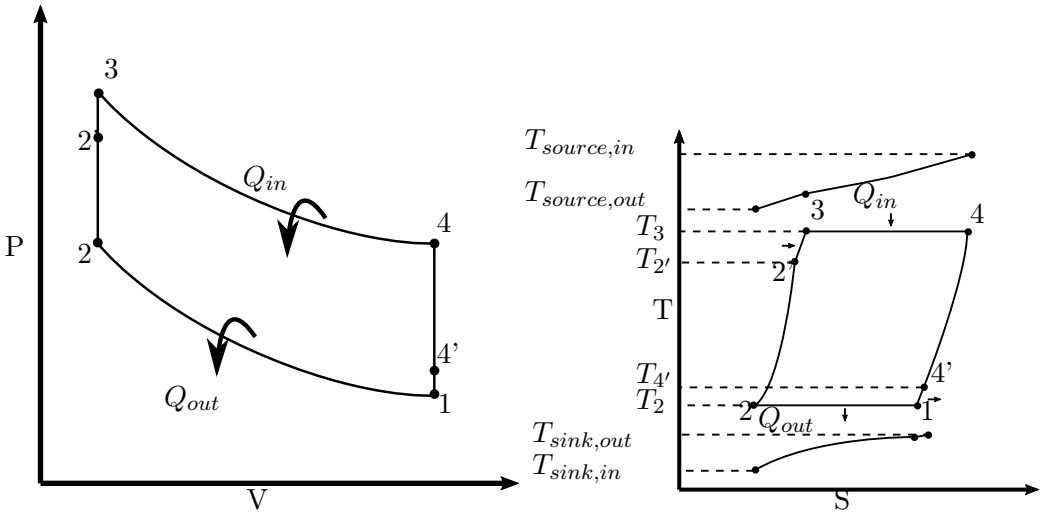

(a) PV diagram

(b) TS diagram

Harrod et al. [37] presented a second law analysis for Stirling engines. The analysis estimated the entropy generated in the cooler, heater and regenerator of the engine. The entropy generation in the heater is given by the difference between the entropy changes of the hot working fluid and the source at the log mean temperature of the fluid stream

$$\begin{aligned} S_{gen,h} &= S_h - S_{source} = S_{34} + S_{2'3} - S_{source} \\ &= \frac{Q_{34}}{T_3} + \dot{m}c_v \ln\left(\frac{T_3}{T_2'}\right) - \frac{Q_{in}}{T'_{source}} \end{aligned} \tag{2.3.14}$$

where T'_{source}

$$T'_{source} = \frac{T_{source,in} - T_{source,out}}{\ln(T_{source,in}/T_{source,out})} \tag{2.3.15}$$

For the cooler

$$\begin{aligned} S_{gen,c} &= S_{sink} - S_c = S_{sink} - S_{12} - S_{4'1} \\ &= \frac{Q_{out}}{T'_{sink}} - \frac{Q_{12}}{T_1} - \dot{m}c_v \ln\left(\frac{T_4'}{T_1}\right) \end{aligned} \tag{2.3.16}$$

where T'_{sink}

$$T'_{sink} = \frac{T_{sink,in} - T_{sink,out}}{\ln(T_{sink,in}/T_{sink,out})} \tag{2.3.17}$$

For the regenerator the entrophy generation is calculated from Eq. 2.3.18

$$S_{gen,R} = S_c - S_h \tag{2.3.18}$$

Substituting Eq. 2.3.14 and Eq. 2.3.16 into Eq. 2.3.18, the resulting entrophy is:

$$S_{gen,R} = \frac{Q_{12}}{T_1} - \frac{Q_{34}}{T_3} + \dot{m}c_v \ln\left(\frac{T_{4'}T_{2'}}{T_1T_3}\right) \tag{2.3.19}$$

The total entrophy generation can be expressed as the sum of the external and internal irreversibilities by adding Eqs. 2.3.14,2.3.16 and 2.3.19.

$$\begin{aligned} S_{gen,total} &= \frac{Q_{out}}{T'_{sink}} - \frac{Q_{in}}{T'_{input}} \\ &= S_{gen,h} + S_{gen,R} + S_{gen,c} \end{aligned} \tag{2.3.20}$$

The heats are calculated from the next equations

$$Q_{12} = W_{12} = \int_{V_1}^{V_2} \omega P dV_c = \dot{m}RT_1 \ln\left(V_1/V_2\right) \tag{2.3.21}$$

$$Q_{34} = W_{34} = \int_{V_1}^{V_2} \omega P dV_h = \dot{m}RT_3 \ln\left(V_1/V_2\right) \tag{2.3.22}$$

$$Q_{22'} = \varepsilon \dot{m}c_v(T_3 - T_1) \tag{2.3.23}$$

where ε is the effectiveness of the regenerator ($\varepsilon = \dfrac{T_{4'} - T_3}{T_1 - T_3} = \dfrac{T_{2'} - T_1}{T_3 - T_1}$)

$$Q_{2'3} = (1 - \varepsilon)\dot{m}c_v(T_3 - T_1) \tag{2.3.24}$$

$$Q_{4'1} = (\varepsilon - 1)\dot{m}c_v(T_3 - T_1) \tag{2.3.25}$$

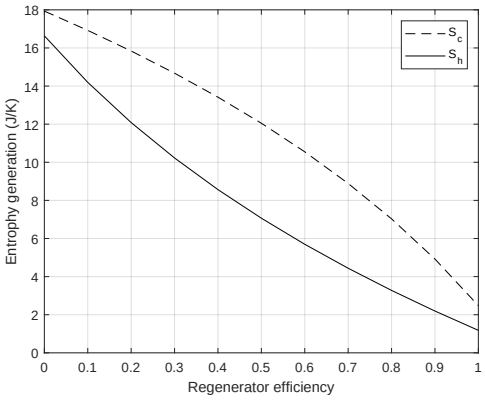

(a) Entropy generared during isothermal and isochoric heating and cooling processes

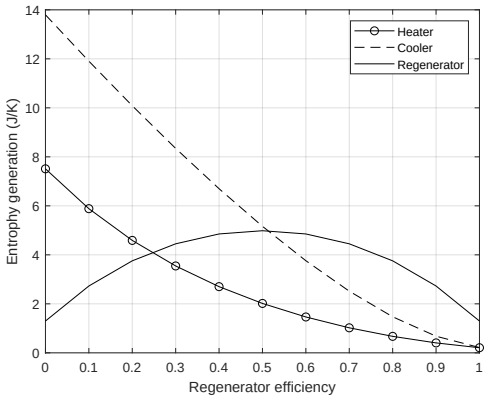

(b) Entropy for each heat exchanger

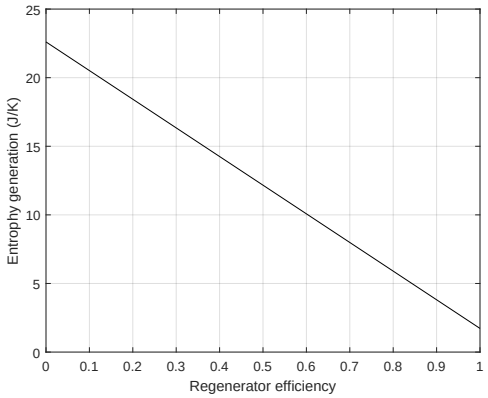

(c) Total entropy generated

Figure 2.14: 502W FPSE

The input heat and the output heat required are

$$Q_{in} = Q_{34} + Q_{2'3} \tag{2.3.26}$$

$$Q_{out} = Q_{12} + Q_{4'1} \tag{2.3.27}$$

In Figure 2.14a the sum of entropies (S_h) and the sum of entropies (S_c) is shown for the sake of understand the entropy generated by the regenerator, which according to Eq. 2.3.18 depends on this two quantities. In Figure 2.14b the entropies for each heat exchanger is displayed as a function of the regenerator's efficiency. The total entropy generated in the cycle is equal to the sum of independent entropies. The results can be seen in Figure 2.14c. Results from Figure 2.14 correspond to a 502W engine listed in Table 2.5.

Similarly for Figures 2.15 and 2.16 the regenerator's efficiency versus entropy generated is displayed. From the results it can be deduced that the amount of entropy generated is going to increase if the difference in the hot and cold temperatures increases, due to the fact that the entropy is defined as the radio of the heat over the temperature and heat is directly proportional to the temperature

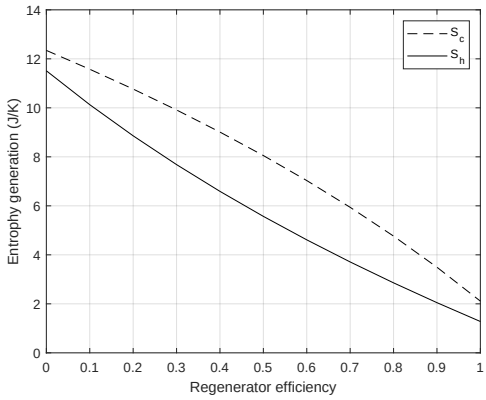

(a) Entropy generared during isothermal and isochoric heating and cooling processes

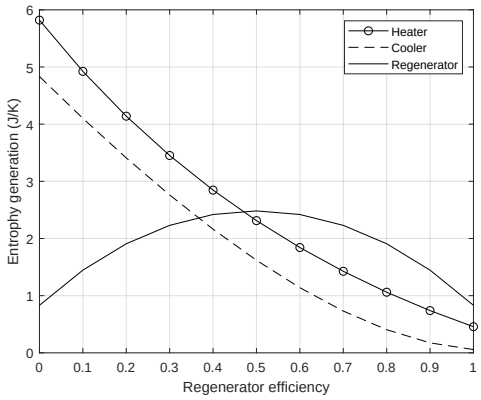

(b) Entropy for each heat exchanger

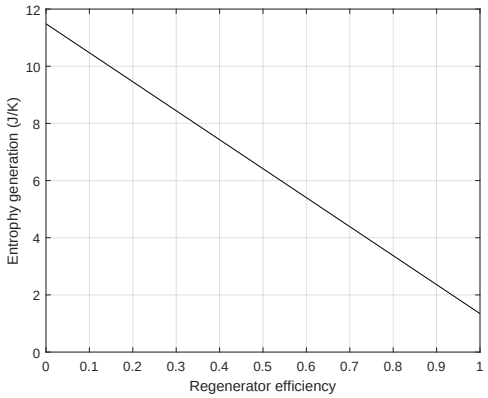

(c) Total entropy generated

Figure 2.15: 439W FPSE

gradient. Therefore for the three engines showed the 505W and 502W produce more entropy than the 439W.

The entropy generation rates for each heat exchanger contributes to the overall entropy generation, Figures (b) show that the entropy generated by the three components is strongly affected by the regenerator's efficiency, the entropy generation is reduced while the effectiveness of the regenerator increases. This decrease is due to the reduction of heat provided by the heater. For low ranges of efficiency the heater and cooler need to provide or sink more heat thus the entropy is greater. The behavior of the regenrator's entropy generated has symmetry from the central point (0.5). If no regenerator is included the engine efficiency would disminish.

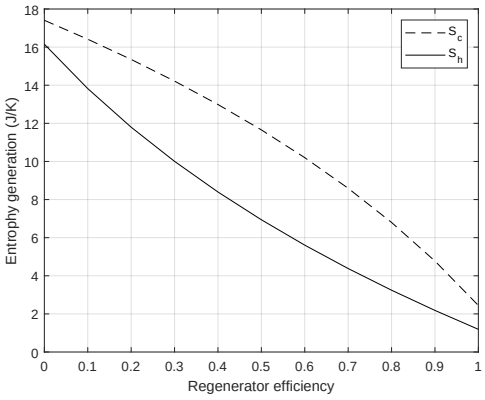

(a) Entropy generared during isothermal and isochoric heating and cooling processes

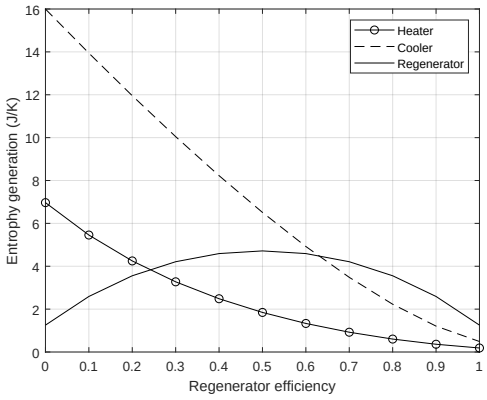

(b) Entropy for each heat exchanger

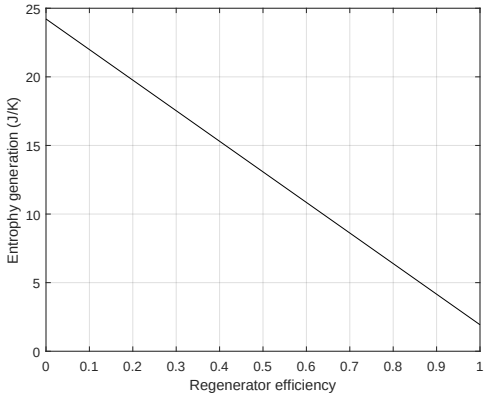

(c) Total entropy generated

Figure 2.16: 505W FPSE

2.4 Electric transformation

Although Stirling engines were first studied a long time ago, the demand for new ways of energy transformation has reborn this technology for clean heat-to electricity power conversion. Stirling power converters typically utilize linear alternators, which transform the motion of the piston into electricity. NASA has been developing Stirling Radioisotope Power Sytems capable of generating electric power with the primary purpose of providing power to future space science missions [38].

Linear Alternator Operation

Based on Faraday's law, a linear alternator can be modeled as an electromotive force (emf), or voltage, is induced along the boundary of a surface through which there is changing magnetic flux [39]. Permanent magnets (PMs) are attached to the piston, which oscillates within the alternator coil. A voltage (V_{emf}) is induced due to the change in the magnetic field crossing through the circular surface contained by the alternator coil (see Figure 2.17). The magnetic flux (φ) is the integral of the magnetic field ($\vec{B}$) through a surface (Eq. 2.4.1) and V_{emf} can be simplified as the total derivative of the flux times the number of turns (N), see Eq. 2.4.2.

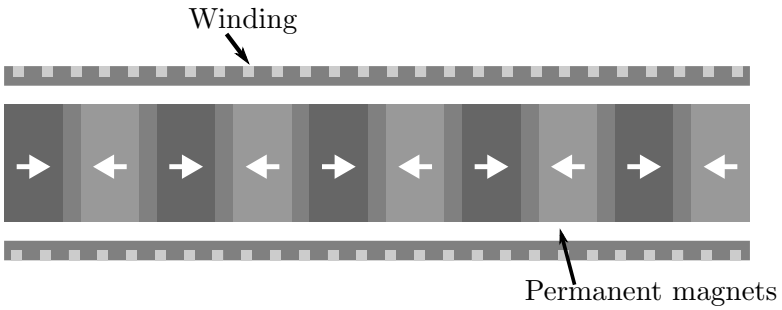

Figure 2.17: Linear alternator

$$\varphi = \int \vec{B} \cdot \hat{n}\, da \tag{2.4.1}$$

$$V_{emf} = N\frac{d\varphi}{dt} \tag{2.4.2}$$

To compute the electrical power output of the alternator a full mathematical model must be developed. In Figure 2.18, the equivalent circuit of the single-phase linear alternator is shown. Equation 2.4.3 describes the circuit in Figure 2.18. The inductance (L) and the linking flux (φ) and the resistance (R) are found from the geometry of the alternator and must be known to calculate the output voltage. The inherent voltage of the engine over one loop is calculated by Eq. 2.4.4 [40][41].

$$V_{out} = V_{emf} - Ri - L\frac{di}{dt} \tag{2.4.3}$$

where the electrical losses are modeled as a voltage drop which is equal to Ri.

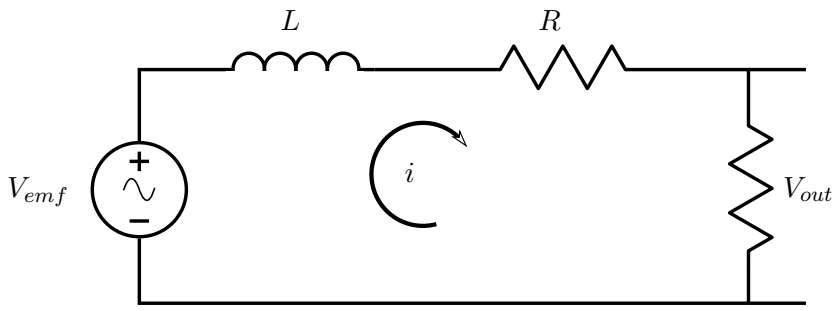

Figure 2.18: Electric representation of the linear alternator

$$V_{emf} = N\frac{d\varphi}{dx}\frac{dx}{dt} \tag{2.4.4}$$

where N is the total number of coil turns and the term $\frac{d\varphi}{dx}$ is a constant, which is often defined as the motor constant or the force constant, and it can be approximated by

$$\frac{d\varphi}{dx} = \frac{2\varphi_{max}}{l_s} \tag{2.4.5}$$

where φ_{max} is the cycle maximum of the winding flux linkage and l_s is the piston stroke [42]. The viscous force generated in the linear alternator is proportional to the piston's velocity and the viscous coefficient is c_P, this parameter is directly connected to the design of the linear alternator.

Chapter 3

Heat exchangers for Stirling engines

The primary purpose of this chapter is to study the heat exchangers, as a crucial part of the engine. Friction or pumping losses are included, which reduce the net power of the machine.

3.1 Urieli heat exchangers simple analysis

The study of heat transfer and flow friction effects for each heat exchanger is important for a well-designed engine. The forced convection is the primary mechanism of transport for heat, which travels from an external source to the working fluid in the heater zone, then part of the heat is absorbed by the regenerator. Finally the purpose of the rejector (cooler) is to use the most energy possible from the gas. It is essential to always have in mind that the heat exchangers should be designed in as compact as possible to limit the "dead volume", which is directly related to the power of the engine. It has been found that effective heat exchange comes at a price of increased flow friction, resulting in the so-called "pumping loss" [43].

Pumping Loss Simple Analysis

A common practice when analyzing a Stirling engine is to assume that the pressure is constant throughout the engine. Yet it has been found that the need for high heat fluxes in the heat exchangers requires a sizeable wetted area (A_w). This increase in the area will rise the void volume which is not desirable due to a drop in pressure. However, a good practice is to design a heat exchanger with many small diameter passages in parallel. The pressure drop is associated with the fluid friction, which is generated between the wall of the heat exchanger and the fluid, who travels from one part of the cylinder to the other. The friction force is strongly related to a power loss, and it is referred to as the "Pumping loss". Urieli evaluates the pressure drop across all the heat exchangers (heater, regenerator, and rejector) concerning the compression space. Then he determines the new value of the work done by integrating over the complete cycle, and isolate the Pumping Loss term [44].

$$W = W_e + W_c = \oint P\, dV_c + \oint (P - \sum \Delta P)\, dV_e \tag{3.1.1}$$

$$W = \oint P(dV_c + dV_e) - \oint \sum \Delta P\, dV_e = W_i - \Delta W \tag{3.1.2}$$

where W_i is the ideal work done per cycle, and ΔW is work loss due to the pressure drop in each heat exchanger.

$$\Delta W = \int_0^{2\pi} \left(\sum_{i=1}^{3} \Delta P_i \frac{dV_e}{d\theta} \right) d\theta \tag{3.1.3}$$

Then the efficiency of the cycle is (see Eq. 3.1.4)

$$\eta = W/Q_{in} \tag{3.1.4}$$

where $Q_{in} = Q_e = W_e$

The pressure drop (ΔP) is due to fluid friction as it moves through the heat exchanger section. Urieli's model assumed one-dimensional flow, although the concept of fluid friction break down under this assumption. Fig. 3.1 shows shear stress (τ) between parallel layers of fluid proportional to the velocity gradient $\left(\frac{du}{dz}\right)$ which is stated in Newton's law of viscosity.

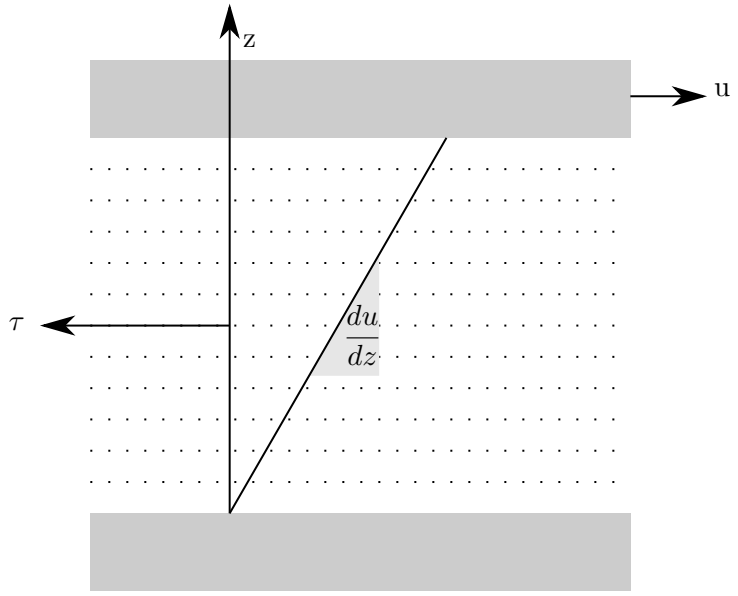

Figure 3.1: Velocity gradient

$$\tau = -\mu \frac{du}{dz} \tag{3.1.5}$$

Eq. 3.1.5 cannot sustain a one-dimensional flow. However, it is stating that the flow is not strictly 1D, but its mean bulk mass flow rate represents it. The dynamic viscosity (μ) is a measure of the internal friction. This internal friction is due to the collision of the particle, which travels at different speeds, and thus

the transfer of momentum occurs from one particle to another [45].

The frictional force is related to the shear stress by Eq. 3.1.6

$$F = \tau \, A_w \tag{3.1.6}$$

Substituting $d = 4V/A_w$ which is the hydraulic diameter at Eq. 3.1.6, where V is the void volume.

$$F = \frac{4\tau V}{d} \tag{3.1.7}$$

For flow in circular pipes, the hydraulic diameter thus becomes the internal diameter of the pipe. Kays and London defined a coefficient of friction (C_f) as the ratio of the shear stress to the "dynamic head". See Eq. 3.1.8 [46].

$$C_f = \frac{\tau}{\frac{1}{2}\rho \, u^2} \tag{3.1.8}$$

Substituting for the shear stress from Eq. 3.1.8 at Eq.3.1.7, the result is an equation that relates the frictional factor with a morphology characteristic value of the heat exchanger like the "hydraulic diameter". See Eq. 3.1.9.

$$F = \frac{2C_f \rho \, u^2 \, V}{d} \tag{3.1.9}$$

When there is no acceleration present in the fluid (quasi-steady flow), the drag force is equal and opposite to the pressure drop force.

$$F + \Delta P A = 0 \tag{3.1.10}$$

Thus, substituting Eq. 3.1.9 at Eq. 3.1.10.

$$\Delta P + \frac{2C_f \rho \, u^2 \, V}{d \, A} = 0 \tag{3.1.11}$$

The second term of the left side is always positive. However, the pressure can be either positive or negative, depending on the direction of flow. Thus the equation violates the momentum conservation principle in the case of reversing flow[44]. This can be fixed by introducing a "Reynolds friction coefficient" (C_{Re}), see Eq. 3.1.12

$$C_{\mathrm{Re}} = \mathrm{Re} \, C_f \tag{3.1.12}$$

Finally the pressure drop is shown in Eq. 3.1.13.

$$\Delta P = \frac{-2 \, C_{\mathrm{Re}} \, \mu \, u \, V}{d^2 A} \tag{3.1.13}$$

Eq. 3.1.13 now satisfies the momentum conservation principle for both directions of the flow, this is represented by the direction of the velocity (u). Empirical data from the friction coefficient is presented as function of the Reynolds number, it is simple to use this data with Eq. 3.1.12. For smooth circular pipes the Moody diagram has been modified to show the Reynolds Friction Coefficient that is shown in Fig. 3.2 [44].

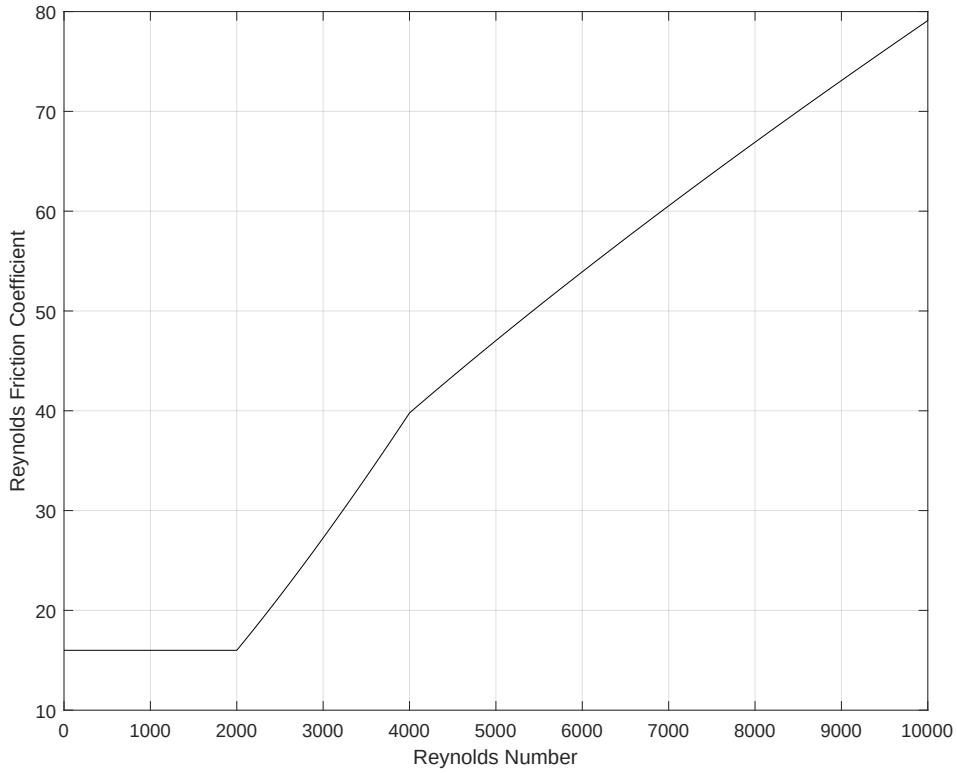

Figure 3.2: Reynolds Friction Coefficient versus Reynolds Number for a smooth circular pipe

- **Hagen-Poiseuille (Laminar)**, for Re less than 2000. It is important to mention that for the Moody diagrams the laminar part is equal to [47][48][49][50]

$$C_f = 64$$

However, due to the hydraulic diameter compensation factor (4) the C_{Re} is equal to

$$C_{\mathrm{Re}} = 16$$

- **Transition**, when the Re is greater than 2000 and less than 4000 the C_{Re} is equal to

$$C_{\mathrm{Re}} = 7.343 \times 10^{-4} \mathrm{Re}^{1.3142}$$

- **Blasius (Turbulent)**, when the Re is gretaer than 4000 then the C_{Re} is equal to

$$C_{\mathrm{Re}} = 0.0791\,\mathrm{Re}^{0.75}$$

3.2 Friction factor and heat transfer correlation

Compact heat exchangers are easy to manufacture and show excellent performance; they allow a rather complex flow channel organization, which makes them suitable for Stirling engines. However, new questions surround their study, primarily if the Navier-Stokes equation still hold for tiny channels and if the classical heat transfer correlations still hold. The main disadvantage lies in the regime of the fluid, due to the small size of the channels the flow is laminar; thus the heat transfer will be less than if the stream was turbulent. It is relevant to mention that compact heat exchangers covered millimeter channel size. Adam and Coll [51] have studied micro-channels (0.76 to 1.09 mm in diameter), their results show that the Nusselt number is higher than the ones predicted by the classical correlations[52] (see Eq. 3.2.1)

$$\mathrm{Nu} = 1.86(\mathrm{Re}\ \mathrm{Pr})^{1/3} \left(\frac{D_h}{L}\right)^{1/3} \left(\frac{\mu}{\mu_p}\right)^{0.14} \qquad \mathrm{Re} < 2000 \qquad (3.2.1a)$$

$$\mathrm{Nu} = 1.116(\mathrm{Re}^{2/3} - 125)\left[1 + \left(\frac{D_h}{L}\right)^{2/3}\right] \left(\frac{\mu}{\mu_p}\right)^{0.14} \qquad 2200 < \mathrm{Re} < 10000 \qquad (3.2.1b)$$

$$\mathrm{Nu} = 0.023\mathrm{Re}^{0.8}\mathrm{Pr}^{0.4} \qquad \mathrm{Re} > 10000 \qquad (3.2.1c)$$

where D_h is the hydraulic diameter, L is the channel length and, μ is the viscosity. For smaller diameters ($D_h < 0.8$) Zhang [53] suggest a new correlation, see Eq. 3.2.2.

$$\mathrm{Nu} = 0.021(\mathrm{RePr})^{0.7} \qquad \mathrm{Re} > 600 \qquad (3.2.2)$$

Experiments done by Luo et. al [54] show that for classical correlations: For Re $<$ 800 the values were 20% lower and Re $>$ 800 the values were 30% higher, which means that even for millimeter size channels, the improvement can be observed to classical heat transfer correlations.

Thomas and Pittman [55] presented an updated overview of different correlations for the friction and heat transfer of Stirling engine regenerator. The first

correlations were developed by Gedeon and Wood [2], who studied the oscillating-Flow inside the regenerator.

As it was discussed early in this chapter, the regenerator is a crucial device when efficiency and effectiveness are needed. Gedeon and Wood first collected the data under the contract of NASA Glenn Research Center. The significant contribution lies in the acquisition of the flow friction and heat transfer under oscillation flow conditions for a variety of Reynold numbers, flush ratio, wire diameter, mesh width and porosity. The correlations were derived for both wire screens, and metal felts. The morphological constraints and the governing equations are presented in Table 3.1 and 3.2.

Table 3.1: Friction factor correlation for the regenerator [2]

Matrix material	Wire screen	Metal felt
Number of samples	3	5
Wire diameter range	$0.0533 \rightarrow 0.094$ mm	$0.0128 \rightarrow 0.0508$ mm
Porosity range	$0.6232 \rightarrow 0.781$	$0.688 \rightarrow 0.8405$
Re_{max} range	$1.04 \rightarrow 3400$	$0.79 \rightarrow 1400$
Valensi range	$0.0052 \rightarrow 21$	$0.0021 \rightarrow 5.6$
Range of tidal amplitude ratio	$0.028 \rightarrow 2.2$	$0.043 \rightarrow 2.6$
Equation for porosity	$\varepsilon = 1 - \frac{V_{mat}}{V_{tot}}$	$\varepsilon = 1 - \frac{V_{mat}}{V_{tot}}$
Equation for flow velocity	$u = \frac{u_0}{\varepsilon}$	$u = \frac{u_0}{\varepsilon}$
Equation for Reynolds number	$\mathrm{Re} = \frac{d\varepsilon u}{(1-\varepsilon)\nu}$	$\mathrm{Re} = \frac{d\varepsilon u}{(1-\varepsilon)\nu}$
Equation for pressure drop	$\Delta P = c_f u^2 \frac{L(1-\varepsilon)\rho}{2d\varepsilon}$	$\Delta P = c_f u^2 \frac{L(1-\varepsilon)\rho}{2d\varepsilon}$
Friction factor correlation	$c_f = \frac{129}{\mathrm{Re}} + \frac{2.91}{\mathrm{Re}^{0.103}}$	$c_f = \frac{192}{\mathrm{Re}} + \frac{4.53}{\mathrm{Re}^{0.067}}$

Table 3.2: Nusselt number correlation for the regenerator [2]

Matrix material	Wire screen	Metal felt
Number of samples	3	5
Wire diameter range	$0.0533 \rightarrow 0.094$ mm	$0.0128 \rightarrow 0.0508$ mm
Porosity range	$0.6232 \rightarrow 0.781$	$0.688 \rightarrow 0.8405$
Re_{max} range	$1.04 \rightarrow 3400$	$0.79 \rightarrow 1400$
Valensi range	$0.0048 \rightarrow 16$	$0.0037 \rightarrow 3.3$
Range of tidal amplitude ratio	$0.17 \rightarrow 3$	$0.17 \rightarrow 3.8$
Equation for porosity	$\varepsilon = 1 - \frac{V_{mat}}{V_{tot}}$	$\varepsilon = 1 - \frac{V_{mat}}{V_{tot}}$
Equation for flow velocity	$u = \frac{u_0}{\varepsilon}$	$u = \frac{u_0}{\varepsilon}$
Equation for Reynolds number	$\mathrm{Re} = \frac{d\varepsilon u}{(1-\varepsilon)\nu}$	$\mathrm{Re} = \frac{d\varepsilon u}{(1-\varepsilon)\nu}$
Equation for specific heat transfer area	$\varphi = \frac{A}{V_{tot}} = \frac{4}{d}(1-\varepsilon)$	$\varphi = \frac{A}{V_{tot}} = \frac{4}{d}(1-\varepsilon)$
Nusselt number	$\mathrm{Nu} = \frac{\alpha d\varepsilon}{\lambda(1-\varepsilon)}$	$\mathrm{Nu} = \frac{\alpha d\varepsilon}{\lambda(1-\varepsilon)}$
Nusselt number correlation	$\mathrm{Nu} = \left(1 + 0.99(\mathrm{RePr})^{0.66}\right)\varepsilon^{1.79}$	$\mathrm{Nu} = \left(1 + 1.16(\mathrm{RePr})^{0.66}\right)\varepsilon^{2.61}$
Overall thermal regenerator loss	$\frac{\dot{Q}_{\text{Reg-loss}}}{\lambda A_{\text{free}}\Delta T} = \frac{0.194(\mathrm{Re}_{max}\mathrm{Pr})^{1.3}}{\varepsilon^{1.81}}$	$\frac{\dot{Q}_{\text{Reg-loss}}}{\lambda A_{\text{free}}\Delta T} = \frac{0.253(\mathrm{Re}_{max}\mathrm{Pr})^{1.24}}{\varepsilon^{2.67}}$

Correlations from Tables 3.1 predict the highest friction factor due to oscillation flow; also Gedeon and Wood measured the p-V power dissipated by the fluid in the regenerator in comparison with Kühl [56] that measured pressure drop. Moreover, the results show that friction factors of metal felt are greater than those for wire screens, especially for higher Reynolds numbers, one possibility is that the random structure of the metal felt yields a higher drag. Thus wire screens are preferred for minimizing regenerator pressure drop according to Thomas et al.[55].

To calculate the correlations from Table 3.2, Gedeon and Wood measured the net axial heat flux along the regenerator as its overall thermal loss [2]. They separate the total loss into a fraction caused by the limited heat transfer, which is the Nusselt number correlation and the rest was attributed to an enhanced axial conduction.

In Tables 3.1 and 3.2, d is the wire diameter, L is the total length of the matrix, A is the gross heat transfer area, A_{net} is the net heat transfer area, V_{mat} is the volume of matrix material, V_{tot} is the total volume of regenerator ν is the kinetic viscosity of the fluid and λ is the thermal conductivity of fluid.

Significant correlations have been developed for heat transfer and pressure loss for the regenerator. To study the phenomena inside the heater and the cooler, Kuosa et al. [57] present a comparison of different correlations and also, the enhancement of heat transfer by adding slots inside the tubes.

Turbulent relationships developed by Dittus and Boelter [58] have been commonly used to calculate the heat transfer coefficient and friction factor for oscillating flow. Unidirectional approximations are accurate when the regime is fully laminar or fully turbulent [57].

In an oscillatory flow, the maximum velocity is achieved near the wall rather than in the center of the channel; this was first discovered by Richardson and Tyler in 1929 [59] the so-called " annular effect" especially applies at higher cycle frequencies [60].

Table 3.3 shows the heat transfer correlations:

1. Tang and Cheng [61] obtained experimental correlations for the cycle-averaged Nusselt number in terms of Re, Re_ω and A_ω, they used air as the working fluid for the range of the following parameters: $7 < \mathrm{Re} < 7000$, $7 < \mathrm{Re}_\omega < 180$ and $0.06 < A_\omega < 2.21$.

2. Zhao and Cheng [62] used only two parameters, Re_ω and A_0 ($0 < \mathrm{Re}_\omega < 500$ and $A_0 = 8.5, 15.3, 20.4$ and 34.9).

3. De Monte et al. correlation for oscillating flow.[63]

4. Walther et al. [60] analyses the influence of developing flow associated with laminar oscillating flow. Their correlation stands for a range of values: $1000 \leq \mathrm{Re}_{max} \leq \mathrm{Re}_{max}^{trans}$, $50 \leq \mathrm{Re}_\omega \leq 900$,$0.2 \leq \Lambda \leq 900$, where $\mathrm{Re}_{max}^{trans} = 400\sqrt{\mathrm{Re}_\omega}$.

5. Dittus-Boelter [64] (Classical correlation)

6. Petukhov and Popov [65] (Classical correlation)

7. Gnielinski [66] (Classical correlation)

The Darcy (c_f) and Fanning (λ) factors are widely used in the literature to calculate losses due to friction. There is a Reynolds number dependency for the drag coefficient λ within the duct. Depending on the regime, either laminar

$$c_f = \frac{64}{\mathrm{Re}}, \qquad \mathrm{Re} < 2000 \tag{3.2.3}$$

or turbulent flow

$$c_f = 0.079\mathrm{Re}^{-0.25}, \qquad \mathrm{Re} > 10^5 \tag{3.2.4}$$

Table 3.3: Classical and oscillating heat transfer correlations for the heater and cooler

1	$\mathrm{Nu} = -0.494 + 0.0777\left(\frac{A_\omega}{1+A_\omega}\right)^2 \mathrm{Re}^{0.7} - 0.00162\mathrm{Re}^{0.4}\mathrm{Re}_\omega^{0.8}$	$A_\omega = \frac{x_{max}}{L} = \frac{\pi u_m}{\omega L} = \frac{d\mathrm{Re}}{L\mathrm{Re}_\omega}$
2	$\mathrm{Nu} = 0.02A_0^{0.85}\mathrm{Re}_\omega^{0.58}$	$A_0 = \frac{x_{max}}{d}$
3	$\mathrm{Nu} = -0.494 + 0.0777\left(\frac{A_R}{1+A_R}\right)^2 \mathrm{Re}^{0.7} - 0.00162\mathrm{Re}^{0.4}\left(4\mathrm{Re}_\omega^{0.8}\right)$	$A_R = \frac{d_h\mathrm{Re}_{max}}{4L\mathrm{Re}_\omega}$
4	$\mathrm{Nu} = 5.78 + 0.00918\mathrm{Re}_\omega^{0.969}\Lambda^{-0.367} - 0.178\left\lvert\frac{\mathrm{Re}}{\mathrm{Re}_{max}}\right\rvert^{0.951}\Lambda^{-0.703}\mathrm{Re}_\omega^{0.526}$	$\Lambda = \frac{L\mathrm{Re}_\omega}{2d\mathrm{Re}_{max}}$
5	$\mathrm{Nu} = 0.023\mathrm{Re}^{0.8}\mathrm{Pr}^{0.4}$	
6	$\mathrm{Nu} = \frac{(f/2)\mathrm{RePr}}{(1+13.6f)+(11.7+1.8\mathrm{Pr}^{-1/3})(f/2)^{1/2})(\mathrm{Pr}^{2/3}-1)}$	$f = (3.64\log\mathrm{Re} - 3.28)^{-2}$
7	$\mathrm{Nu} = \frac{(f/8)(\mathrm{Re}-1000)\mathrm{Pr}}{1+12.7(f/8)(\mathrm{Pr}^{2/3}-1)}$	$f = (0.79\ln\mathrm{Re} - 1.64)^{-2}$ $3000 < \mathrm{Re} < 10^6$

However, Zhao and Cheng [67] presented a friction coefficient for cyclically turbulent oscillatory flow Eq. 3.2.5, which covers a range of $81 \leq \mathrm{Re}_\omega \leq 540$ and $54.4 \leq A_0 \leq 113.5$

$$c_f = \frac{1}{A_0}\left(\frac{76.6}{\mathrm{Re}_\omega^{1.2}} + 0.406624\right) \tag{3.2.5}$$

"Sage Software for Engineering modeling and optimization" is software for professional developers. The software not only can simulate Stirling engines but also a variety of cryocoolers. Sage does not compete with standard CFD software. However, it provides gas flow, heat transfer, and other modeling details within several specialized model components. Sage uses many of the Nusselt number and friction factor correlations of Gedeon and Wood [2] to compute heat transfer and pressure drop. A description for more common heat exchangers is presented next along with their parameters [68]:

- Length: Heat exchanger length (m) L in the x direction.
- Roughness: The relative roughness of the surface is defined as the average height (ϵ) of surface irregularities divided by the hydraulic diameter, which is the distance among high and low points on the surface [69]. Depending on the process, roughness is determined, see Table 3.4.

Process	ϵ(microns)
cold-rolling	2 to 6
drawing	2 to 6
extruding	2 to 6
drilling	3 to 13

Table 3.4: Roughness for some processes

- A_f: Mean flow cross-sectional area (m^2), which is the void volume divided by the length.

- A_s: Mean solid cross-sectional area (m^2).
- S_x: Wetted perimeter (m) is the surface area per unit length for gas-to-solid heat transfer.
- Porosity: Porosity (β) is the void volume divided by the total volume. For matrix heat exchangers, the mean flow cross-section area A_f is defined as Eq. 3.2.6.

$$A_f = \beta A_c \tag{3.2.6}$$

- For the duct type heat exchangers, t_{wall}: Wall thickness (m) used for to determine the solid cross-sectional area.

For each heat exchanger, the correlation for friction and Nusselt number are independent. Moreover, Valensi number is another parameter used in the correlations. It is mathematically described in Eq. 3.2.7.

$$V_a = \frac{\rho \omega d_h^2}{4\mu} \tag{3.2.7}$$

Previously in Tables 3.1 and 3.2, correlations for different types of matrices have been shown. However, the purpose is to include more options for the designer.

- Random Fiber matrix, this correlation is derived from an oscillating-flow regenerator test reported by the NASA Contractor Report [2] based on the porosity dependence curve fits for the following round-wire test samples, see Table 3.5:

Table 3.5: Wire diameters studied

Type	Material	Wire diameter (microns)	Porosity
2 mil Brunswick	inconel	52.2	0.68
1 mil Brunswick	Stainless steel	27.4	0.82
12 micron Bekaert	Stainless steel	31	0.85, 0.90, 0.93 and 96
30 micron Bekaert	Fecralloy	24	0.9

The peak Reynolds number for the combined test ranged from about 1 to 3500. For the correlations below the parameter, α is porosity dependence.

Friction factor

$$c_f = \frac{a_1}{\mathrm{Re}} + a_2 \mathrm{Re}^{a_3} \tag{3.2.8}$$

where

$$\alpha = \frac{\beta}{1-\beta} \tag{3.2.9}$$

$a_1 = 25.7\alpha + 79.8$
$a_2 = 0.146\alpha + 3.76$
$a_3 = -0.00283\alpha - 0.0748$

Nusselt number

$$\mathrm{Nu} = 1 + b_1 \mathrm{Pe}^{b_2} \tag{3.2.10}$$

where
$b_1 = 0.186\alpha$
$b_2 = 0.55$
$\mathrm{Pe} = \mathrm{RePr}$

- Sphere matrix, for the wetted perimeter (S_x)

$$S_x = 6(1-\beta)A_c/d_s \tag{3.2.11}$$

where A_c is the canister cross-section area, and d_s is the sphere diameter. The correlations are based on unpublished oscillating-flow regenerator test [68].

Friction factor

$$c_f = \left(\frac{157}{\mathrm{Re}} + 5.15\mathrm{Re}^{-0.137}\right)\left(\frac{\beta}{0.39}\right)^{3.48} \tag{3.2.12}$$

Nusselt number

$$\mathrm{Nu} = 1 + 0.48\mathrm{Pe}^{0.65} \tag{3.2.13}$$

- Foil matrix, for the wetted perimeter (S_x),

$$S_x = 2A_f/g \tag{3.2.14}$$

and the porosity is defined as

$$\beta = \frac{1}{1 + b/g} \tag{3.2.15}$$

Friction factor

  - Laminar regime

$$c_f = 96/\mathrm{Re} \tag{3.2.16}$$

  - Turbulent regime

$$c_f = 0.121\left(\frac{\epsilon}{d_h} + \frac{68}{\mathrm{Re}}\right)^{0.25} \tag{3.2.17}$$

Nusselt number

The laminar case is based on exact theory for fully-developed flow,uniform heat flux, and turbulent case is from reference [46].

  - Laminar regime

$$\mathrm{Nu} = 8.23 \tag{3.2.18}$$

– Turbulent regime

$$\mathrm{Nu} = 0.025\mathrm{Re}^{0.79}\mathrm{Pr}^{0.33} \tag{3.2.19}$$

- Tubular bundle, for the flow area (A_f)

$$A_f = n\frac{\pi}{4}d_i^2 \tag{3.2.20}$$

where,
n: number of elements.
Solid cross-section area is calculated in terms of outside diameter and wall thickness,

$$d_o = d_i + 2t_w \tag{3.2.21}$$

$$A_s = n\frac{\pi}{4}\left(d_o^2 - d_i^2\right) \tag{3.2.22}$$

and the wetted perimeter is calculated

$$S_x = n\pi d_i \tag{3.2.23}$$

Friction factor for the tubular case depends on the Valensi number (V_a). It is calculated from Eq. 3.2.24

– Laminar regime

$$c_f = \frac{16s}{\mathrm{Re}} \tag{3.2.24}$$

$s = 4$ if $V_a \leq 32$
$s = \sqrt{V_a/2}$ if $V_a > 32$

– Turbulent regime

$$c_f = 0.11\left(\epsilon/d_h + 68/\mathrm{Re}\right)^{0.25} \tag{3.2.25}$$

Nusselt number

– Laminar regime

$$\mathrm{Nu} = 6 \tag{3.2.26}$$

– Turbulent regime

$$\mathrm{Nu} = 0.036\mathrm{Re}^{0.8}\left(L/d_h\right)^{-0.055}\mathrm{Pr}^{0.33} \tag{3.2.27}$$

- Rectangular channels, the flow area is

$$A_f = nw_ih_i \tag{3.2.28}$$

where,
n: number of elements,
the solid cross-section area is

$$A_s = n(w_oh_o - w_ih_i) \tag{3.2.29}$$

where $w_o = w_i + 2t_w$ and $h_o = h_i + 2t_w$

the wetted perimeter is $S_x = 2n(w_i + h_i)$
$a = w_i/h_i$
$b = 1.47 - 1.48a + 0.92a^2$
$c = 0.438 + 0.562(1 - a)^3$

Friction factor

- Laminar regime, friction factor is calculated from Eq.3.2.24
  $s = 4b$ if $V_a \leq 32b^2$
  $s = \sqrt{V_a/2}$ if $V_a > 32b^2$
- Turbulent regime

$$c_f = 0.11(\epsilon/d_h + 68/\mathrm{Re})^{0.25} \tag{3.2.30}$$

Nusselt number

- Laminar regime

$$\mathrm{Nu} = 10c \tag{3.2.31}$$

- Turbulent regime

$$\mathrm{Nu} = 0.035\mathrm{Re}^{0.75}\mathrm{Pr}^{0.33} \tag{3.2.32}$$

The Nusselt number (Nu) is defined as the ratio of heat transfer due to convection over the heat transfer due to conduction, see Eq. 3.2.33 .

$$\mathrm{Nu} = \frac{\dot{q}_{conv}}{\dot{q}_{cond}} \tag{3.2.33}$$

In Fig. 3.3a a fluid with temperature T_1 passes around a body with temperature T_2, while the fluid moves it exchanges some heat with the body, this phenomenon is known as convection. In Fig. 3.3b two blocks are in contact with each other; there is no moving part; the heat is transferred due to conduction.

(a) Heat transferred due to convection (b) Heat transferred due to conduction

Figure 3.3: Transport mechanisms

$$\dot{q}_{conv} = h\Delta T \tag{3.2.34}$$

where,
h: Convection heat transferred unit $\left(\frac{W}{m^2\,K}\right)$

$$\dot{q}_{cond} = k\frac{\Delta T}{L} \tag{3.2.35}$$

where,
k: thermal conductivity and depends on the material $\left(\frac{W}{m\,K}\right)$.

Thus,

$$\mathrm{Nu} = \frac{\dot{q}_{conv}}{\dot{q}_{cond}} = \frac{h\Delta T}{k\dfrac{\Delta T}{L}} = \frac{h\,L}{k} \tag{3.2.36}$$

Besides, Nusselt number is an important parameter because it described how the heat is transferred, if there is a high convective force, the Nusselt number will be greater, but if there is a low Nusselt number, it means that most of the heat transfer has been done due to conduction. Then, from Eq. 3.2.36 the convection heat transferred unit (h) can be calculated.

The volume calculation for the three heat exchangers is essential. Those volumes are required by Eq. 2.2.4. Then, it can be computed base on their matrix type and canister (if needed). Based on Eq. 3.2.37 and Eq. 3.2.6 the volumes can be quantified.

$$V = A_f L \tag{3.2.37}$$

All the mentioned correlations are the basement for the design of the heat exchangers, which are essential devices within the Stirling engine. Depending on the type of matrix of the heat exchangers, in the calculation of the engine. The next chapter includes software designed to calculate the friction factor and the Nusselt correlation readily.

Chapter 4

Design methodology for free piston Stirling engines

In compliance with the general objective of this thesis, this chapter presents the design methodology for a FPSE with the support of a user interface. This includes a procedure to be used as a guide, designed to help the engineer, for completing a functional design of a FPSE. This methodology is different from a simple performance evaluation, given the fact that the initial design is not available, but it is entirely developed from the initial design steps. This implies the assumption of boundary conditions, or inputs, in order to obtain a FPSE which accomplishes those input conditions.

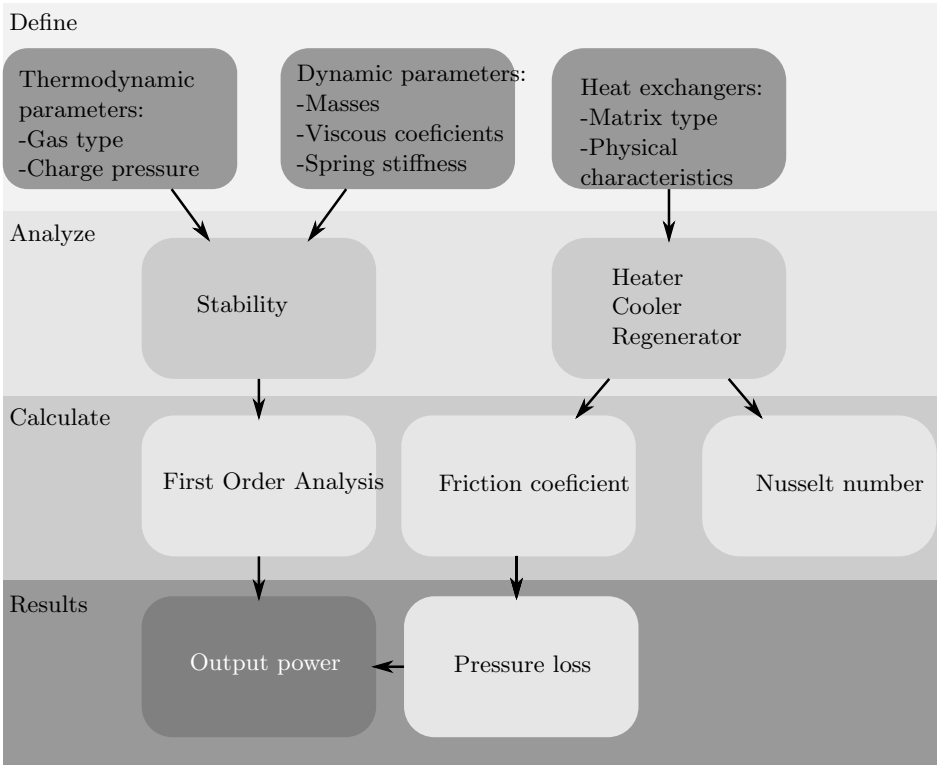

Figure 4.1: Methodology diagram

A Graphical User Interphase (GUI) was developed in this thesis in order to accomplish the design procedure in a faster way, because of the amount of design parameters involved. A deeper explanation regarding the GUI is given in detail in next sections. Several steps are needed to successfully design a FPSE. Roughly, four tasks are executed: Define, Analyze, Calculate and show the results. See Figure 4.1

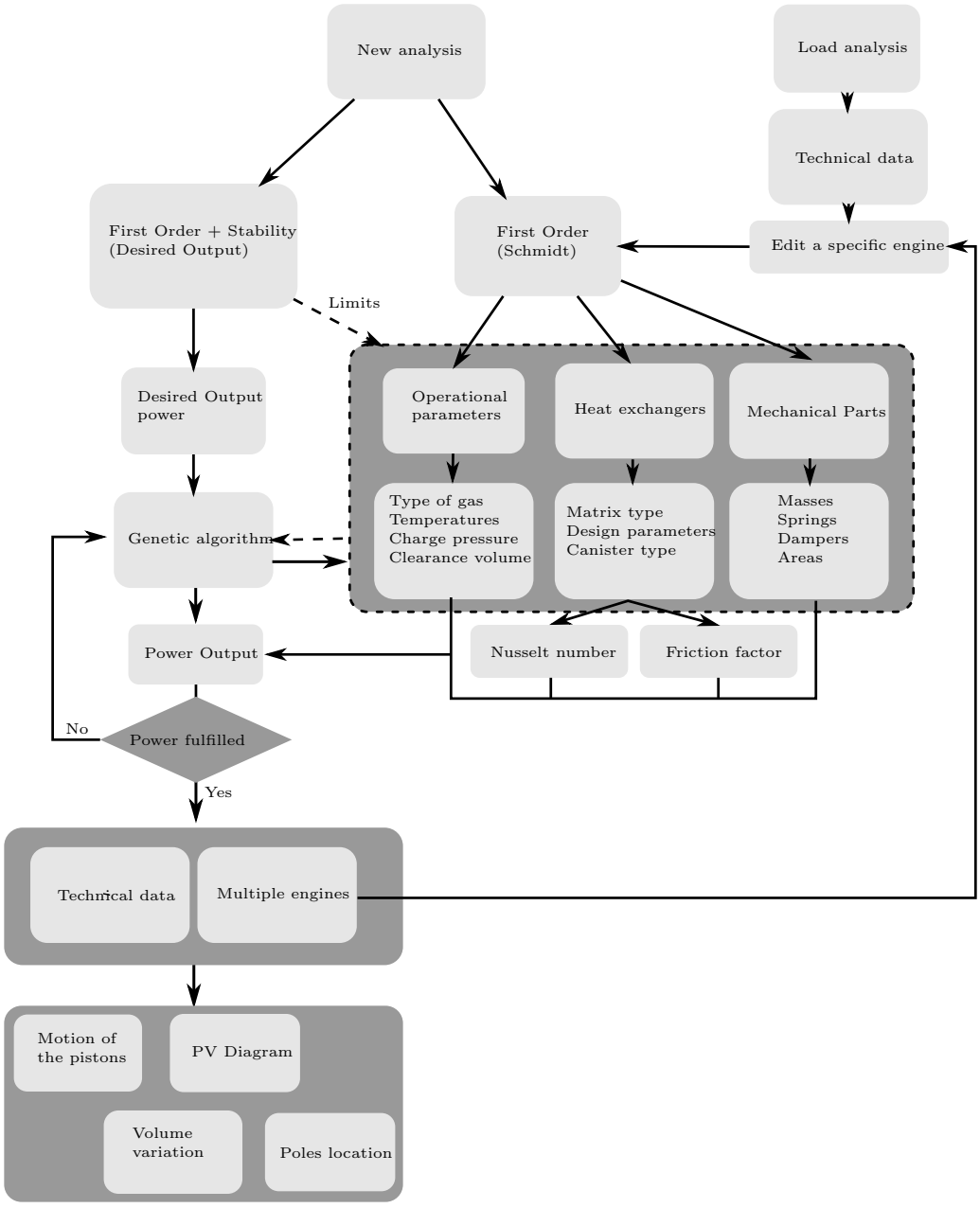

Figure 4.2: GUI Structure diagram

The design procedure consists in using primary the "Schmidt+stability analysis" and then the "first order analysis" (Fig. 4.2). The former allows obtaining the appropriate engine configuration to fulfill the desired power and the stability criterion. The later allows refining the values of the corresponding design parameters.

The designer can decide the number of different engines that meet the required input power. The criteria for selecting one engine can be summarized as follows: An important criterion is the engine efficiency. The designer can choose the machine with higher efficiency, but several considerations must be taken into account. The developed code can offer operational conditions that deserve attention like, for instance, gas temperatures difficult to implement, say 2000 K in the hot space. This is because the code does not limit the temperature value, due to the computational cost that this implies. This means that in order to save calculation time, a limit value for the gas temperature is not set. Then, it is easier that the designer himself can make this differentiation. An acceptable range for a given engine can be from 300K to 700K.

Another criterion is the ratio of the displacer and piston masses. Because the FPSE is a purely dynamical engine, this parameter is also important. The mass of the displacer should be less than that of the piston, as discussed in Section 1.2.

4.1 Solution based on nature

Evolution has played the primary roll in nature, the mixing and mutation of genes create new combinations in the DNA, despite the similar characteristics, a new offspring can be better than its predecessor. This though is the foundation for the Genetic Algorithm.

The algorithm tries to mimic the logic of nature; the more fitted chromosomes are allowed to "reproduce" their genes to form a next and probably a better generation and the less capable "died" then the new generation repeat the cycle, so the enhancement of the species continues, on this case till the convergence of a solution [70].

The implementation of the algorithm simplifies the natural evolution in five steps; those are going to be more in-depth described in the next section, for know they mention below:

1. Initial Population
2. Fitness function
3. Selection
4. Crossover
5. Mutation

Initial population

To begin with the algorithm it's necessary to create the first generation of individuals, each of them are a particular solution for the problem tended to solve (not necessary a good solution). These individuals are described by a set of parameters named genes which are equivalent to variables; a collection of genes creates a chromosome that is a solution.

Fitness function

A fitness function determines how capable an individual compares to the rest of the population; each is graded, and this will determine the availability to reproduce itself. The fitness function score is proportional to the difference between the desired power and the computed power.

$$e = (1 - P_c/P_d) \times 100$$

where e is the score, P_c is the power computed and P_d is the power desired, if P_c is greater than P_d then.

$$e = (1 - P_d/P_c) \times 100$$

Selection

As natural selection determines how a population could grow and the fittest individual can pass their genes to the next generation, something similar occurs with the population in the algorithm, based on their fitness function score they are either killed or allow to reproduce.

Crossover

Crossover is used to mix some genes from their parents to a couple of newborn individuals with new genes and probably with better capabilities, in the algorithm how genes mix can be defined either arbitrary or in a deterministic manner.

Mutation

Stagnation in the community can be prevented using a method called mutation, although it is used randomly also is found to be helpful. It consists of modifying specific genes with a different value thus it enhance a significant diversity in the population.

4.2 Free piston Stirling engine design tool (FPSE-DT)

As the number of calculations is proportional to the number of design parameters, thus it results unpractical to use a simple machine code without a GUI. Even when the code is well-structured the job would result tedious.

As above commented, there are two options for a new analysis, named "First order+Stability" and "First order". Figure 4.3 shows the main menu of the "Free piston Stirling engine design tool". At this stage the user can select either start a new analysis or load a complete study to edit.

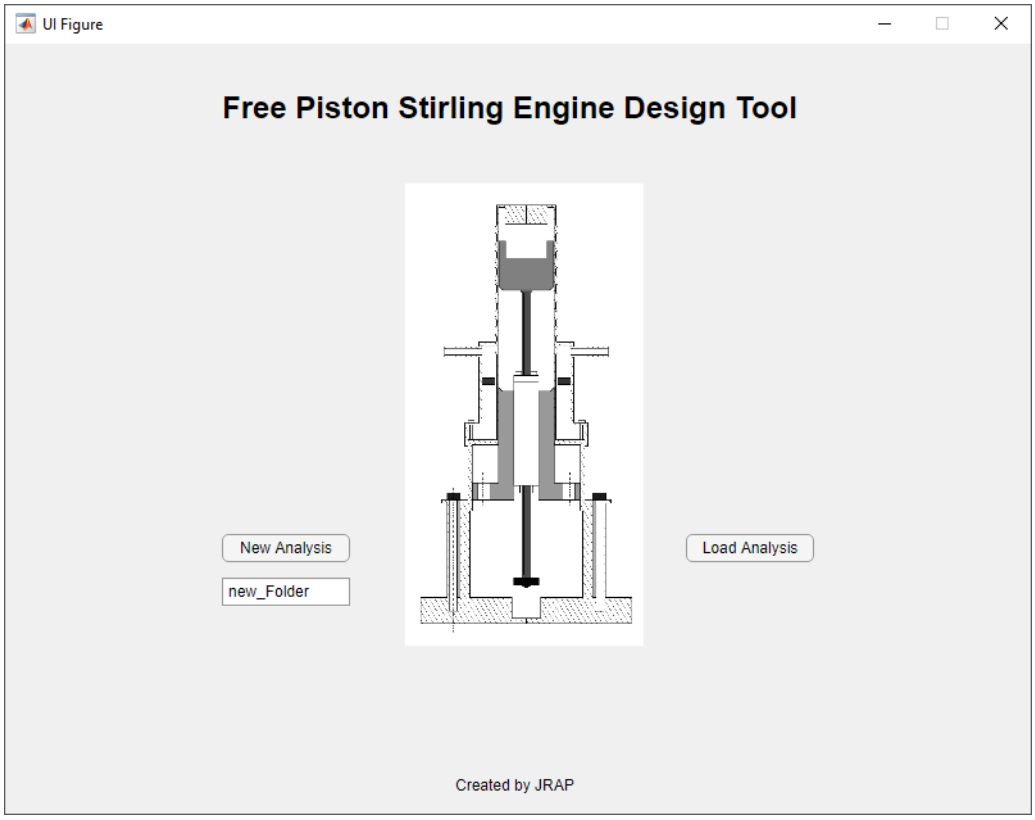

Figure 4.3: Main menu

If the user selects a “new analysis”, then a type of analysis must be chosen (Figure 4.4a). If the user selected ”First Order plus stability (Desired power)” (Figure 4.4) the software will try to find the correct settings to fulfill the power requirement.

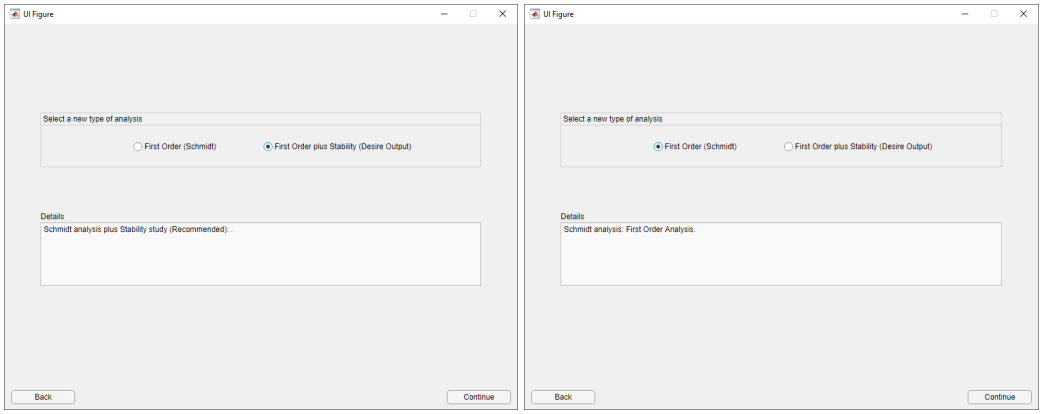

(a) New analysis menu

(b) First order analysis with desire output as main input

Figure 4.4: Analysis type selection

Figure 4.5a presents the menu for three options: Operational Parameters, Heat exchangers and Mechanical Parts, with the corresponding submenu (Figure 4.5b). Moreover, at this stage the designer can establish the desire power output.

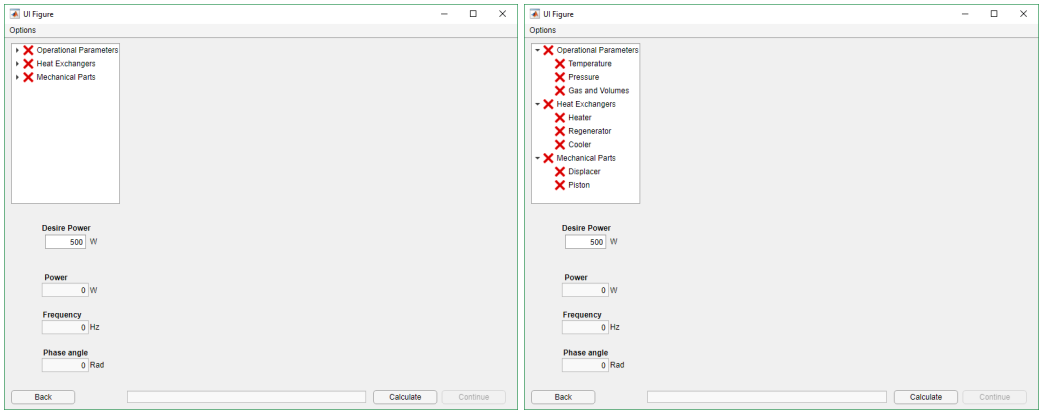

(a) Main “First Order plus stability (Desire power)” menu for the input limits

(b) Subfamilies of the three main type of parameters

Figure 4.5: Main input menu

Once an option is selected, the panel of input parameters is going visible so that the designer can fill in the requested limits, saving the data later. If the red cross changes to a green check, then it was successfully stored (Figure 4.6a and 4.6b). For the specific case of the option "Temperature" the regenerator temperature is not an input parameter, instead it is calculated from the heater and cooler temperatures. Then, after the data is saved, the regenerators temperature is displayed.

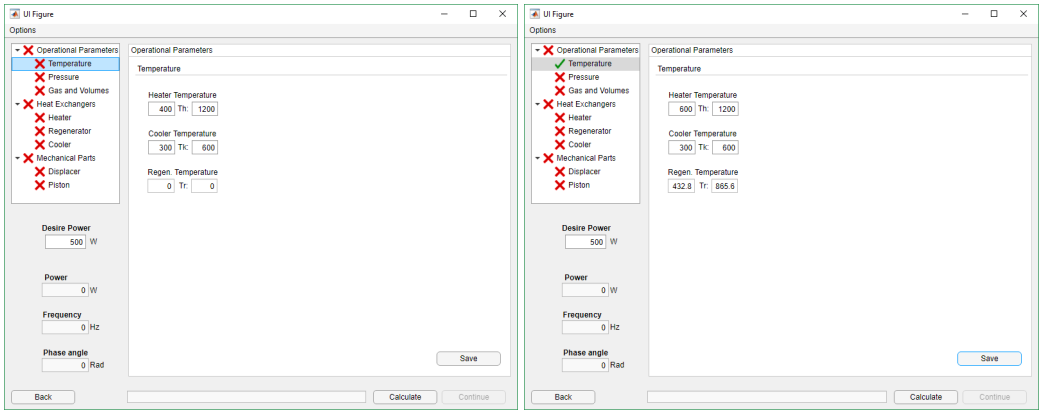

(a) Temperature input limit fields (b) Temperature parameters saved

Figure 4.6: Temperature limits input menu

Figure 4.7a shows the option “Pressure” which only includes the initial charge pressure, an important parameter to calculate the mass of the working gas, as well as other parameters for the analysis.

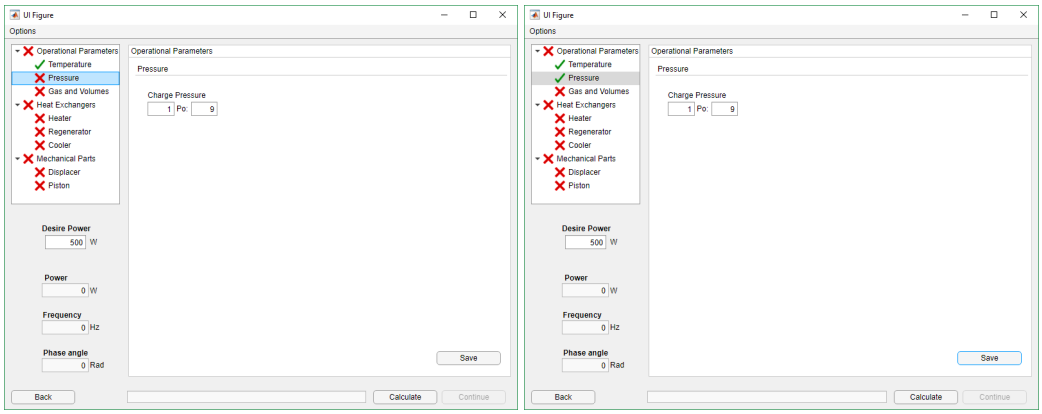

(a) Pressure menu (b) Pressure data saved

Figure 4.7: Pressure limits input menu

Similarly, the option “Gas and Volumes” deploys the working gas and the clearance volumes within the cylinder (Figure 4.8a). The gas drop menu includes Helium, Hydrogen and Air. The gas selected will establish the gas properties, e.g. dynamic viscosity, gas constant, Prantl number and density. A green check mark will appear to the left of the main menu once all submenu are filled, as illustrated in Figure 4.8b.

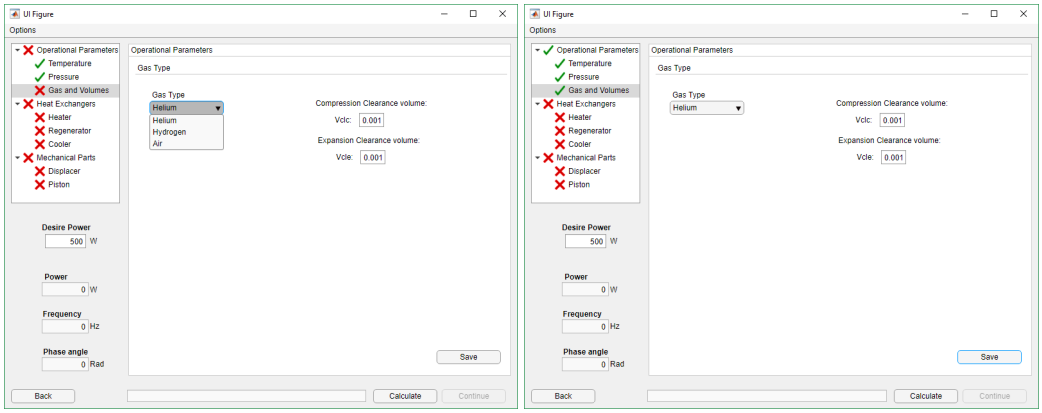

(a) Gas and Volume subfamily (b) Gas and Volume data checked and Operational Parameters successfully saved

Figure 4.8: Gas and volumes limits input menu

The heat exchanger design is one of the most important parameters for Stirling engines and one of the most complicated subsystems for the designer. Figure 4.9a shows the Heat Exchanger option, which include: Heater, Regenerator and Cooler. Each of them has a unique set of design settings, from the "Canister" shape to the "Matrix" configuration. The primary result of this section is the calculation of the Nusselt number and the friction coefficient. These two factors are critical for determining mechanical losses. Moreover, the volume for each heat exchanger is calculated based on canister morphology (Figure 4.9b) and the matrix type (Figure 4.9c).

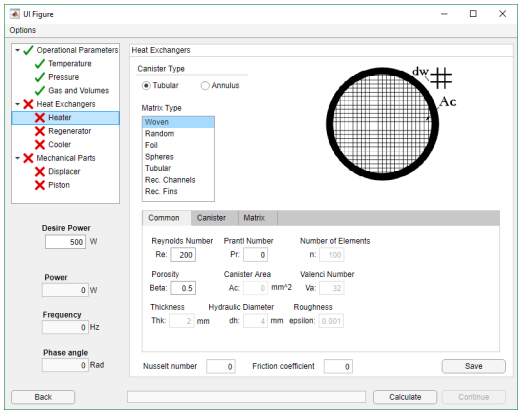

(a) Heat exchangers main menu

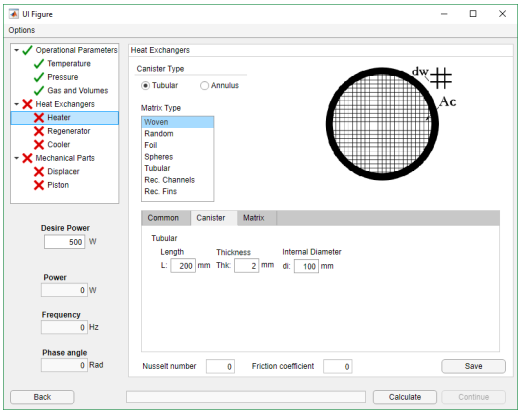

(b) Canister input variables

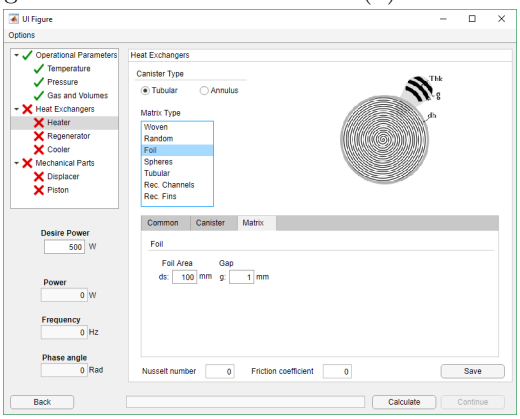

(c) Matrix parameters

Figure 4.9: Heat exchanger, canister and matrix input menus

Each subfamily has a “Save” button to confirm the filled in data. After saving the “Heater” settings the green check substitute the red cross, thus the data has been successfully loaded. The calculation of the Nusselt number and the friction coefficient is displayed after the “Save” button is clicked, see Figure 4.10a, only then the user can continue the process. This process is executed at least two more times, one for each heat exchanger, see Figures 4.10b and 4.10c.

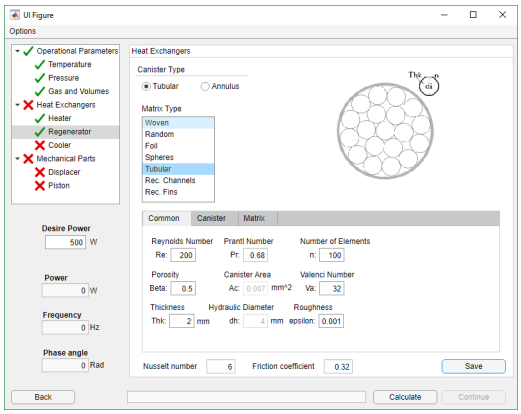

(a) Regenerator’s design menu

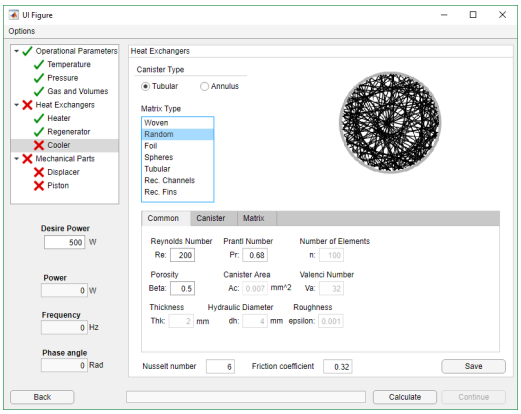

(b) Cooler’s design menu

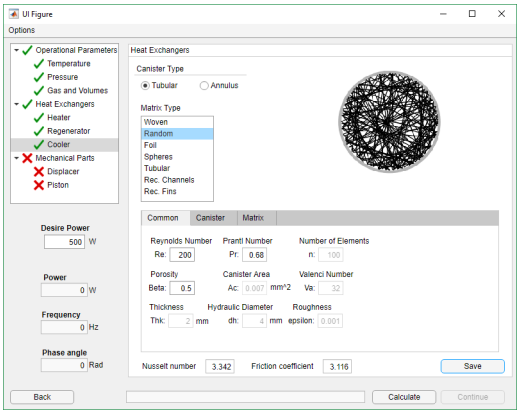

(c) Heat exchanger data loaded to the system

Figure 4.10: Heat exchangers input menu

The last parameters needed to carry out the calculations are the mechanical settings, e.g., the mass of the piston and the displacer, the spring stiffness, the areas of the pistons, among others. The major part of these parameters is directly connected to the oscillation of the system (frequency) and the phase angle between both pistons. The designer must take care of specific human considerations (the difference in the radius of the displacer and the rod diameter limits and, the ratio of mass among the piston and displacer, which needs to be positive) in order to obtain a working engine, see Figures 4.11a.

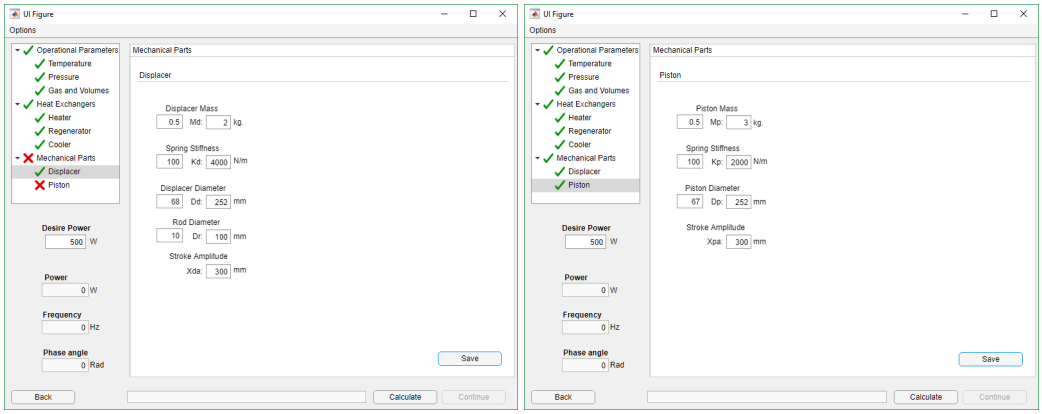

(a) Displacer input data (b) All data filled in

Figure 4.11: Mechanical Parts input menu

Once completed, the user can proceed to click the “Calculate” button, as shown in Figure 4.11b, then the algorithm starts trying to find a set of parameters that fulfill the desired power output, as in Figure 4.12a. This process may take some seconds depending on the input limits.

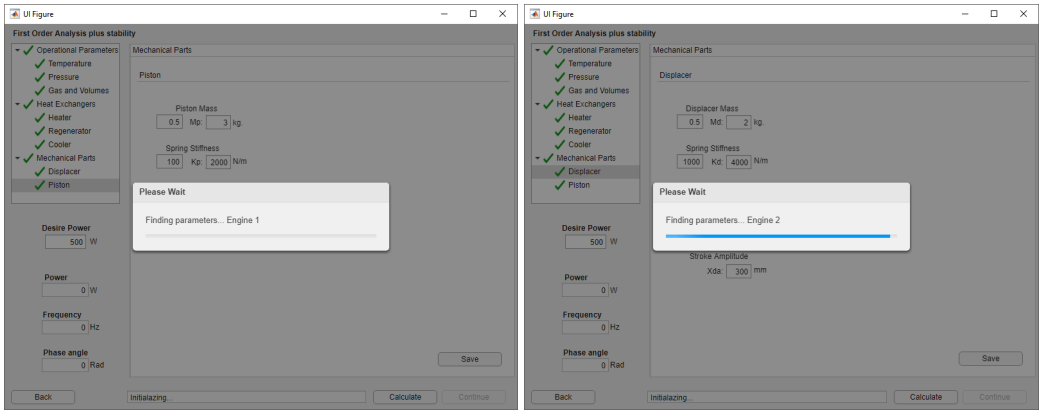

(a) Genetic Algorithm executed

(b) The blue bar will continuously show the progress of the search

Figure 4.12: Initialization and execution of the search algorithm

After the search is completed, the GUI will generate a file with the technical data of the engine. The name of this file will depend on the power achieved by the software and it is always round out to the closest greater integer, for this example the name of the file is "Data_504w_FPSE.dat", as Figure 4.13 shows. Fig. 4.14 shows a number of engines, representing diferent options which acomplish the desired power

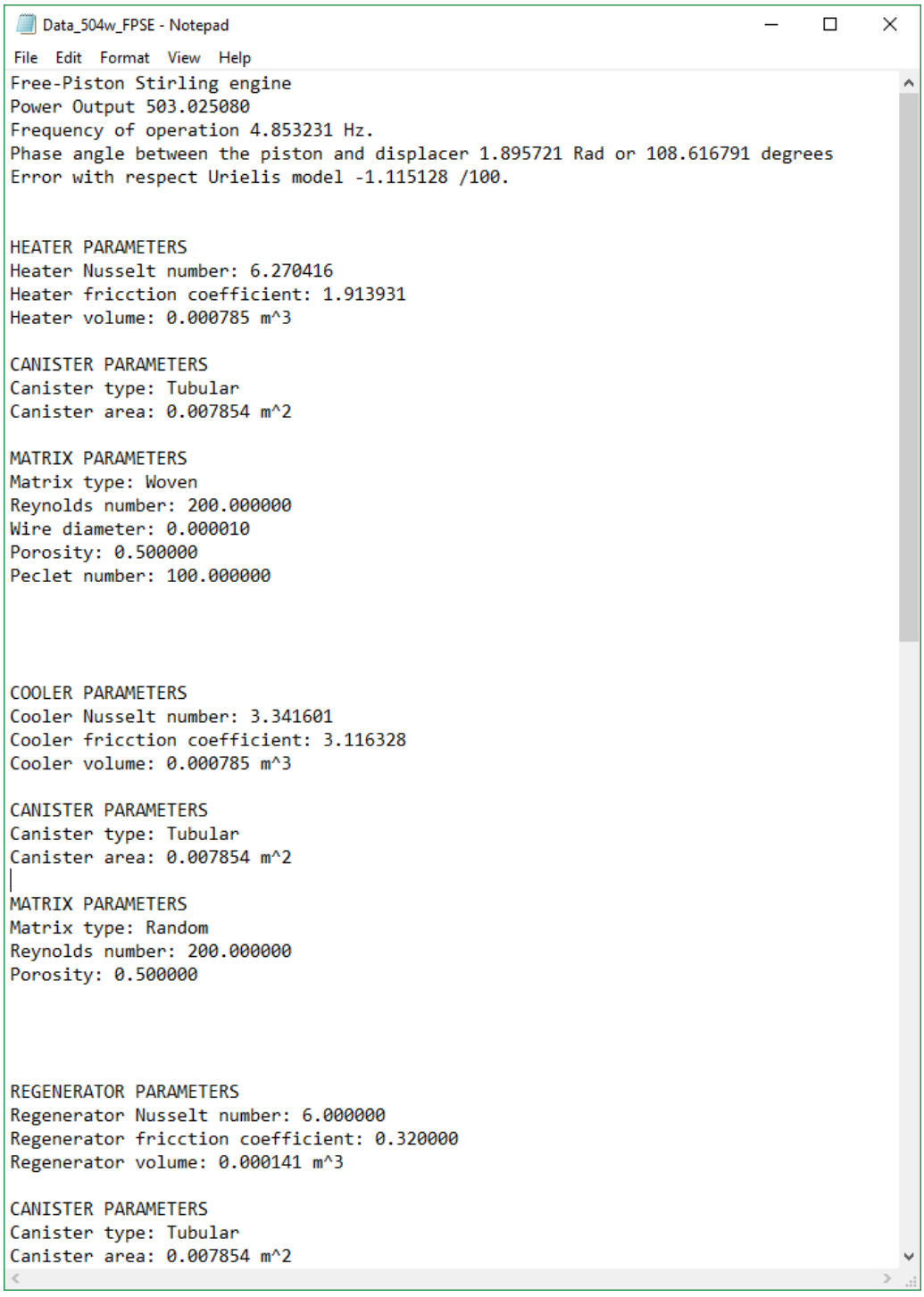

Figure 4.13: File generated by the software with the technical data

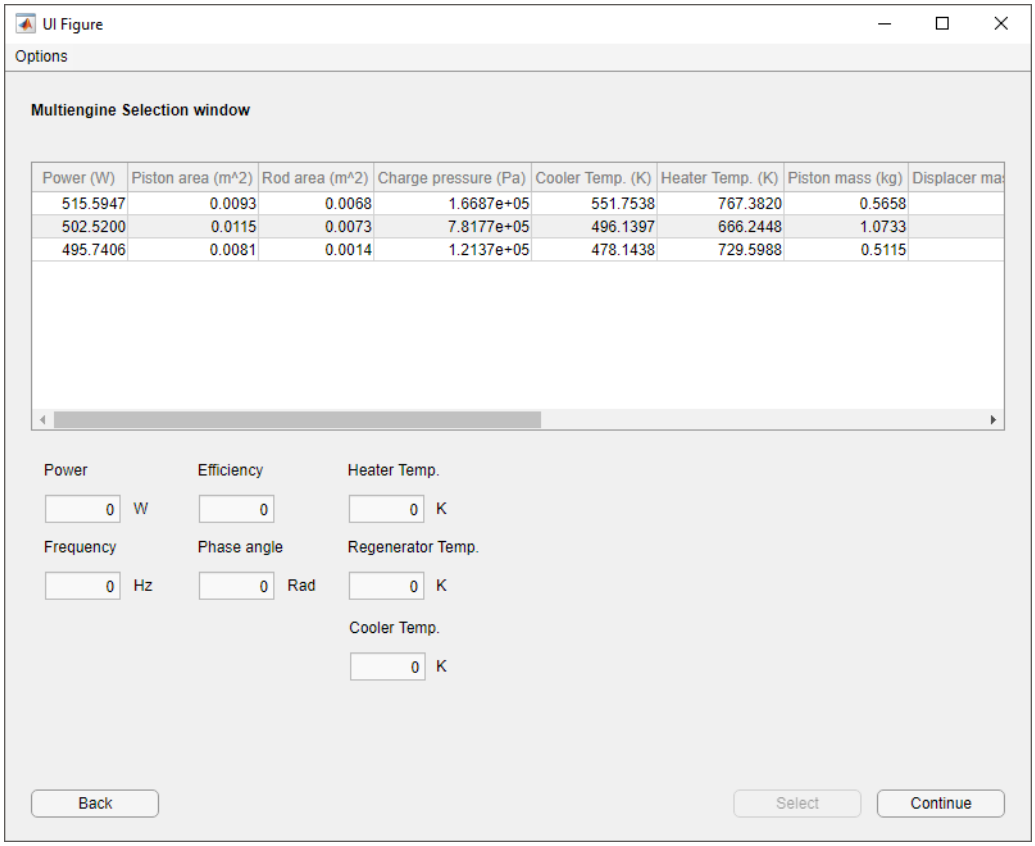

Figure 4.14: Multiple solutions

At this stage of the design, the user can finish the analysis, but if a modification is desired to refine the design values, then the GUI provides a solution for this (on the menu bar on top of the tree menu, see Figure 4.15). The option "Open in FPSE First order" must be selected. This will execute a similar interface, like the one in "First Order (Schmidt)" but with the data from the previews analysis (Figure 4.16a). However, the user has to save the data each time it is modified so the green check marks will appear again, as Figures 4.16b and 4.16c display.

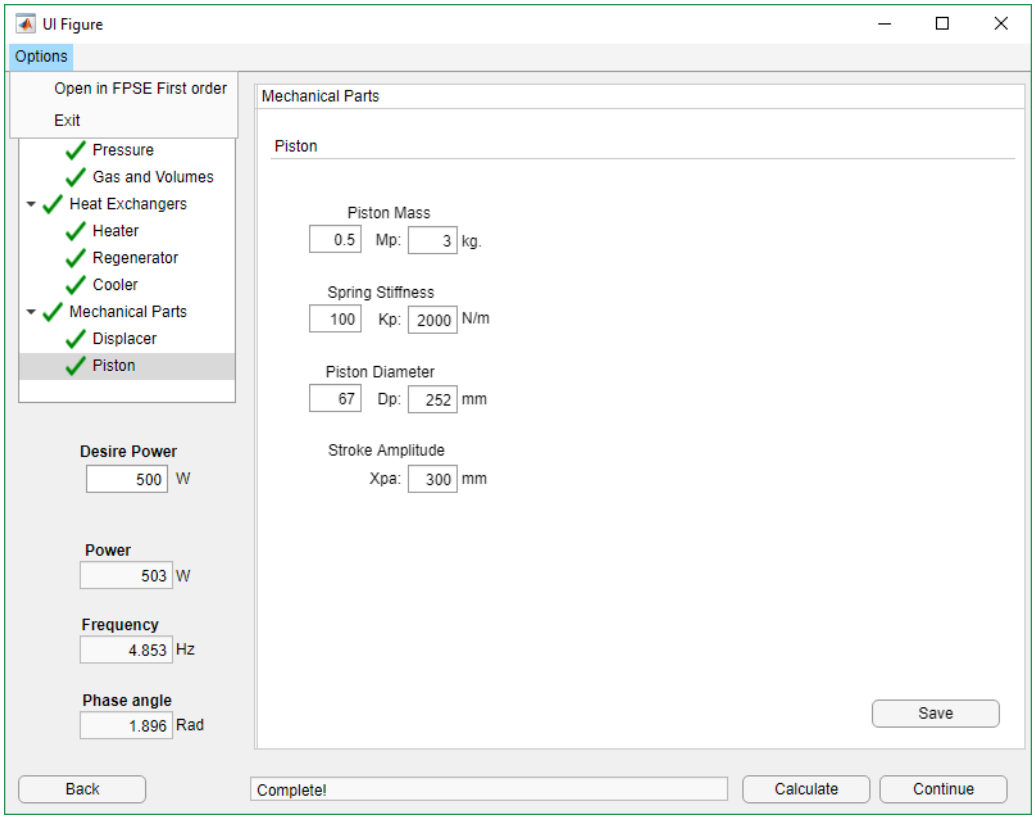

Figure 4.15: Transfer the data found to a editable environment

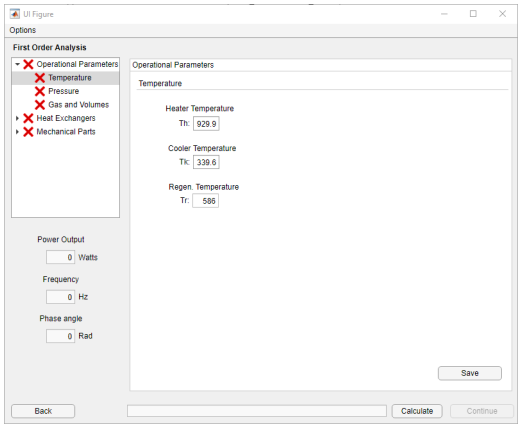

(a) Data loaded but not saved

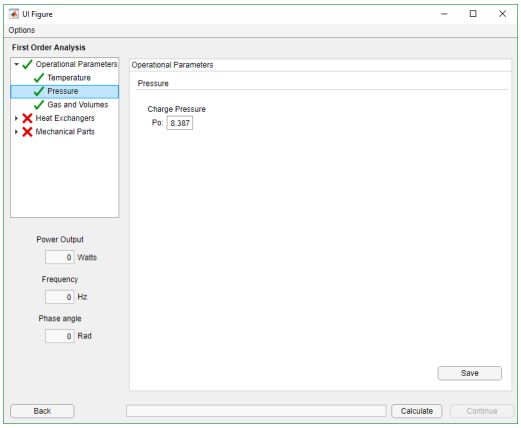

(b) Operational Parameters successfully loaded

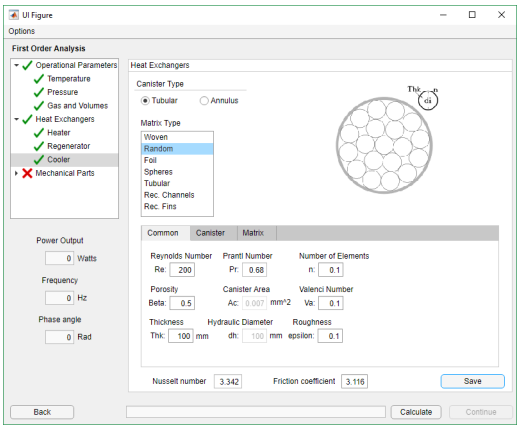

(c) Heat exchangers completed

Figure 4.16: Data loaded in the First order panel

Likewise, the “Mechanical Parts” tree item will load the data from the previews analysis (Figures 4.17a and 4.17b). Until then, the GUI allows proceeding with the calculation, and the power output, the frequency and the phase angle will be displayed in the left part of the panel, see Figure 4.18.

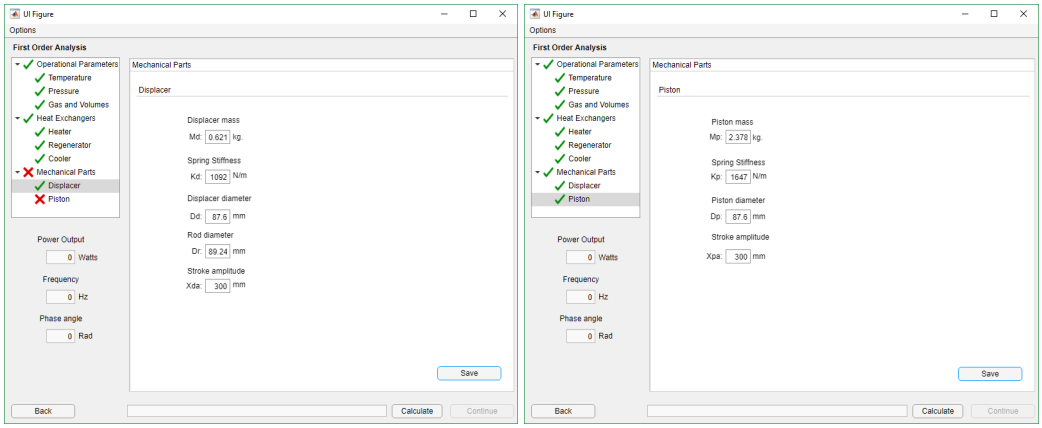

(a) Displacer parameters saved (b) Piston and displacer data saved

Figure 4.17: Mechanical Parts updated data

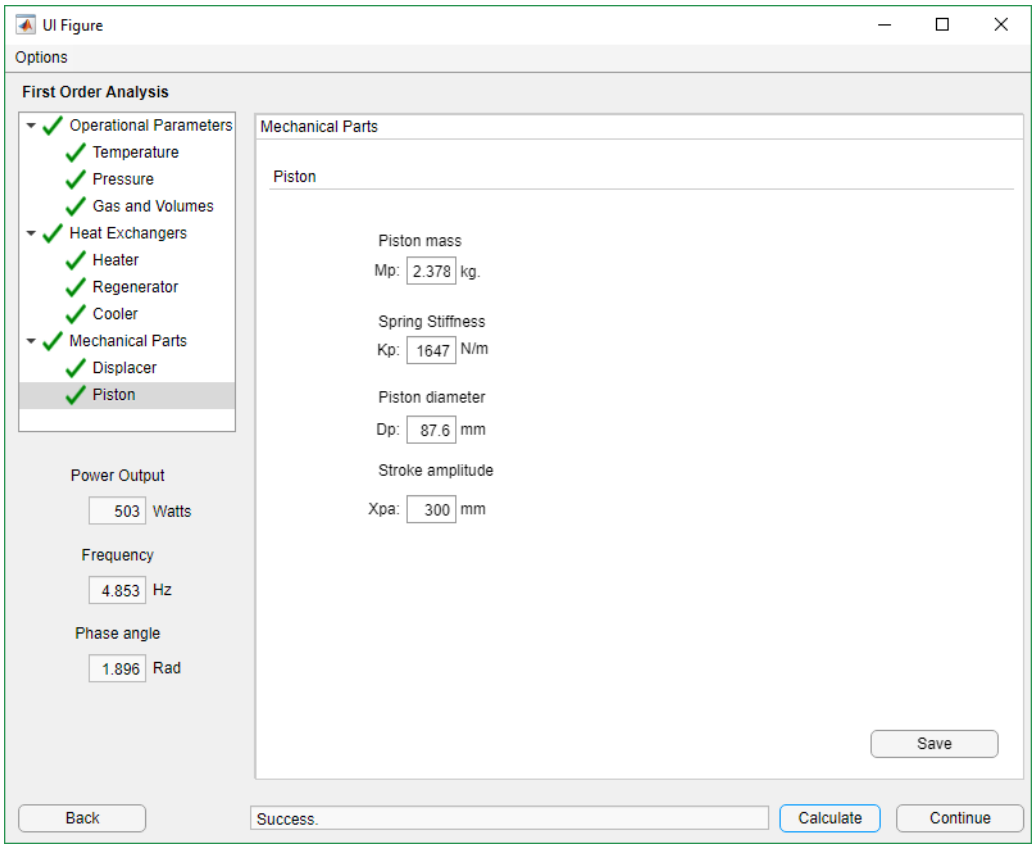

Figure 4.18: Power calculated from the search environment

After the power calculation, the user can click the “Continue” button a new window will open, and with it a group of buttons. Each button will display some results graphically. Three families group the results, “Pistons and Volumes”, “Stability” and “Heat exchangers.” See Figure 4.19.

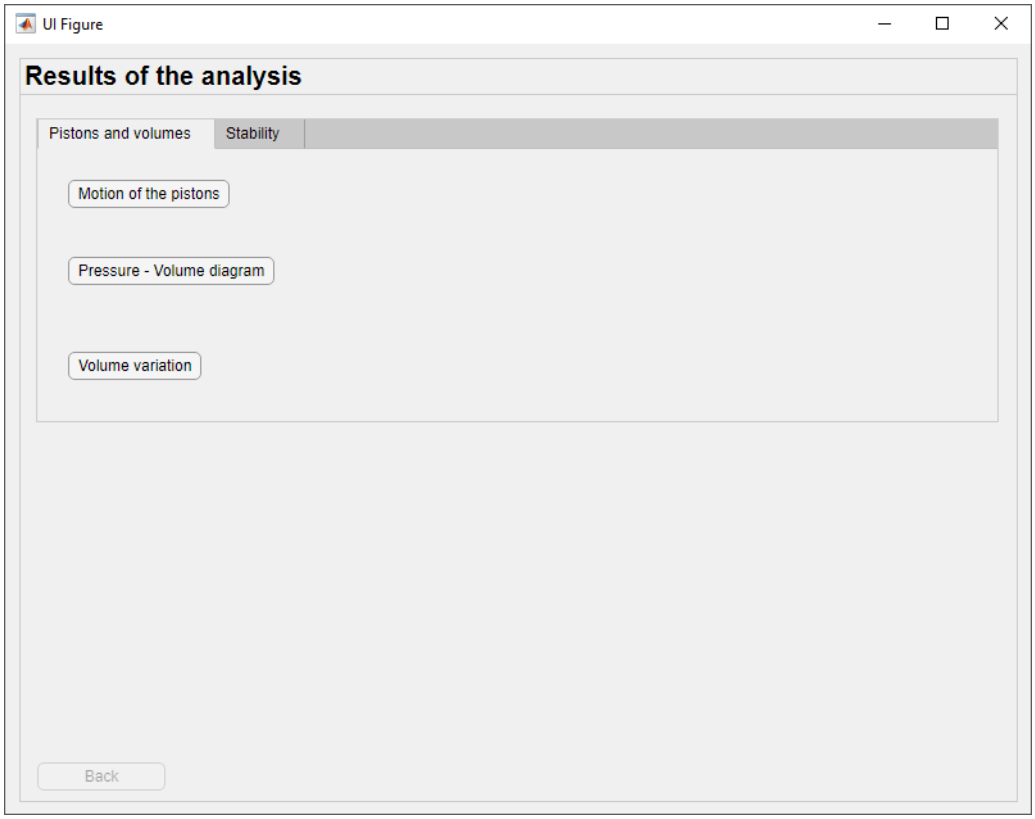

Figure 4.19: Results selection window

For a specific engine, the results are shown in Figure 4.20a for the "Motion of pistons", Figure 4.20b for the "PV Diagram", and Figure 4.20c for the "Volume variation".

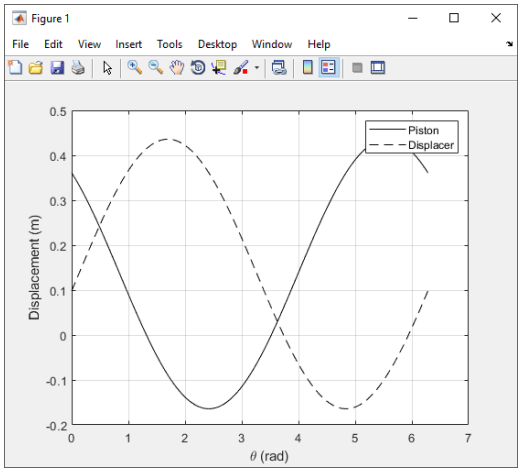

(a) Motion of pistons

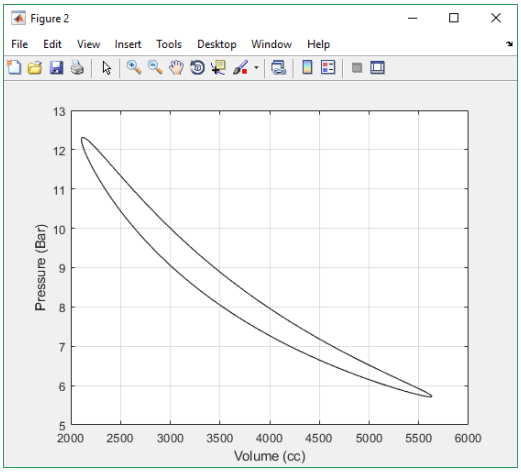

(b) PV Diagram

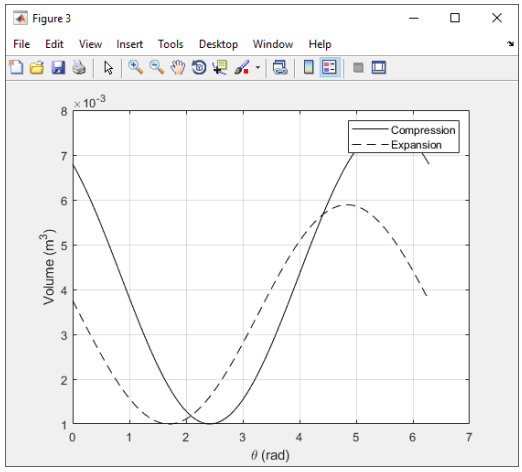

(c) Volume variation

Figure 4.20: Results for the group "Pistons and volumes"

Similarly, the results related to the stability are shown in Figure 4.21.

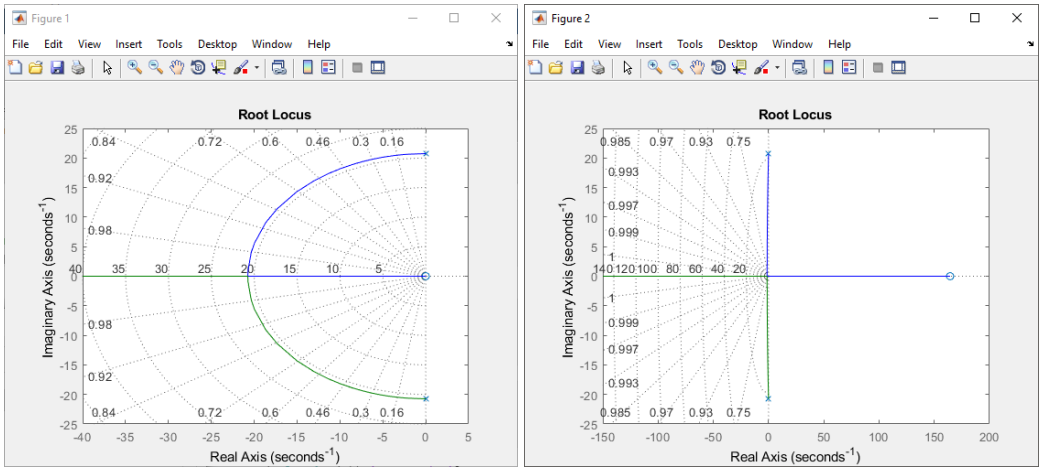

(a) Localization of piston's poles (b) Localization of displacer's poles

Figure 4.21: Localization of the system

4.3 Considerations while using the FPSE-DT

This section's primary purpose is to expose some situations while using the FPSE-DT. Although for the whole development of the thesis, the software found each time a solution to the engines that were intended to be designed, maybe the code could not find a configuration for the desired output power. Different factors could lead to this situation; the most common is that the range of values for the input limits is too narrow, so there is no solution or could take an indefinite amount of time to find it. Some analysis last over 10 minutes, but the progress bar was almost full, so probably the time spent was worthed. It is always recommended to put attention in the progress bar, and its behavior to either continue or abort the analysis. Additionally, the program has the feature to stop the study if the number of iterations for a simple engine surpasses 9000.

The next part will illustrate the design methodology using the application. The first step is to create a new analysis and name it, see Figure 4.22. Then, it is recommended to begin with the "First Order plus Stability (Desired power)" so it is selected, see Figure 4.23.

Figures 4.24 to 4.26 are the input of the "Operational parameters" this part will remain the same as the initial parameters. However, if the designer wants to narrow the limits or change them, this is the stage to do it.

For the heat exchanger part, the tubular arrangement is selected for the heater (Figure 4.27), for the regenerator, the woven matrix type is preferred (Figure 4.28), and the fin composition is selected for the cooler (Figure 4.29); the selections were made base on studies [2].

For the "Mechanical parts", it is important to take in consideration that the displacer must be lighter than the power piston. Therefore, the user has to con-

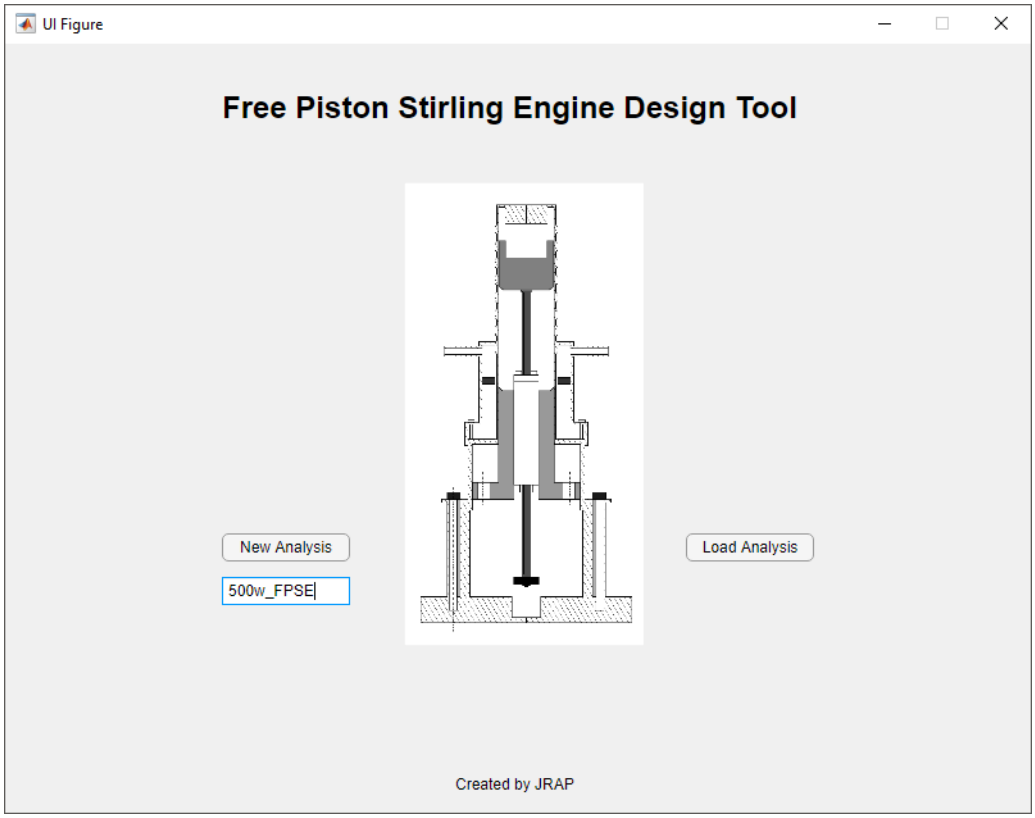

Figure 4.22: GUI's Main menu

sider this when inputting the limits of the masses; a good practice is to reduce the number of common number among the design parameters, in this case, the mass of the displacer has to be between 0.5 and 2 kg and the piston's mass among 1 and 3 kg. Similar to other parameters like the areas, the piston's area must be bigger than the rod's area. Because the areas are directly related to the force applied, it is more crucial for the design. Despite this, the limits between the piston's and rod's area have no values in common (unless the 100), see Figures 4.30 and 4.31. After the values are saved the calculation will start, see Figure 4.32.

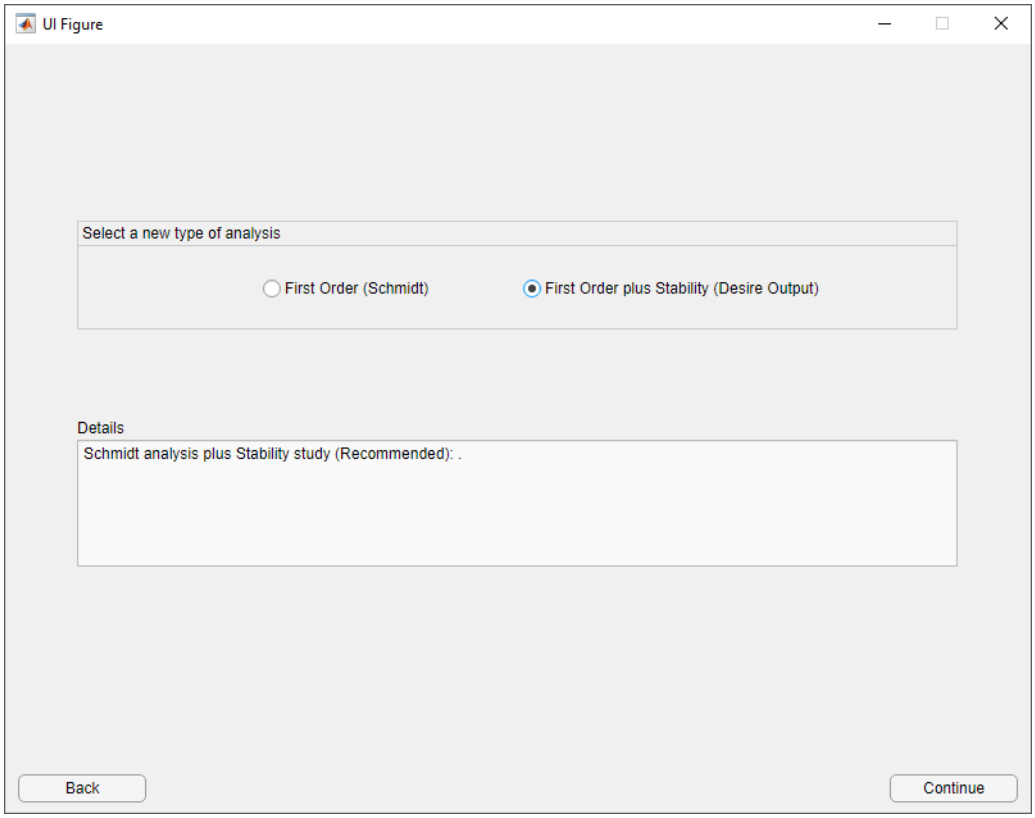

Figure 4.23: Selection of the study

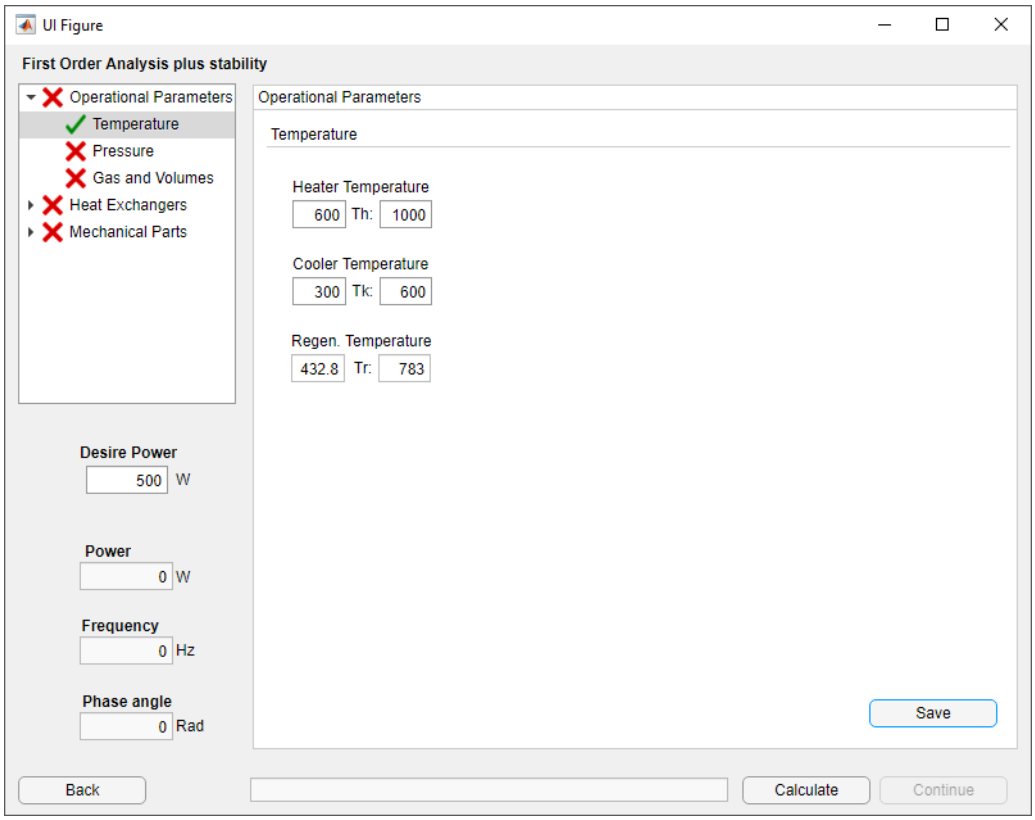

Figure 4.24: Temperature limits

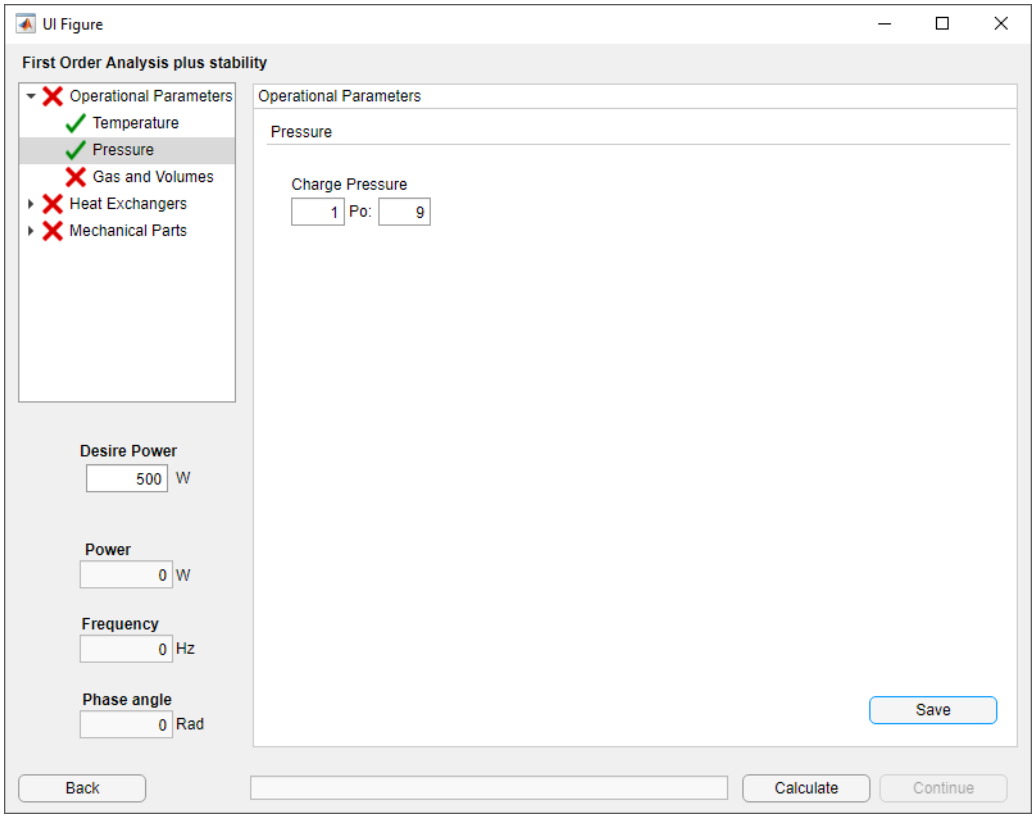

Figure 4.25: Pressure limits

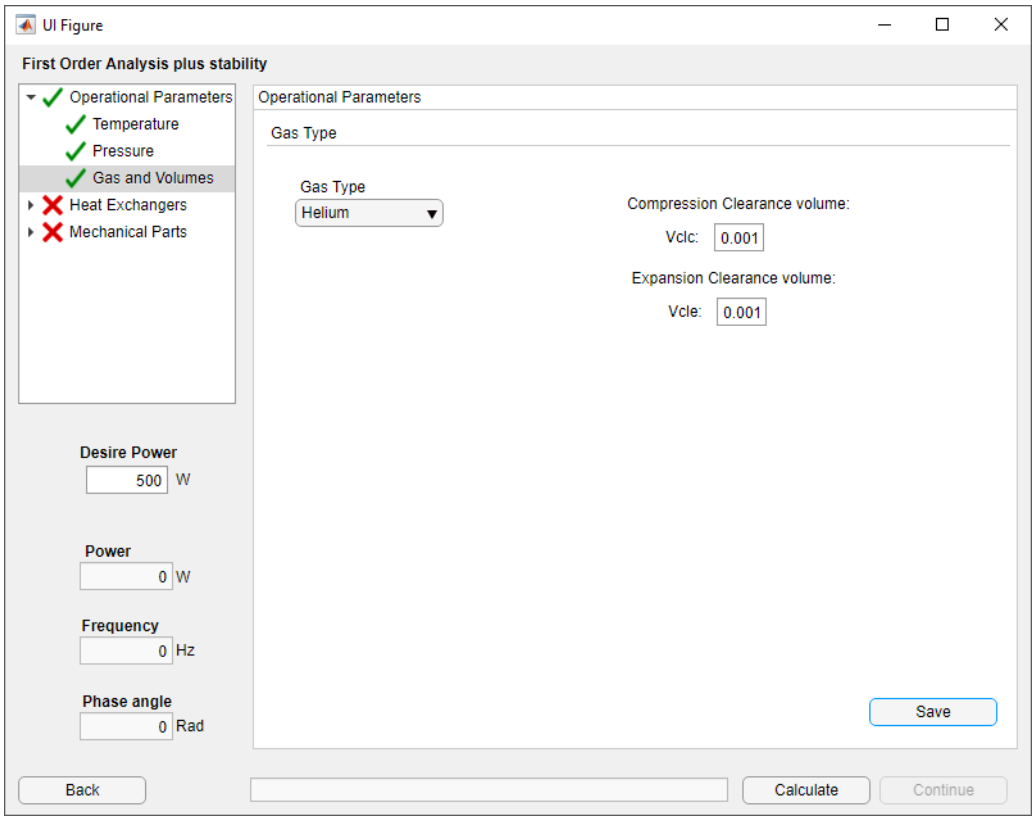

Figure 4.26: Gas type

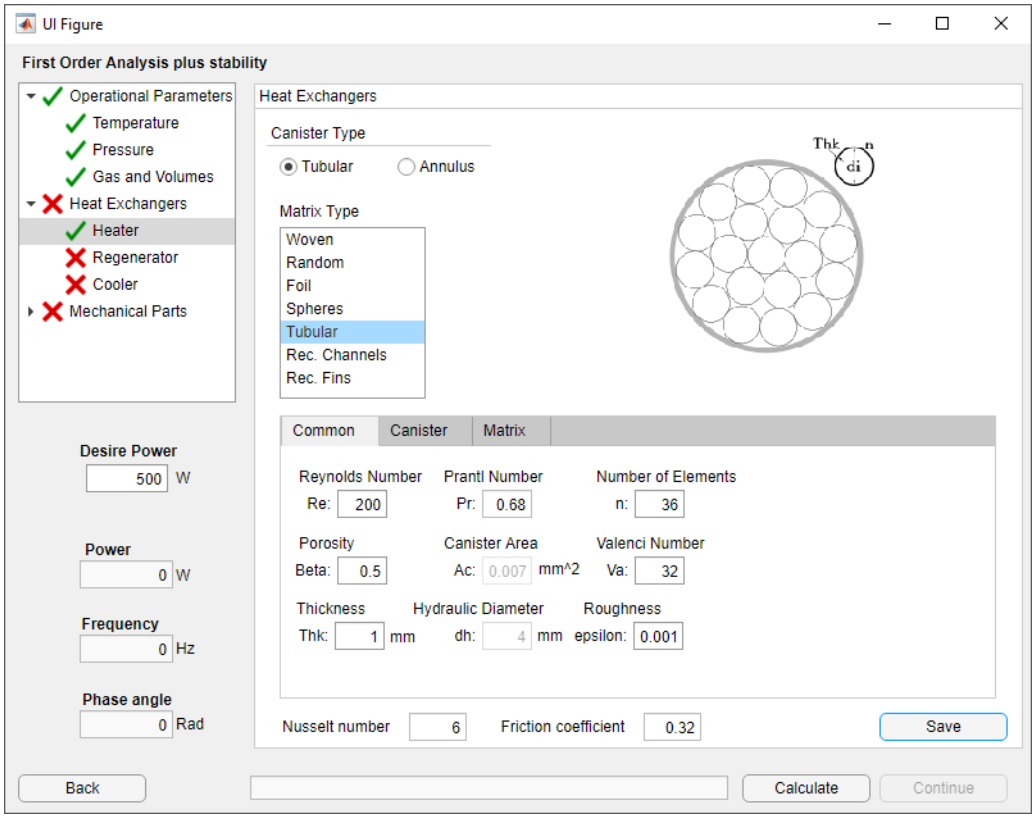

Figure 4.27: Heater parameters

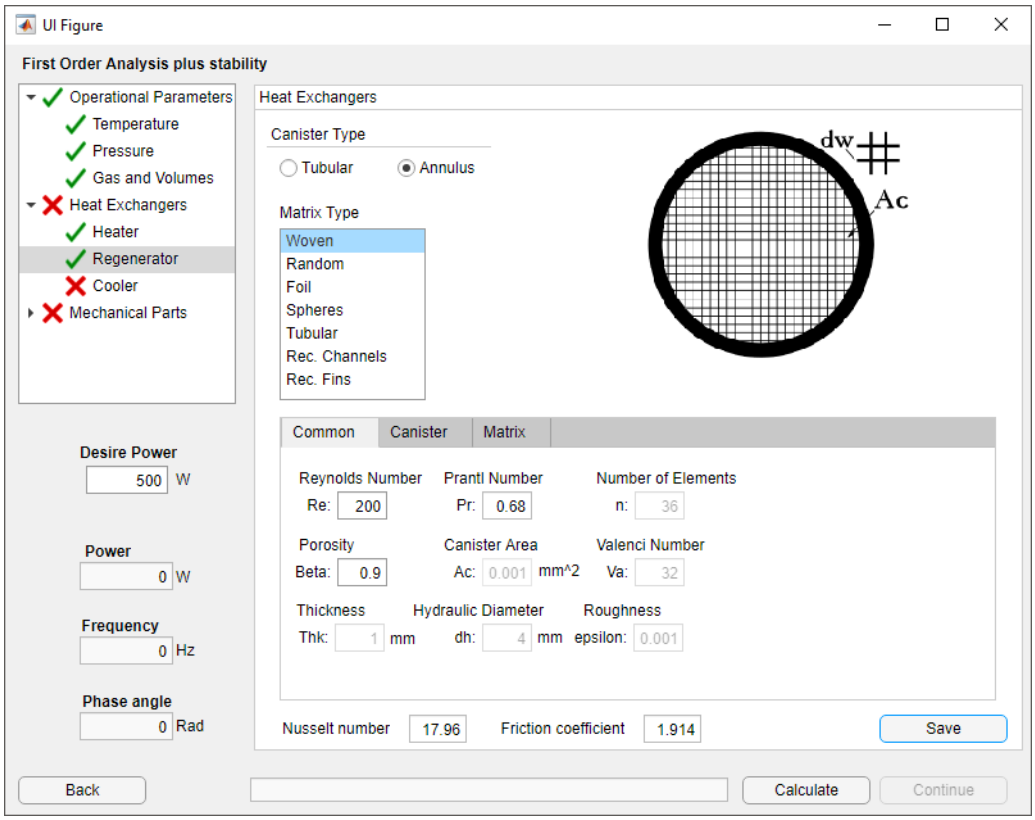

Figure 4.28: Regenerator parameters

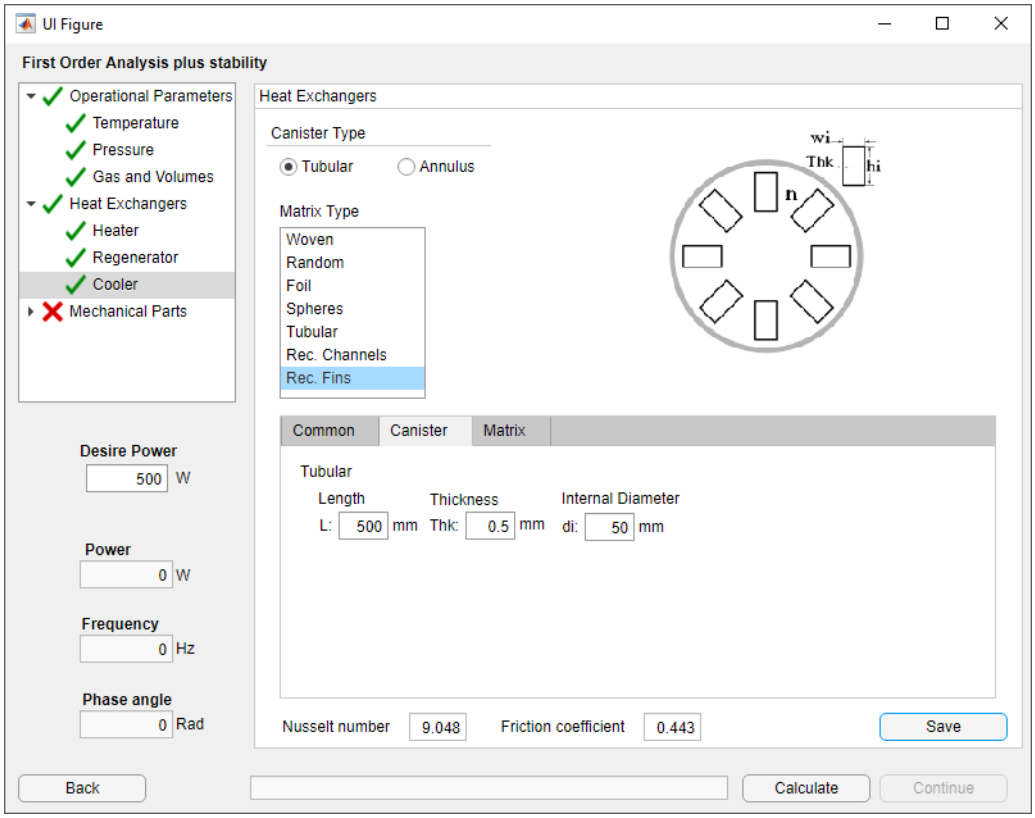

Figure 4.29: Cooler parameters

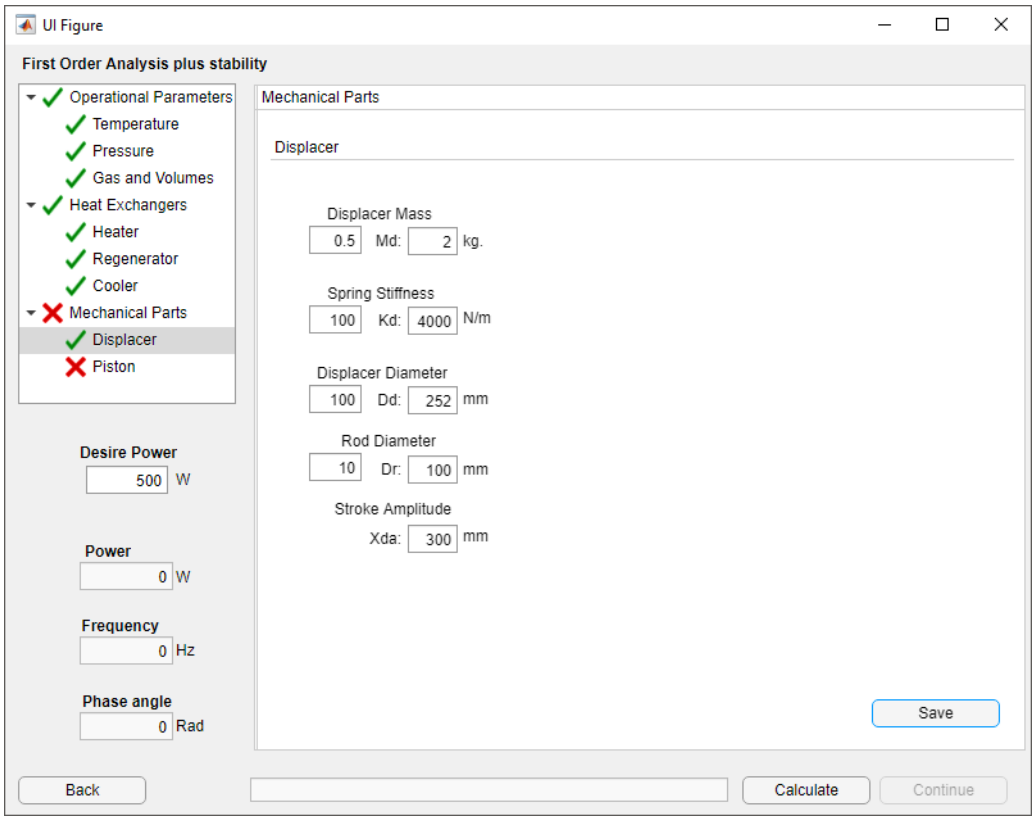

Figure 4.30: Displacer parameters

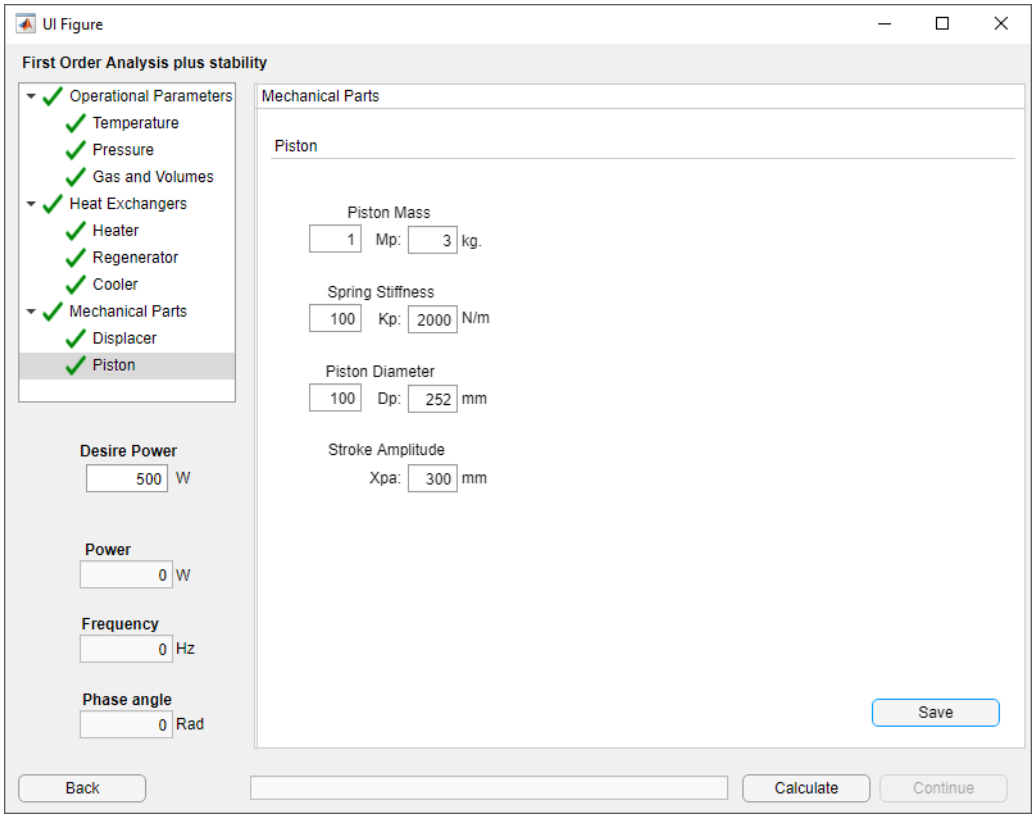

Figure 4.31: Piston parameters

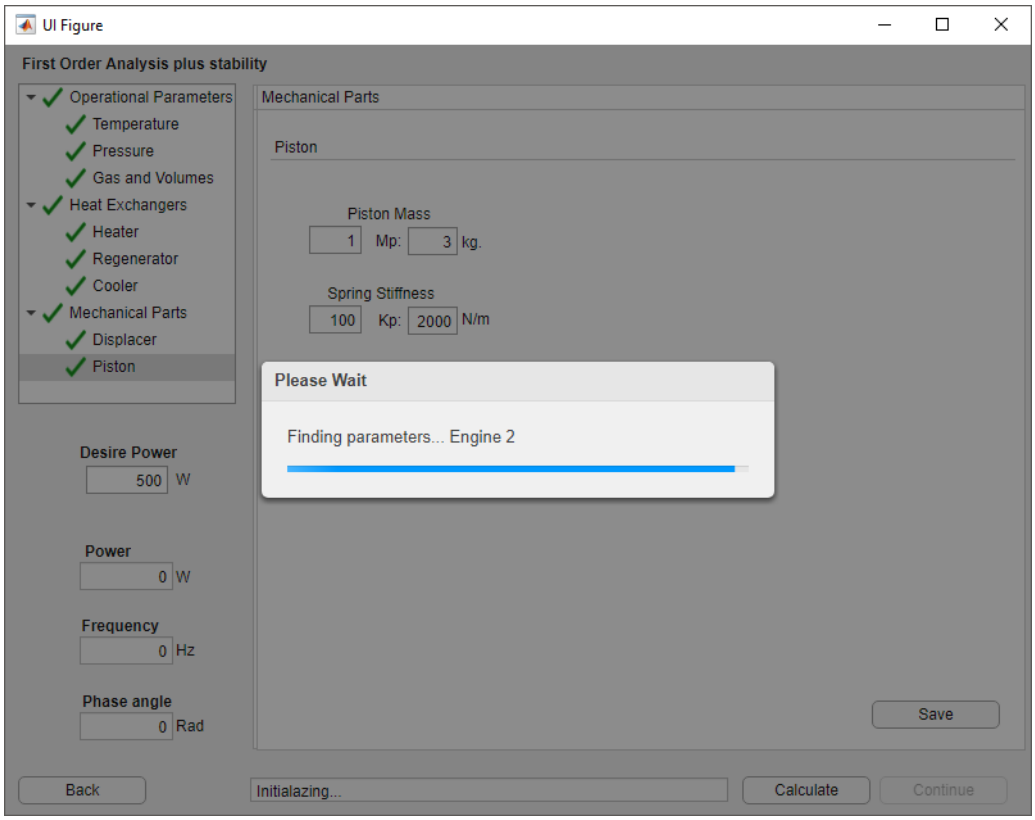

Figure 4.32: Searching of the engines

Then a set of engines are displayed; in this menu, the designer can select a specific set of parameters and edit them if its performance satisfies the requirements the design is finished. However, for the sake demonstration, the first option is shown. Figure 4.34 shows how power output and efficiency change when the temperature limits are modified. Similarly, when the values of masses, spring stiffness, and areas are rounded the output changes (Figures 4.35 and 4.36). Finally the results of the modified engine are generated, see Figure 4.37.

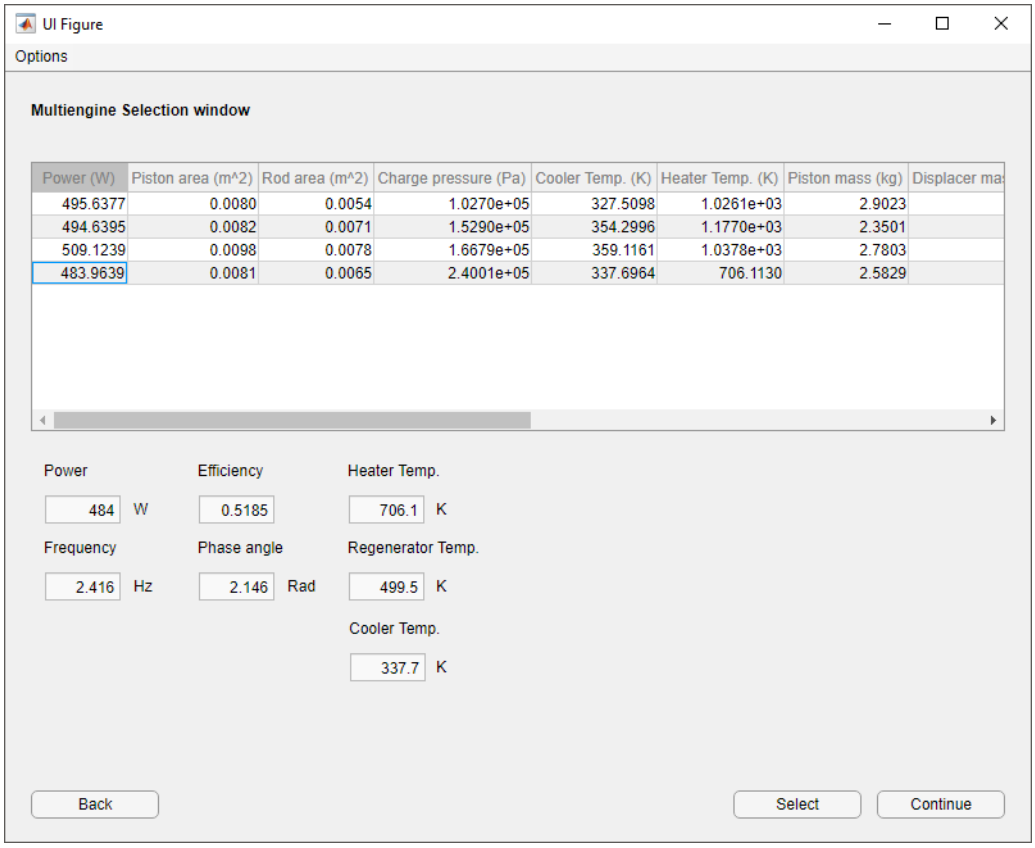

Figure 4.33: Multiple solutions

As shown in Fig. 4.33, the designer can decide the number of different engines that meet the required input power. The criteria for selecting one engine can be summarized as follows: The first criterion is the engine efficiency. The designer can choose the machine with higher efficiency, but several considerations must be taken into account. The developed code can offer operational conditions that deserve attention like, for instance, gas temperatures difficult to implement, say 2000 K in the hot space. This is because the code does not limit the temperature value, due to the computational cost that this implies. This means that in order to save calculation time, a limit value for the gas temperature is not set. Then, it is easier that the designer himself can make this differentiation. An acceptable range for a given engine can be from 300 k to 700K. Another criterion is the ratio of the displacer and piston masses. Because the FPSE is a purely dynamical engine, this parameter is also important. The mass of the displacer should be less than that of the piston, as discussed in Section 1.2.

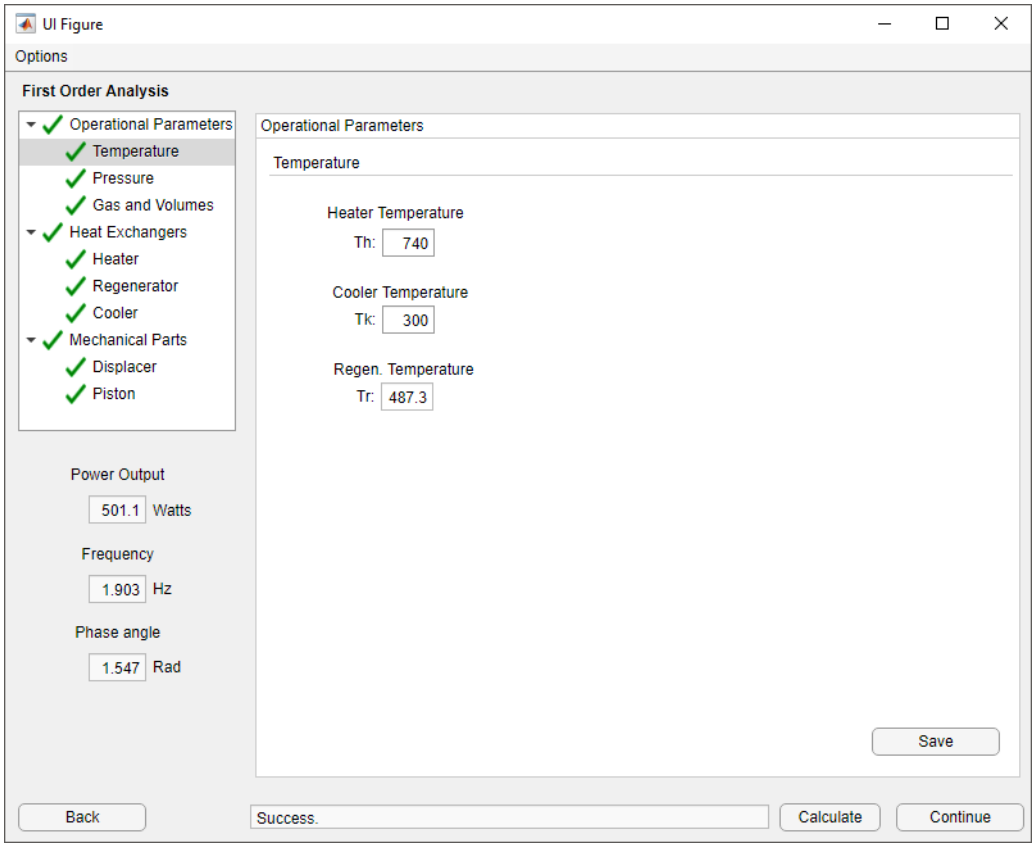

Figure 4.34: Temperature modifications

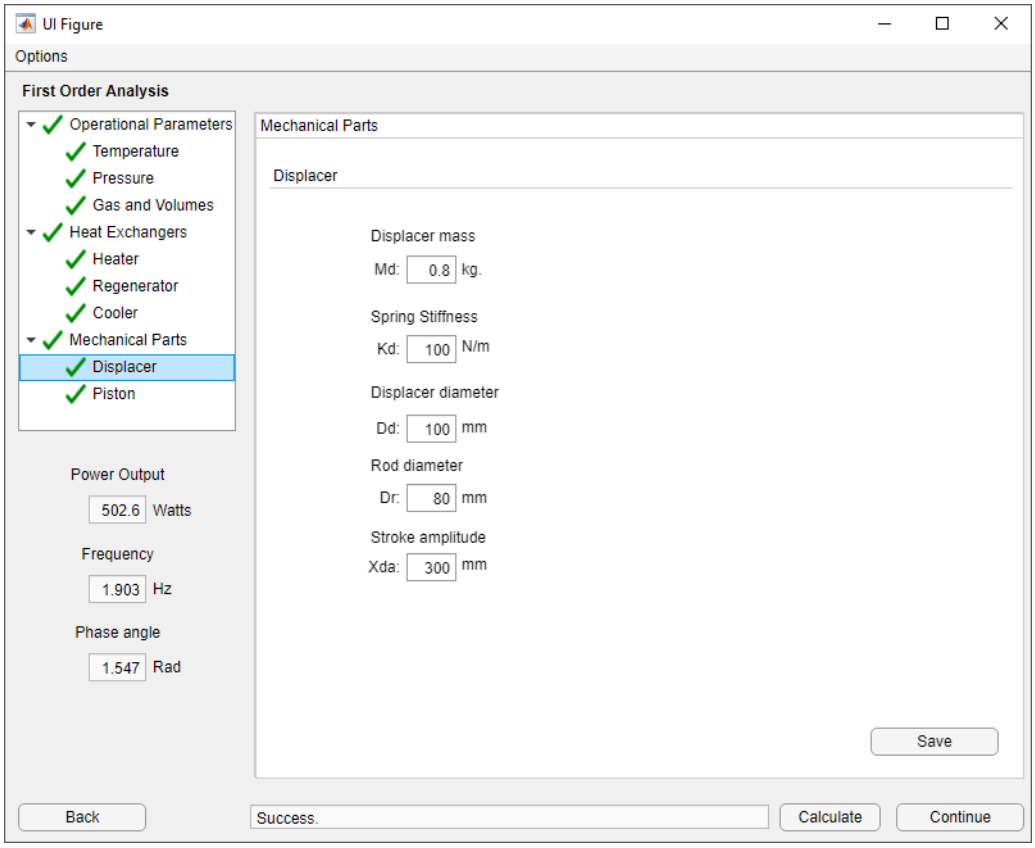

Figure 4.35: Displacer modifications

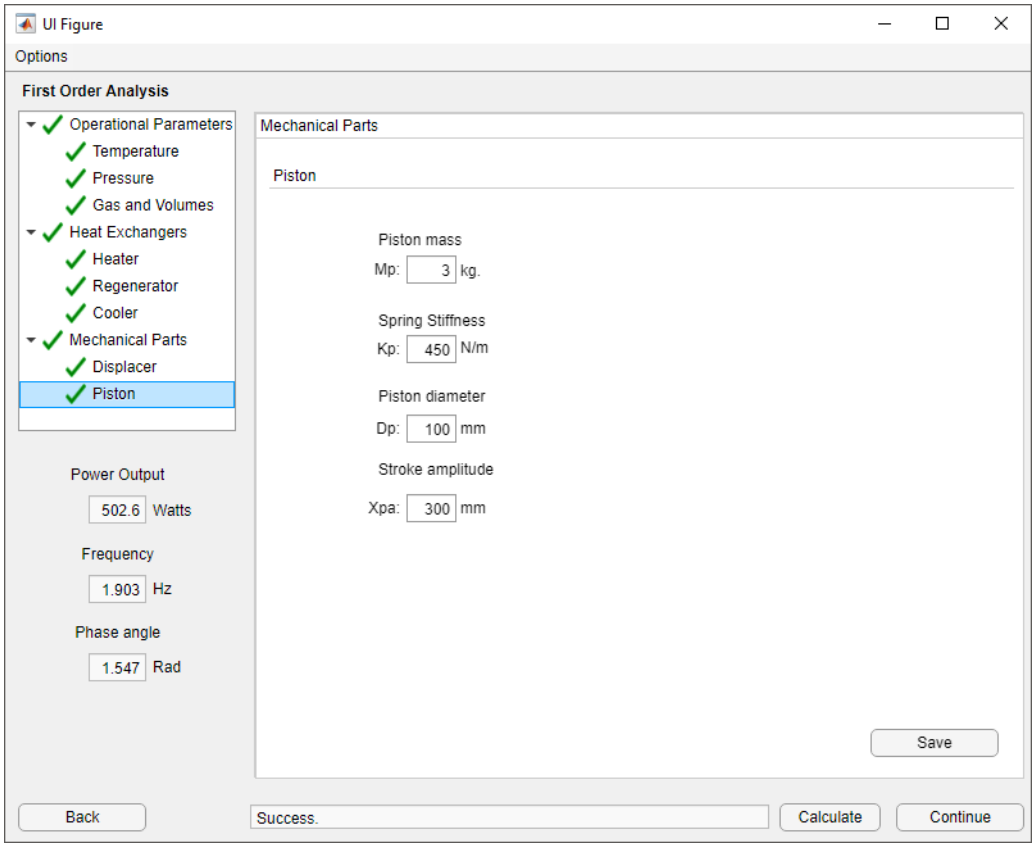

Figure 4.36: Piston modifications

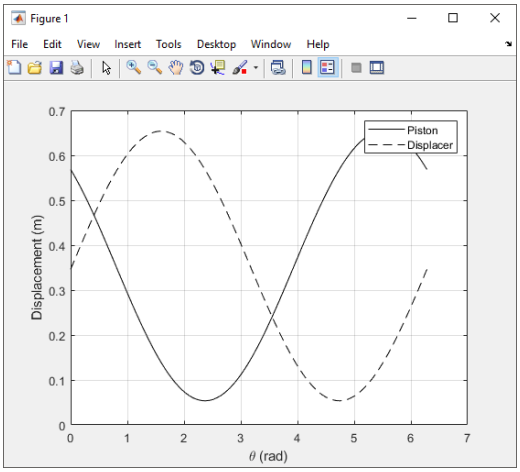

(a) Motion of the pistons

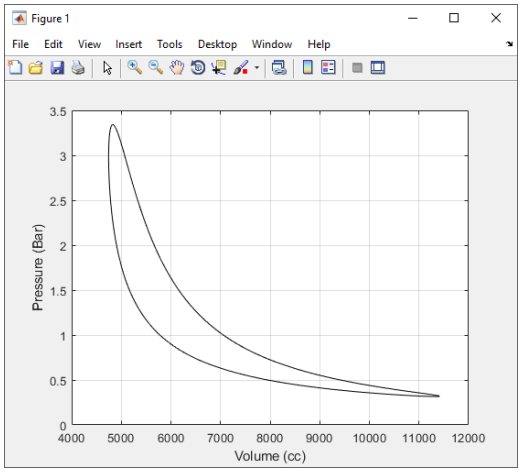

(b) PV Diagram

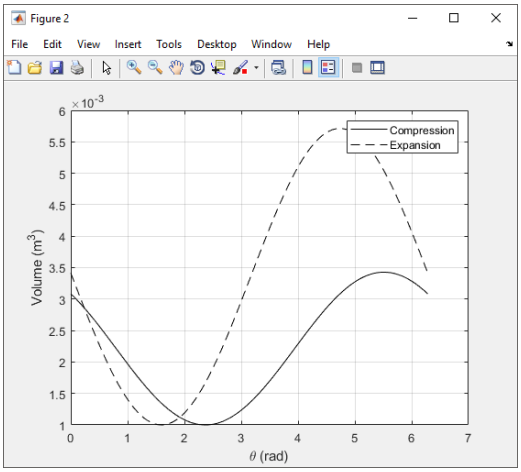

(c) Volume variation

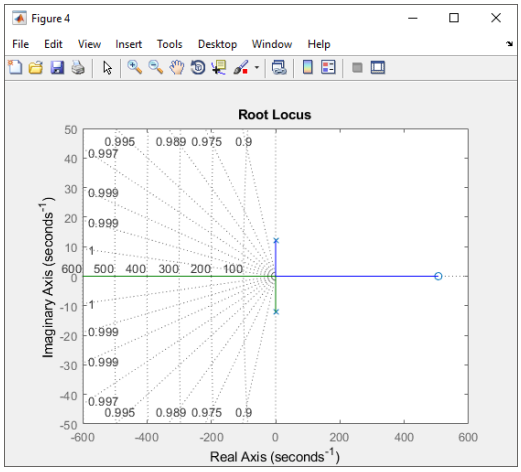

(d) Mapping of the displacer poles in the complex plane

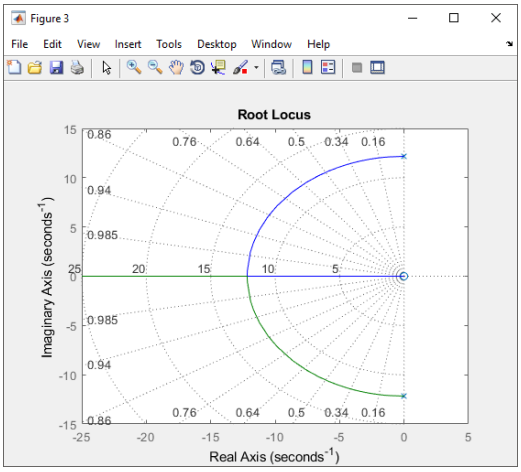

(e) Mapping of the piston poles in the complex plane

Figure 4.37: Results

"What if" questions may surge regarding the operation of the engine when it is already build and operating. This is not part of the objective nor the scope of this work. Nevertheless, a discussion regarding several engine operation variables is offered in the following.

Amplitudes

In a design process, certain border conditions are established as the starting point, which represent an objective. This objective in the case of FPSE can be, for instance, the engine power. Once the objective is determined, the rest of the operational parameters are obtained based on such objective and having a set of input parameters, summarized by [27].

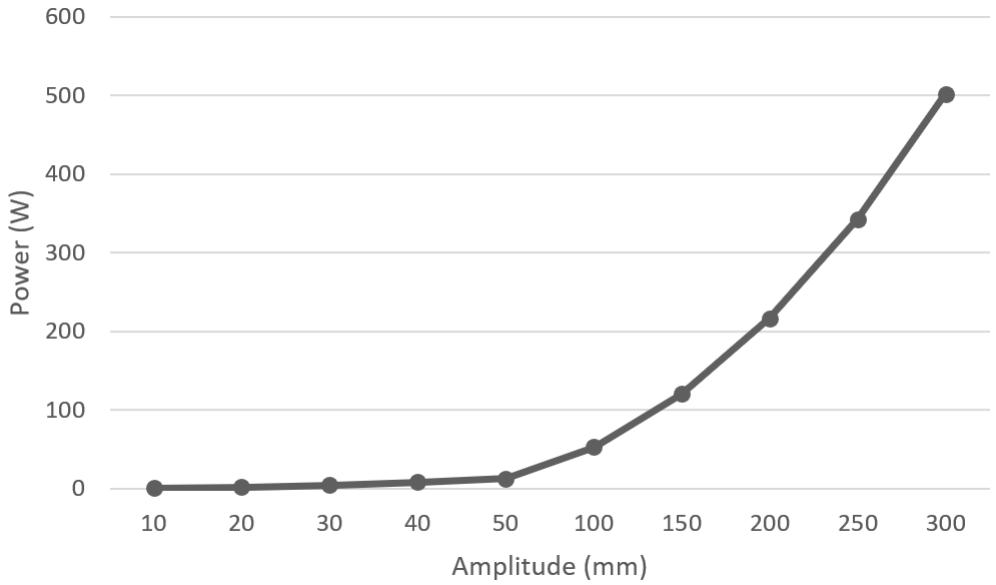

Figure 4.38: Power as a function of amplitude

Considering the above paragraph, the values for the amplitude in the designed engine is a result, obtained and limited by the physical constrains of input parameters. As explained by [34], the amplitude ratio (piston-displacer) is defined if one of the amplitudes in known (from geometry, for example). Therefore, amplitude values are demarcated according to the resulting target parameters, but also according to stability criterion: in order to guaranty the stability (the engine oscillates continuously), it must operate at that obtained amplitude. Lower values are not contemplated because the complete design indeed obtains all geometric and operating values that ensure one oscillation value so that the motor is functional. It is important to mention that certain combination of parameters would make the piston and displacer collide, and therefore the engine will not work. Therefore, the proposed methodology is able to find the combinations of parameters to assure the engine oscillations and avoid collision.

The variation of amplitudes is studied in recent researches, from a point of view of control strategy. The motion of power and displacer pistons are set as objective function in the work reported recently by [71], considering a control technique. They used a nonlinear dynamic model and define the error equation between motion, velocity, and acceleration of the pistons. Another researcher [72]

in which several similar studies are well resumed, consists of a current feedback decoupling control with respect to the output voltage adjusting time and fluctuation amplitude under the variations of piston displacement and output load. Incorporation of these techniques, or a new one, is addressed in future works as perturbation analysis.

The amplitude in the calculation process can also be considered an input parameter, if a sensibility analysis is desired. The GUI allows the variation of this parameter for this kind of purpuses. Figure 4.38 shows the variation of power as a function of amplitude. Every point represents a different run (different designs) to observe the effect of oscillations over the power. It is clear that for a certain power, there is a corresponding value in which the engine has to oscillate. This means that in order to vary the amplitude, the power must be modified accordingly. For instance, if the amplitude is increased from 150 mm to 300 mm, the power increases from 130 to 500 w.

Temperatures

Countless reported works on FPSE uses the Schmidt's theory, with the corresponding assumptions (explained in section 2.2), being one of them that the workspace of the engine contains of isothermal regions, adding the assumption of source/sink temperatures as input design parameters [27]. The gas temperature variation in expansion and compression spaces, Te and Tc, is considered by [7] in which the effect of this variation over the FPSE performance is studied. As a summary, such effects are: For a given range of regenerator efficiency, the gradients in the expansion space were greater that in the compression one. When the gas temperature in the expansion Te space is increased, the strokes of pistons, phase angle, and frequency show an increasing trend. The increase of gas temperature within the compression space Tc reduces all these parameters. The corresponding influence over the power and engine efficiency is given: both parameters are higher when Te increases and Tc decreases, also reported in [73, 74].

Conclusions

In the present work, an innovative design tool for Free Piston Stirling Engines is developed. Initially, a preliminary analysis is carried out based on a First order Smith with stability analysis to assure the operating conditions for which the FPSE is functional. Summary of the main conclusions is presented below:

- The first order calculation in conjunction with the stability analysis, based on the dynamics of the engine, is described and implemented in the design. A criterion is deduced based on the localization of the complex poles, whose physical meaning is related to the natural frequency of the whole system. At this stage, the engineer can select the operation parameters in order to fulfill the power and efficiency desired. This is not an easy task because of the sensibility of the model when an engine setting are changed. The implementation of a based on genetic reproduction algorithm resulted in a powerful tool to find parameters that successfully satisfy the output power desired. The results presented are obtained through a novel and automatic way.

- A crucial part of the Stirling engines, heat exchangers, is included in the design. For the heater, regenerator and cooler, an approach for calculation of the friction factor and the Nusselt number is obtained, using well-known experimental correlations. Therefore, a pressure loss and heat transfer coefficients can be estimated and a more realistic output power estimation. The variety of matrix types included, and their design parameters, add more calculation and this suggest a more practical tool to automate the design process.

- A Graphical User Interface (GUI) is developed, considering the above findings, which comprises from the calculation of the natural oscillation frequency of the engine, based on the dynamic analysis, stability analysis and its representation in the complex plane. In addition to this, it offers the heat exchanger's friction factor and Nusselt number correlations. The interface results in a faster solution to design a sophisticated engine like a Free-piston Stirling engine, given the significant amount of variables and the number of iterations needed to accomplish the desired parameters. Furthermore, the interface creates technical data that encompass all the design and operational parameters in one document. The purpose of this sheet is to guide designers, not only to calculate theoretical engines, but also to prototype them.

- For a given output power, the designer can select an appropriate engine according to an efficiency criterion, but considering the practical implemen-

tation of the temperatures and the ratio of the displacer and piston masses, as explained in section 2.3.

Future work

As already commented several times in this work, the design of FPSE is a very challenging and a complex task, with many areas of research still to work. Every study has a scope and therefore, several topics can be developed with this work as the basis. To continue this study and guide other researchers, the future work should be oriented to:

- Perturbation analysis that include engine start and stop, external operating conditions (temperature variations in the heat exchangers, for example) and oscillation control.
- Design Optimization, which is though as an additional stage of the design procedure, not a substituting technique. This is a future master thesis.
- Building and testing of a prototype for different operational parameters and comparison with theoretical data.

References

[1] J. S. G. Walker, *Free Piston Stirling Engines (Lecture Notes in Engineering)*, vol. 12. Springer-Verlag, 1985.

[2] J. G. Gedeon, D.; Wood, "Oscillating-flow regenerator test rig: Hardware and theory with derived correlations for screens and felts," tech. rep., NASA Glenn Research Center, 1996.

[3] G. Walker, *Stirling Engines*, vol. 1. Clarendon Press, Oxford, 1980.

[4] G. Conroy, A. Duffy, and L. Ayompe, "Economic, energy and ghg emissions performance evaluation of a whispergen mk iv stirling engine microchp unit in a domestic dwelling," *Energy Conversion and Management*, vol. 81, pp. 465 – 474, 2014.

[5] S. Zhu, G. Yu, J. O, T. Xu, Z. Wu, W. Dai, and E. Luo, "Modeling and experimental investigation of a free-piston stirling engine-based micro-combined heat and power system," *Applied Energy*, vol. 226, pp. 522 – 533, 2018.

[6] A. Tavakolpour-Saleh, S. Zare, and H. Bahreman, "A novel active free piston stirling engine: Modeling, development, and experiment," *Applied Energy*, vol. 199, pp. 400 – 415, 2017.

[7] A. Tavakolpour-Saleh, S. Zare, and A. Omidvar, "Applying perturbation technique to analysis of a free piston stirling engine possessing nonlinear springs," *Applied Energy*, vol. 183, pp. 526 – 541, 2016.

[8] S. Zare and A. Tavakolpour-Saleh, "Frequency-based design of a free piston stirling engine using genetic algorithm," *Energy*, vol. 109, pp. 466 – 480, 2016.

[9] J. Mou, W. Li, J. Li, and G. Hong, "Gas action effect of free piston stirling engine," *Energy Conversion and Management*, vol. 110, pp. 278 – 286, 2016.

[10] L. Remiorz, J. Kotowicz, and W. Uchman, "Comparative assessment of the effectiveness of a free-piston stirling engine-based micro-cogeneration unit and a heat pump," *Energy*, vol. 148, pp. 134 – 147, 2018.

[11] F. Formosa, "Coupled thermodynamic dynamic semianalytical model of free piston stirling engines," *Energy Conversion and Management*, vol. 52, no. 5, pp. 2098 – 2109, 2011.

[12] F. Formosa and G. Despesse, "Analytical model for stirling cycle machine design," *Energy Conversion and Management*, vol. 51, no. 10, pp. 1855 – 1863, 2010.

[13] F. Formosa and L. G. Frechette, "Scaling laws for free piston stirling engine design: Benefits and challenges of miniaturization," *Energy*, vol. 57, pp. 796 – 808, 2013.

[14] H. Karabulut, "Dynamic analysis of a free piston stirling engine working with closed and open thermodynamic cycles," *Renewable Energy*, vol. 36, no. 6, pp. 1704 – 1709, 2011.

[15] M. Motamedi, R. Ahmadi, and H. Jokar, "A solar pressurizable liquid piston stirling engine: Part 1, mathematical modeling, simulation and validation," *Energy*, vol. 155, pp. 796 – 814, 2018.

[16] S. Langdon-Arms, M. Gschwendtner, and M. Neumaier, "A novel solar-powered liquid piston stirling refrigerator," *Applied Energy*, vol. 229, pp. 603 – 613, 2018.

[17] A. Skorek-Osikowska, L. Remiorz, u. Bartela, and J. Kotowicz, "Potential for the use of micro-cogeneration prosumer systems based on the Stirling engine with an example in the Polish market," *Energy*, vol. 133, no. C, pp. 46–61, 2017.

[18] S. Zare and A. Tavakolpour-Saleh, "Frequency-based design of a free piston stirling engine using genetic algorithm," *Energy*, vol. 109, pp. 466 – 480, 2016.

[19] W. R. Martini, *Stirling Engine Design Manual*. National Aeronautics and Space Administration, 1983.

[20] P. Needham, *The Carnot Cycle and Reversible Changes*, pp. 85–97. Dordrecht: Springer Netherlands, 2011.

[21] J. P. D. Hartog, *Mechanical vibrations*. Dover Publications, 4th ed., 1985.

[22] K. Ogata, *Modern Control Engineering*. Upper Saddle River, NJ, USA: Prentice Hall PTR, 4th ed., 2001.

[23] T. L. Schmitz and K. S. Smith, *Two Degree of Freedom Forced Vibration*, pp. 167–198. Boston, MA: Springer US, 2012.

[24] M. Hussey, *Harmonic Analysis and Transform Techniques in Damped Harmonic Oscillator Systems*, pp. 97–126. London: Macmillan Education UK, 1983.

[25] S. Grinnel, "Flow of compressible fluid in the thin passage," *A.S.M.E.*, pp. 765 – 771, 1956.

[26] C. West, "Theoretical basis for beale number," *16th I.E.C.E.C. No. 819787*, pp. 1886–1887, 1981.

[27] S. Zare and A. Tavakolpour-Saleh, "Free piston stirling engines: A review," *International Journal of Energy Research*, vol. 0, no. 0.

[28] L. Meirovitch, *Methods of Analytical Dynamics*. Dover, 1998.

[29] J. A. Riofrio, K. Al-Dakkan, M. E. Hofacker, and E. J. Barth, "Control-based design of free-piston stirling engines," in *2008 American Control Conference*, pp. 1533–1538, June 2008.

[30] S.-J. Jang, M. J. Brennan, F. Dohnal, and Y.-P. Lee, "A design method for selecting the physical parameters of a free piston stirling engine," *Proceedings of the Institution of Mechanical Engineers, Part C: Journal of Mechanical Engineering Science*, vol. 231, no. 13, pp. 2441–2450, 2017.

[31] B. B. Farhan Choudhary, "Hopf instabilities in free piston stirling engines," *ASME. J. Comput. Nonlinear Dynam.*, vol. 9, no. 2, 2013.

[32] R. W. Redlich and D. M. Berchowitz, "Linear dynamics of free-piston stirling engines," *Proceedings of the Institution of Mechanical Engineers, Part A: Power and Process Engineering*, vol. 199, no. 3, pp. 203–213, 1985.

[33] B. Sylvie, L. Guillaume, L. Francois, and N. Philippe, "Stability analysis of free piston stirling engines," *The European Physical Journal Applied Physics*, vol. 61, no. 3, p. 30901, 2013.

[34] D. V. Z. Lev Y. Lezhnev, Denis Alekseevich Ivanov, "The basics of controlling a free piston stirling engine," *Biosciences Biotechnology Research Asia*, vol. 12, no. 2, 2015.

[35] J. G. Martinez, *Some mathematical models to describe the dynamic behavior of the B-10 Free piston Striling engine.* Ohio university, 1994.

[36] I. Urieli, "Schmidt analysis - equation summary." `https://www.ohio.edu/mechanical/stirling/isothermal/Schm_summary.html`, 2018.

[37] K. S. J Harrod, PJ Mago, "First and second law analysis of a stirling engine with imperfect regeneration and dead volume," 2009.

[38] S. M. Geng and N. A. Schifer, "Development of a low inductance linear alternator for stirling power convertors," in *15th International Energy Conversion Engineering Conference*, p. 4961, 2017.

[39] J. F. Metscher and E. J. Lewandowski, "Development and validation of linear alternator models for the advanced stirling convertor," 2015.

[40] W. Cawthorne, P. Famouri, and N. Clark, "Integrated design of linear alternator/engine system for hev auxiliary power unit," in *IEMDC 2001. IEEE International Electric Machines and Drives Conference (Cat. No. 01EX485)*, pp. 267–274, IEEE, 2001.

[41] Q.-F. Li, J. Xiao, and Z. Huang, "Parametric study of a free piston linear alternator," *International Journal of Automotive Technology*, vol. 11, no. 1, pp. 111–117, 2010.

[42] S. Qiu and J. Augenblick, "Development and magnetic analysis of a stirling convertor assembly linear alternator," in *3rd International Energy Conversion Engineering Conference*, p. 5653, 2005.

[43] I. Urieli, "Stirling engine simple analysis." `https://www.ohio.edu/mechanical/stirling/simple/simple.html`, 2018.

[44] I. Urieli, "Pumping loss simple analysis." `https://www.ohio.edu/mechanical/stirling/simple/pumping.html`, 2018.

[45] S. Bretsznajder, "Chapter 3 - viscosities of gases," in *Prediction of Transport and Other Physical Properties of Fluids* (S. Bretsznajder, ed.), International Series of Monographs in Chemical Engineering, pp. 136 – 188, Pergamon, 1971.

[46] W. Kays and A. London, *Compact Heat Exchangers*. Krieger Publishing Company, 1984.

[47] K. Hutter and Y. Wang, *Pipe Flows*, pp. 577–620. Cham: Springer International Publishing, 2016.

[48] G. Brenn, *Laminar Two-Dimensional Flow*, pp. 51–84. Berlin, Heidelberg: Springer Berlin Heidelberg, 2017.

[49] J. McGovern, "Technical note: Friction factor diagrams for pipe flow," *School of Mechanical and Transport Engineering at ARROW DIT*, 2011.

[50] G. Brown, "The darcy-weisbach equation," 2000.

[51] T. Adams, S. Abdel-Khalik, S. Jeter, and Z. Qureshi, "An experimental investigation of single-phase forced convection in microchannels," *International Journal of Heat and Mass Transfer*, vol. 41, no. 6, pp. 851 – 857, 1998.

[52] Beek and Muttzal, *Transport Phenomena*. Ed. Wiley, 1980.

[53] N. Zhang and M. Xin, "Liquid flow and convective heat transfer in microtube," *Proc. China National Heat Transfer*, 1991.

[54] L. A. Luo, U. D'Ortona, and D. Tondeur, "Compact heat exchangers," in *Microreaction Technology: Industrial Prospects* (W. Ehrfeld, ed.), (Berlin, Heidelberg), pp. 556–565, Springer Berlin Heidelberg, 2000.

[55] B. Thomas and D. Pittman, "Update on the evaluation of different correlations for the flow friction factor and heat transfer of stirling engine regenerators," in *Collection of Technical Papers. 35th Intersociety Energy Conversion Engineering Conference and Exhibit (IECEC) (Cat. No.00CH37022)*, vol. 1, pp. 76–84 vol.1, July 2000.

[56] W. C. Kuhl H., Schulz S., "Theoretical models and correlations for the flow friction and heat transfer characteristics of random wire regenerator materials," *IECEC*, 1998.

[57] M. Kuosa, K. Saari, A. Kankkunen, and T.-M. Tveit, "Oscillating flow in a stirling engine heat exchanger," *Applied Thermal Engineering*, vol. 45-46, pp. 15 – 23, 2012.

[58] M. Porter, *Turbulent Flow*. William Andrew Publishing/Noyes, 1990.

[59] E. Richardson and E. Tyler, "The transverse velocity gradient near the mouths of pipes in which an alternating or continuous flow of air is established," *Proceedings of the Physical Society*, vol. 42, no. 1, p. 1, 1929.

[60] C. Walther, H.-D. Kühl, T. Pfeffer, and S. Schulz, "Influence of developing flow on the heat transfer in laminar oscillating pipe flow," *Forschung im Ingenieurwesen*, vol. 64, no. 3, pp. 55–63, 1998.

[61] T. Xiaoguo and P. Cheng, "Correlations of the cycle-averaged nusselt number in a periodically reversing pipe flow," *International Communications in Heat and Mass Transfer*, vol. 20, no. 2, pp. 161–172, 1993.

[62] T. Zhao and P. Cheng, "Oscillatory heat transfer in a pipe subjected to a laminar reciprocating flow," *Journal of heat transfer*, vol. 118, no. 3, pp. 592–597, 1996.

[63] F. de Monte, G. Galli, and F. Marcotullio, "An analytical oscillating-flow thermal analysis of the heat exchangers and regenerator in stirling machines," in *IECEC 96. Proceedings of the 31st Intersociety Energy Conversion Engineering Conference*, vol. 2, pp. 1421–1427 vol.2, Aug 1996.

[64] R. Winterton, "Where did the dittus and boelter equation come from?," *International Journal of Heat and Mass Transfer*, vol. 41, no. 4, pp. 809 – 810, 1998.

[65] Shah Ramesh K, Sekulic Dusan P, *Turbulent Flow*. John Wiley and Sons, 2003.

[66] C. L. I. Yuhiro, *Compared with Heat Transfer Experimental Data*. IGI Global, 2017.

[67] T. Zhao and P. Cheng, "Experimental studies on the onset of turbulence and frictional losses in an oscillatory turbulent pipe flow," *International Journal of Heat and Fluid Flow*, vol. 17, no. 4, pp. 356–362, 1996.

[68] D. Gedeon, "Sage users guide," January 2016.

[69] *Flow Resistance: A Design Guide for Engineers*. Routledge, 1989.

[70] V. Mallawaarachchi, "Introduction of genetic algorithms." `https://tinyurl.com/yy9rxw3t`, 2017.

[71] S. Zare, A. Tavakolpour-Saleh, and T. Binazadeh, "Passivity based-control technique incorporating genetic algorithm for design of a free piston stirling engine," *Renewable Energy Focus*, vol. 28, pp. 66 – 77, 2019.

[72] P. Zheng, B. Yu, S. Zhu, Q. Gong, and J. Liu, "Research on control strategy of free-piston stirling-engine linear-generator system," in *2014 17th International Conference on Electrical Machines and Systems (ICEMS)*, pp. 2300–2304, Oct 2014.

[73] A. Sowale and A. Kolios, "Thermodynamic performance of heat exchangers in a free piston stirling engine," *Energies*, vol. 11, p. 505, 02 2018.

[74] S. Qiu, Y. Gao, G. Rinker, and K. Yanaga, "Development of an advanced free-piston stirling engine for micro combined heating and power application," *Applied Energy*, vol. 235, pp. 987 – 1000, 2019.